Lukas Wagner, BSc

Concept and realisation of a distributed fibre-optic sensing system for direct and continuous strain measurement in a shotcrete lining

Master's Thesis

Submitted in fulfilment of the requirements for the degree of

Master of Science/Diplom-Ingenieur

Master's programme Geotechnical and Hydraulic Engineering

at

Graz University of Technology

Supervisor

O.Univ.-Prof. Dipl.-Ing. Dr.mont. Wulf Schubert

Institute of Rock Mechanics and Tunnelling
Graz University of Technology

Additional supervisor

Dipl.-Ing. Alexander Kluckner, BSc

Institute of Rock Mechanics and Tunnelling
Graz University of Technology

Graz, September 2017

Affidavit
Eidesstattliche Erklärung

I declare that I have authored this thesis independently, that I have not used other than the declared sources/resources, and that I have explicitly marked all material which has been quoted either literally or by content from the used sources. The text document uploaded to TUGRAZonline is identical to the present master‘s thesis.

Ich erkläre an Eides statt, dass ich die vorliegende Arbeit selbstständig verfasst, andere als die angegebenen Quellen/Hilfsmittel nicht benutzt, und die den benutzten Quellen wörtlich und inhaltlich entnommenen Stellen als solche kenntlich gemacht habe. Das in TUGRAZonline hochgeladene Textdokument ist mit der vorliegenden Masterarbeit identisch.

Date/Datum

Signature/Unterschrift

Acknowledgements

I want to thank the ÖBB-Infrastruktur AG for making it possible to conduct such an ambitious venture at one of their project sites currently under construction. I thank all the people who have been involved, especially Oliver Kai Wagner, Petra Wolf and Tobias Schachinger.

I thank Markus Brandtner and Wolfgang Obermüller from IGT Geotechnik und Tunnelbau Ziviltechniker Gesellschaft m.b.H. for providing me with computational data of the software Tunnel:Suite and additional technical advice.

I am very thankful for all the support we got on site on the one hand by the companies of the construction joint venture SBT 1.1 Tunnel Gloggnitz – Implenia Österreich, HOCHTIEF Infrastructure Austria, Thyssen Schachtbau – who always have been a great help from the very beginning at the pre-test in Göstritz and later at the main test in Gloggnitz.

On the other hand I particularly want to thank the Geotechnical Team Underground (GTU) on site for their support, mainly Gerold Lenz, Karoline Prall and Sascha Oswald who managed the coordination and the implementation works and provided me with a lot of geotechnical insight.

I also want to thank the Institute of Engineering Geodesy and Measurement Systems (IGMS) from Graz University of Technology for providing the fibre-optic measurement equipment used in this project and specifically Christoph Monsberger who did the instrumentation and measuring work on site as well as the data processing afterwards.

I express my gratitude to the members of staff at the Institute of Rock Mechanics and Tunnelling, Prof. Wulf Schubert for the opportunity to realise such a project within my master's thesis by pulling some strings in the background, Andreas Buyer for doing the photo documentation on site and Anton Kaufmann for the help with all the preparations prior to the tests. I gratefully thank my supervising assistant Alexander Kluckner for his tremendous support from day one of this project until the very end. Without you, this project would never have been possible. Thank you.

Last but certainly not least I want to thank my friends and family who always supported me throughout my time in Graz. I thank my sister Katrin and my parents Leonhard and Gisela for their never-ending help and encouragement during my studies. I thank my girlfriend Anja for always being there for me, thank you for everything.

Abstract

This thesis shows the successful implementation of fibre-optic sensing cables for direct and continuous strain measurement within the shotcrete lining of a conventional tunnel drive. Precise planning of this project concerning aspects such as accurate, swift and safe installation of the measurement system during ongoing tunnelling works as well as a detailed processing and evaluation of the obtained data are the major tasks of this thesis.

The shotcrete lining of the top-heading as well as of the invert is equipped with two layers (rock side and cavity side) of fibre-optic sensing cables, which are installed in circumferential and longitudinal direction. A cable line for temperature compensation of the measured changes in strain is also installed.

All cables are measured autonomously for several weeks to capture the strain evolution inside the lining from the day of the construction to a posterior, well-hardened state. An additional follow-up measurement is conducted two months afterwards. At an accuracy of up to 1 µm/m a resolution of 2 cm can be achieved.

Besides the conventional monitoring targets used for displacement recordings, additional measurement equipment like strain gages and pressure cells are installed in the cross-section under investigation. Back calculated strains from absolute displacements and the readings from the strain gages are in good agreement with the results of the conducted fibre-optic measurements.

Kurzfassung

Diese Arbeit zeigt die erfolgreiche Realisierung des Einbaus von faseroptischen Sensorenkabel zur direkten und kontinuierlichen Dehnungsmessung in einer Spritzbetonaußenschale eines konventionell aufgefahrenen Tunnels. Präzise Planung im Hinblick auf eine genaue, rasche und sichere Installation des Messsystems während laufender Vortriebsarbeiten vor Ort sowie eine ausführliche Auswertung der gewonnenen Daten sind die wesentlichen Aufgaben dieser Arbeit.

Die Spritzbetonschale der Kalotte sowie der Sohle ist in zwei Lagen (bergseitig und hohlraumseitig) mit faseroptischen Sensorenkabel, welche in Umfangsrichtung und Längsrichtung verlegt sind, instrumentiert. Ein Kabelstrang zur Temperaturkompensation der gemessenen Dehnungsänderungen ist ebenfalls installiert.

Sämtliche Kabel werden über mehrere Wochen autonom gemessen, um die Dehnungsentwicklung innerhalb der Schale vom Tag der Herstellung bis zu einem späteren, gut ausgehärteten Zustand aufzuzeichnen. Eine zusätzliche Folgemessung wird zwei Monate später durchgeführt. Bei einer Präzision von bis zu 1 µm/m kann eine Auflösung von 2 cm erreicht werden.

Neben den heutzutage üblichen Messprismen zur Aufzeichnung von absoluten Verschiebungen werden zusätzlich Sensoren wie Dehnungsgeber und Druckmessdosen im betrachteten Querschnitt installiert. Die Daten der Dehnungsgeber sowie Dehnungen, welche aus den Verschiebedaten rückgerechnet sind, zeigen gute Übereinstimmung mit den Ergebnissen der durchgeführten faseroptischen Messungen.

Contents

1 Introduction

1.1 General

The main objective of this thesis is the installation of fibre-optic sensors for a direct and continuous strain measurement in the shotcrete lining of a conventional tunnelling section at the Semmering Base Tunnel in Austria. The following list comprises the major aspects considered in terms of theoretical considerations and actual implementations:

- Selection of the most suitable measurement system (measurement unit and fibre-optic sensing cables) for this project including a pre-test evaluating all determining conditions.
- Design of the layout (e.g. position) for the fibre-optic sensing cables to do as much research with the recorded data as possible and to be simultaneously simple and efficient enough to withstand the rough conditions on site.
- A quick and safe installation concept to cause as little inconvenience as possible for the contractor during the ongoing tunnelling.
- Evaluation of the measured data to draw conclusions about the strain distribution and history within the shotcrete lining.
- Considerations regarding the capabilities and limits for this kind of measurement system.
- Considerations regarding benefits and downsides over conventional used measurement techniques.
- Considerations regarding economical optimisations by means of lowering material cost and minimisation of the time loss due to the construction delay at the moment of installation.

With all this in mind, the planning, realisation and data analysis is done and described in this thesis. Comparisons to conventional measurement techniques are made and a final conclusion stating the overall performance as well as the advantages and disadvantages of the installed system is given at the end.

1.2 Motivation

The major part of the motivation behind this thesis results from the geotechnical engineering point of view. Very little is known about the real time strain and therefore stress distribution as well as history inside the outer tunnel lining. With conventional monitoring equipment, the strains within the shotcrete lining can only be back calculated using displacement data from monitoring targets. At best, strain gages can be installed at defined points along the circumference of the tunnel to locally record the strain development. Everything in between has to be interpolated with a natural degree of uncertainty.

The other essential part comes from pure intellectual interest to design and realise a project with this innovative measurement technique with all accompanying challenges. As fibre-optic measurements are still a new and upcoming technology within constructional and civil

engineering, only very few undertakings similar to this one have been realised by now in the tunnelling sector worldwide.

This project in particular is the very first project of this kind, that shows the installation of fibre-optic sensing cables for direct strain measurements during regular tunnelling work of a conventional drive at an ongoing construction project located in Austria.

The time factor is one of the big advantages of fibre-optic measurements. Usually readings of installed geodetic targets are done once a day – the fibre-optic measurement system records data up to every minute or even faster. In other words, hundreds of data sets are already accessible when the first follow-up reading is done for the targets the day after excavation/installation of a monitoring section.

With this data, inferences can be drawn regarding the loading situation of the tunnel lining throughout the stages of the conducted measurements. This has certainly always to be done in combination with other important knowledge like the geological situation, advance- sequence and rate, shotcrete properties, supplementary support measures and groundwater conditions. Furthermore, the degree of utilisation of the lining can be calculated which is often a basis for geotechnical judgements made on site every day by the engineers.

The application of this measurement system is yet far from being used in tunnelling on a regular basis, but this project shows the application capabilities (and the current limits) of such a system with a promising future ahead.

1.3 The Semmering Base Tunnel

The scheme to overcome the Semmering mountain pass with a railway has quite a long history. Carl von Ghega was the first to plan and build a railway across the pass connecting Mürzzuschlag in Styria and Gloggnitz in Lower Austria. The high altitude difference and the difficult terrain made the construction a very ambitious task. Nevertheless after only six years of construction time, the 41 km long track including 14 tunnels, 16 viaducts and over 100 bridges was opened for public transport in 1854. In the year 1998 the Semmering railway was declared an UNESCO World Heritage site.

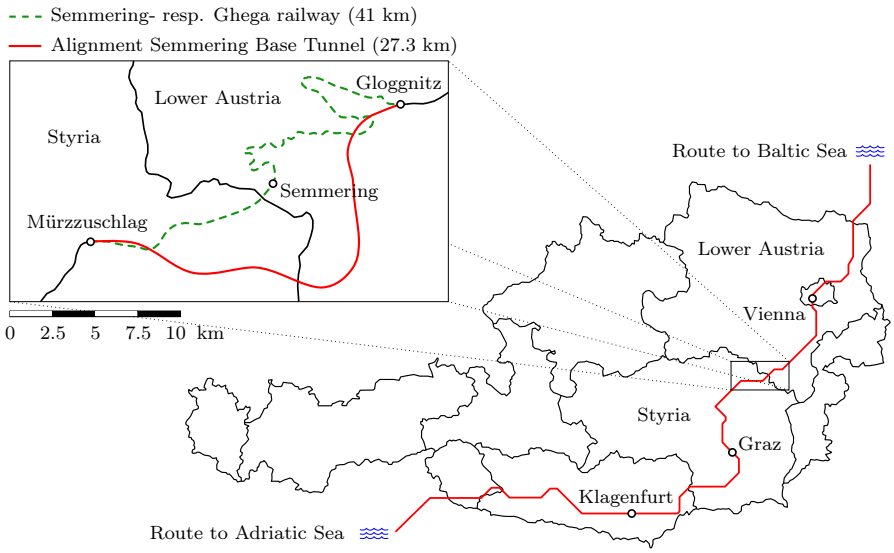

Figure 1.1: Alignment of the old Ghega railway in comparison with the new Semmering Base Tunnel between Styria and Lower Austria.

With a maximum gradient of 28 ‰ and a minimal curve radius of 190 m, the so called Ghega railway is a challenge for modern passenger traffic as well as for heavy goods trains. The demands concerning travel time, cargo weight and wagon size have increased over the years and despite several improvements of the track, the Semmering railway has reached its maximum capacity and the need for a new, more efficient solution was inevitable.

Therefore, the idea of a new tunnel through the Semmering was born to meet all the upcoming demands. The Semmering Base Tunnel (SBT) will be part of the high capacity north-south railway corridor, the so called Baltic-Adriatic Axis connecting Gdańsk (Poland) at the Baltic Sea with Bologna (Italy) near the Adriatic Sea.

The first design for the Semmering Base Tunnel was submitted to the committee in 1989. Political, environmental and other reasons postponed the construction for years. After several changes of the alignment and the agreement on the final design, the construction works for the Semmering Base Tunnel started in 2012. Figure 1.1 displays an overview of the alignment of the current Semmering railway and the new Semmering Base Tunnel.

When finished the twin-tubed railway tunnel will have a total length of 27.3 km with a maximum slope of 8.3 ‰. For safety reasons cross-passages will be constructed at least every 500 m. With a planned top speed of 230 km/h the travel time between the cities of Vienna and Graz will be reduced by 45 minutes (ÖBB-Infrastruktur, 2016).

1.4 Project Location

The implementation of the fibre-optic measurement system in the shotcrete lining is called *'main test'* in this thesis. It is conducted at the project section SBT 1.1, Tunnel Gloggnitz, track 1 of the Semmering Base Tunnel at the monitoring section *MS-1439*.

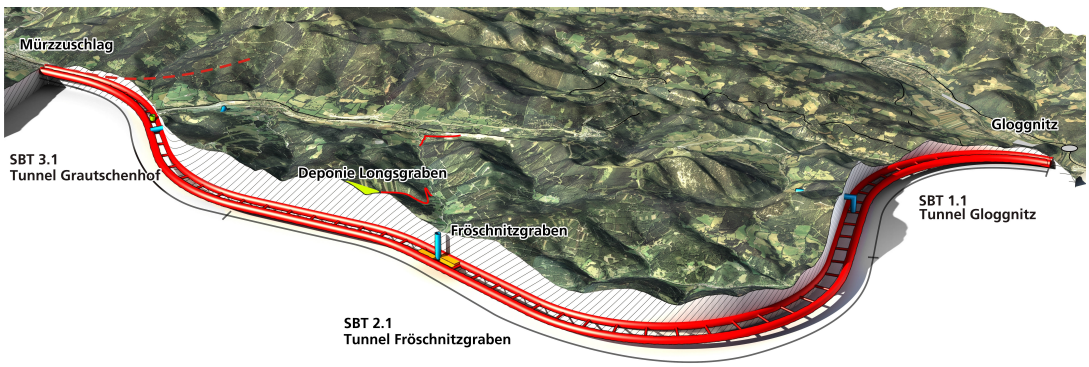

Figure 1.2: Individual project sections of the Semmering Base Tunnel (ÖBB-Infrastruktur, 2015).

Prior to that, the so-called *'pre-test'* to evaluate certain parameters for the main test is conducted at the access tunnel Göstritz which also belongs to the same contract (intermediate access for SBT 1.1). Figure 1.2 shows the alignment of the Semmering Base Tunnel with all project sections.

2 Geological Conditions

Located at the eastern boarder of the Eastern Alps, the Semmering Base Tunnel runs through a highly complex geologic-hydrologic mountain range. The whole area is a so-called tectonic window where old rocks (crystalline) of the Central Eastern Alps are located above younger ones. It is divided into two major tectonic units.

The first one is called the *Lower East Alpine Semmering Unit* consisting of fractured and faulted crystalline rock which are mainly composed of quartz-phyllites, phyllitic mica schists, gneisses and amphibolites. At the northern border the *Lower East Alpine Semmering Unit* contains cataclastic chlorite-phyllites overlain by Semmering-quartzites as well as carbonatic rocks (dolomite, marble, greywacke).

The second major geological unit is called *Upper East Alpine of the Greywacke Zone* and is located north of the Semmering Unit. From north to south this unit can be divided into the lower *Veitscher Nappe*, with its early Palaeozoic graphite phyllites, quartz conglomerate and weak metamorphic sandstones and the higher *Noric Nappe*, predominantly consisting of phyllites and schists.

The main test is located at monitoring section *MS-1439* of Tunnel Gloggnitz, track 1 at project section SBT 1.1. The average overburden at this section is 135 m. Geographically this area is situated in the *Noric Nappe* (including Silbersberg Series) of the Greywacke Zone, more specific in the core of the so-called *Eichberg* fault system. Figure 2.1 shows a sub-horizontal section with the location of the main test comprising main geological features.

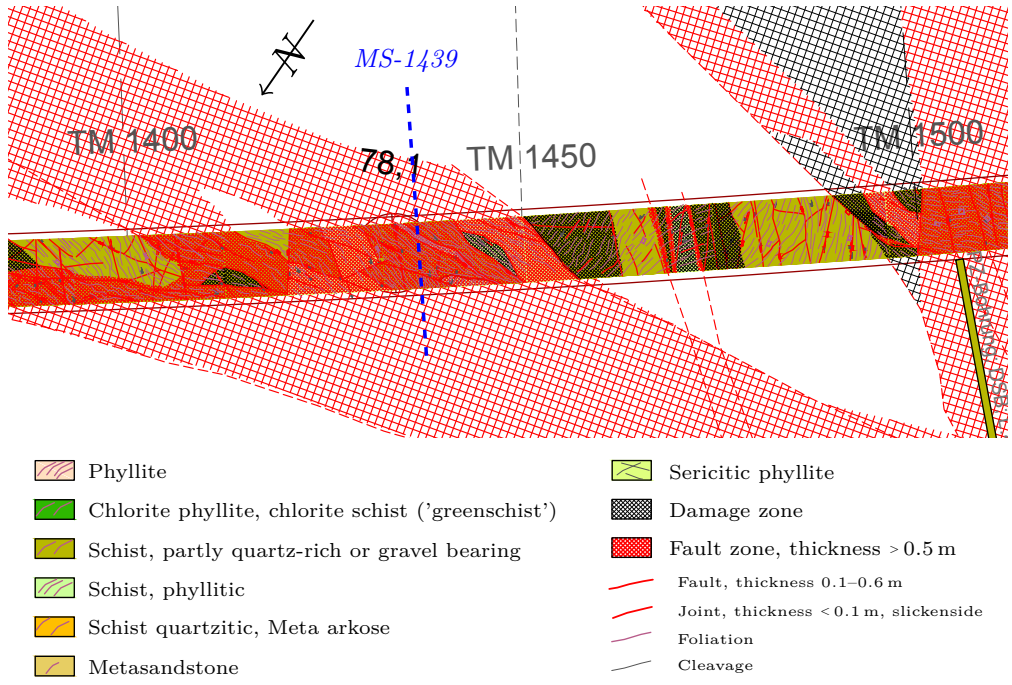

Figure 2.1: Sub-horizontal section of Tunnel Gloggnitz, track 1 at project section SBT 1.1 showing the geological features around *MS-1439*. Figure modified after ÖBB-Infrastruktur (2017a).

The rock mass in this zone predominantly comprises fault rocks, partly with high amount of sandy-silty to silty-clayey (in the core of the fault zone) cohesive cataclasites, which resulted from intensely shearing of schists and phyllites during tectonic events.

To a minor extent more competent quartzitic and carbonatic components with the size of a few centimetres are embedded in the cataclastic material. The rock mass is heavily fractured and moderately disintegrated with an uniaxial compressive strength of the fault rocks being less than 5 MPa.

The foliation, hardly observable due to the intense tectonic overprinting of the rock mass, primarily strikes almost parallel to the tunnel face, dipping steeply against the direction of the drive. In Figure 2.2 the orientations of different discontinuity types mapped at the face at *MS-1439* as well as three rounds before and after are displayed in stereonets.

Due to the unfavourable orientation of the discontinuities (slickensides and shear-bands) and the poor interlocking, locally small-scale rock falls and overbreaks (falling of small-scale blocks) occurred. Large-scale collapse did not appear on the account of the cohesive character of the fault rocks. Water inflow is limited to single trickling at bolts and drainage drillings.

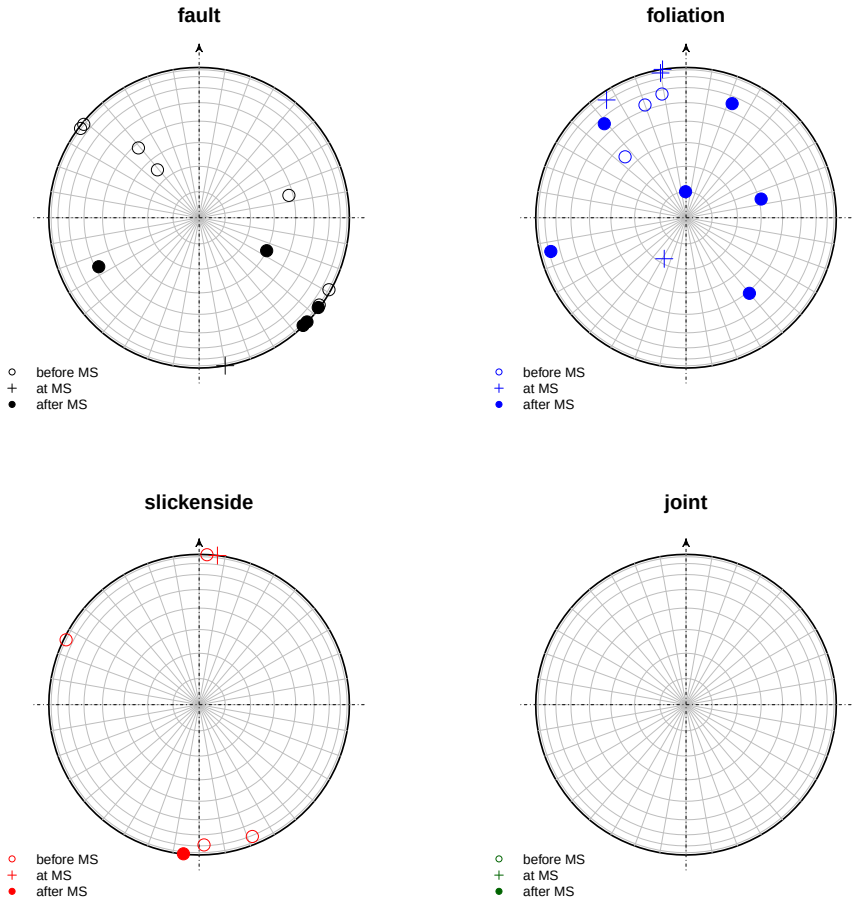

Figure 2.2: Orientations of mapped discontinuities before, after and at *MS-1439* (vertical axis = tunnel axis).

Figure 2.3 shows on the left-hand side sketches of the mapped tunnel face at chainage 1439.2 m where the fibre-optic measurement system is installed as well as one face before (chainage 1423.2 m) and after (chainage 1441.2 m) that. The right-hand side displays the corresponding photograph of the face. The rock types are as follows:

- At chainage 1423.2 m (Figure 2.3(a)) the recorded rock types for the specific areas are

schist - phyllitic (A), sericite schist – cataclasite (B) and schist – cataclasite (C and D).

- At chainage 1439.2 m (Figure 2.3(c)) the recorded rock types for the specific areas are schist – cataclasite (A and C) as well as cataclasite (B).
- At chainage 1441.2 m (Figure 2.3(e)) the recorded rock types for the specific areas are sericitic phyllite – cataclasite (A), schist – cataclasite (B and D) and cataclasite (C).

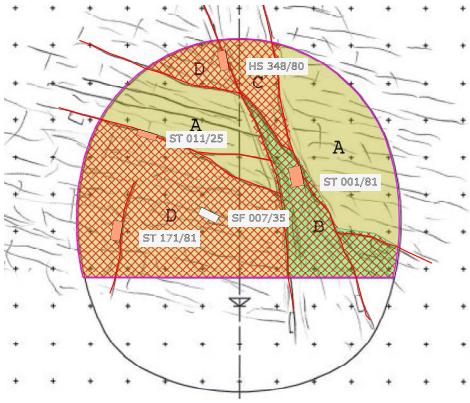

(a) Mapped face at chainage 1423.2 m

(b) Picture of face at chainage 1423.2 m.

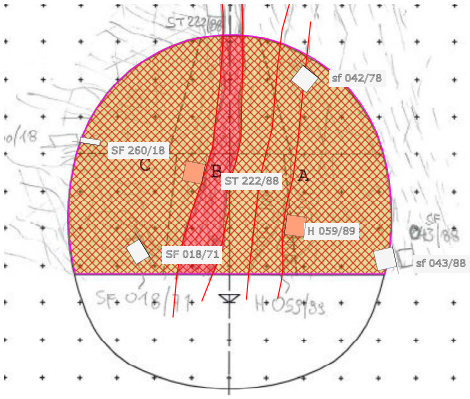

(c) Mapped face at chainage 1439.2 m.

(d) Picture of face at chainage 1439.2 m

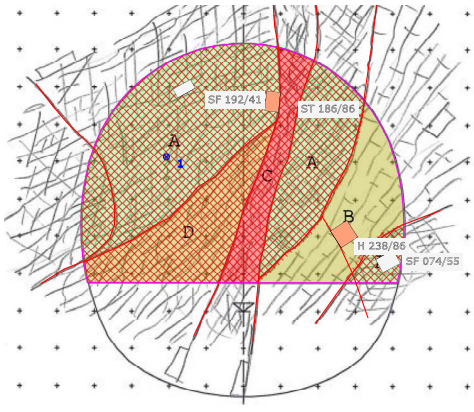

(e) Mapped face at chainage 1441.2 m.

(f) Picture of face at chainage 1441.2 m.

Figure 2.3: Geological mappings and pictures of tunnel faces at chainage 1423.2 m, chainage 1439.2 m and chainage 1441.2 m with: H/S . . . slickenside, SF . . . foliation and ST . . . fault. Figures and pictures taken from ÖBB-Infrastruktur (2017b).

3 Measurement System

As part of monitoring of structural properties of buildings and other objects in civil engineering, distributed fibre-optic measurement systems (DFOS) represent a significant extension to the existing and currently used sensing technology.

There are numerous advantages of such fibre-optic systems. As the entire fibre is the sensor, they provide a continuous, static or dynamic measurement with likewise very small size and low weight of the sensing cable itself. The cable management is relatively easy compared to conventional systems and it can be built-in or attached to almost any object. In addition, the system is insensitive to electromagnetic interference and can also operate under extreme temperature conditions. The sensor requires no external power supply (measurement with light) and can be hundreds of meters away from the actual measurement instrument (data logger).

This technology is used more frequently in geotechnics for monitoring purposes. For instance, Schuller et al. (2014) implemented a FOS in a reinforced earth structure as part of the slope stabilisation measures at the project section SBT 2.3 of the Semmering Base Tunnel (Moser et al., 2016). Further Monsberger et al. (2016) show another application of fibre-optic sensing, in this case deformation measurements for a ductile driven pile.

In the field of tunnelling de Battista et al. (2015) have successfully used distributed fibre-optic sensors for monitoring strains in a shotcrete lining during the excavation of cross-passages at the Crossrail project in London. To measure deformations within tunnel segments during the ring building process at continuous tunnelling, Gehwolf et al. (2016) developed a completely new test rig for the segments, which are also equipped with a fibre-optic instrumentation.

All conducted fibre-optic measurements for this project are carried out by the Institute of Engineering Geodesy and Measurement Systems (IGMS) from Graz University of Technology.

3.1 Optical Backscatter Reflectometer

For this project a distributed fibre-optical measurement system from Luna Innovations Inc. (USA) is used for all performed fibre-optic measuring work. This instrument operates on the basis of the so-called Rayleigh scattering and can capture strain and temperature changes at a very high accuracy of up to 1 µm/m and 0.1 °C with a spatial resolution within the centimetre range (Luna Innovations, 2014).

The basic working principal of such a distributed system is as follows: A short pulse of light is injected at one end of the optical fibre (Figure 3.1). As the light propagates through the fibre it is scattered on natural impurities of the glass (Rayleigh backscatter) or is reflected on the other end of the fibre. The Rayleigh scattering is one of the main reasons for the intensity loss of the original signal and is caused by variations of the refraction index of the glass core within the fibre.

The reflected light carries information about the local strain and temperature at a certain point in time. If the fibre is exposed to external influences during the measuring process like a change in strain or temperature, the relative frequency shifts (Δf) in the locally reflected

frequency spectrum. This change in frequency is directly proportional to the local change in strain or temperature.

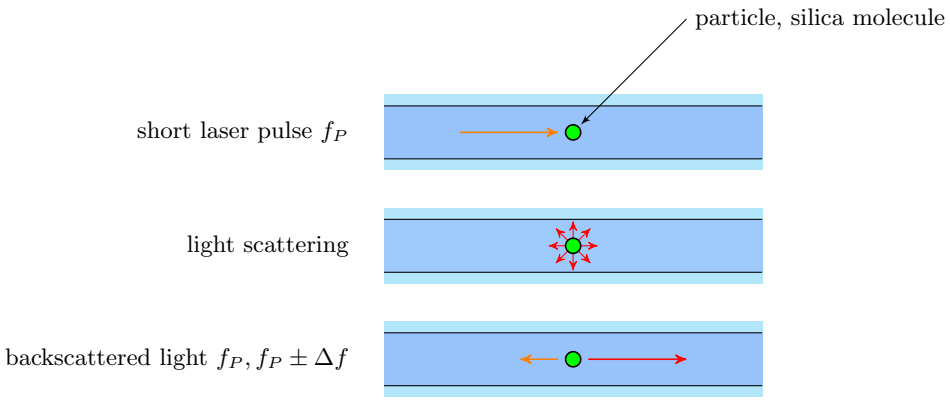

Figure 3.1: Schematic working principle of backscattering. Figure after Lienhart (2015).

As any external temperature not only affects, but also alters the measured strain arising from the external loading situation of the fibre-optic sensing cable, all measurements have to be carried out separately for strain and temperature respectively. The strain component due to mechanical loading can then be calculated by subtracting the pure strain resulting due to the mentioned temperature loading (called temperature compensation).

With this technique only relative changes in strain and temperature can be recorded. Therefore all measurements have to be referred to a zero measurement conducted at the beginning. To determine, for example, the absolute changes in temperature, the starting value has to be known and added as a static offset to all measurements.

3.2 Fibre-optic Sensing Cables

Due to the harsh environmental conditions inside a tunnel, the fibre-optic sensor must be protected to ensure the operative usage after the installation process and during the monitoring procedure. Also a proper compound between the fibre and its surrounding protective layers as well as a good bond between the cable itself and the concrete is necessary to get an undistorted transfer of the strain inside the concrete to the strain inside the fibre.

Therefore special armoured fibre-optic sensing cables of Brugg Cables (Switzerland) are used as they provide the necessary protection as well as accuracy. To meet the variable requirements of this project, a total of three different cable types are used. Their main technical specifications are described below.

The cable *BRUsens strain V3* (Figure 3.2 and Table 3.1) has an outer diameter of 7.2 mm and comprises a single optical fibre embedded in a metal tube which is hermetically sealed in a first protective plastic layer. The special steel armouring and a secondary polyamide outer sheath with a structured surface for maximum bonding properties makes this cable particularly durable.

The cable *BRUsens strain V9* (Figure 3.3 and Table 3.2) has an outer diameter of 3.2 mm and comprises a single optical fibre embedded in a metal tube which is hermetically sealed within a polyamide outer sheath. The structured surface guarantees maximum bonding properties.

Designed especially for temperature measurement, the cable *BRUsens temperature* 85 °C (Figure 3.4 and Table 3.3) has an outer diameter of 4.8 mm. The optical fibres are loosely

embedded in a protective steel tube to prevent any mechanical stress acting on them. This cables has a polyamide outer sheath with a smooth surface.

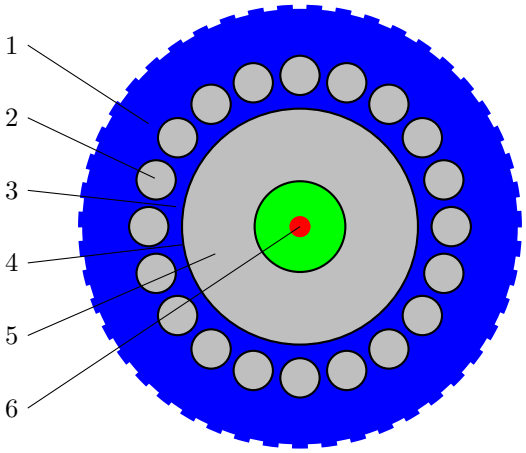

Figure 3.2: Schematic cross-section of *BRUsens strain V3* ∅ 7.2 mm (Brugg Kabel, 2012a) with: **1** Polyamid outer sheath, with structured surface, **2** Special grade galvanised steel armouring, **3** Plastic protection layer with interlocking system, **4** Metal tube SS316L for protection and hermetic seal, **5** Multi layer buffer and strain transfer layer with interlocking system, **6** Special strain optical single mode fibre.

Table 3.1: Technical data *BRUsens strain V3* (Brugg Kabel, 2012a).

Type	Max. no. of fibres [units]	Cable ∅ [mm]	Weight [kg/km]	Max. tensile strength installation [N]	Typical load at 1 % elongation [N]
1F	1	7.2	75	600	1600

Type	Min. bending radius with tensile [mm]	Min. bending radius without tensile [mm]	Max. crush resistance [N/cm]
1F	144 (20 × ∅)	108 (15 × ∅)	500

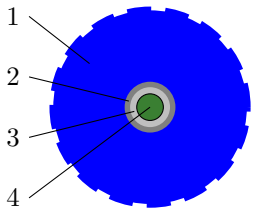

Figure 3.3: Schematic cross-section of *BRUsens strain V9* ∅ 3.2 mm (Brugg Kabel, 2012b) with: **1** Polyamid outer sheath, with structured surface with interlocking system, **2** Metal tube SS316L for protection and hermetic seal, **3** Multi layer buffer and strain transfer layer with interlocking system, **4** Special strain sensing optical single mode fibre.

Table 3.2: Technical data *BRUsens strain V9* (Brugg Kabel, 2012b).

Type	Max. no. of fibres [units]	Cable ⌀ [mm]	Weight [kg/km]	Max. tensile strength installation [N]	Typical load at 1 % elongation [N]
1F	1	3.2	10.5	260	470

Type	Min. bending radius with tensile [mm]	Min. bending radius without tensile [mm]	Max. crush resistance [N/cm]
1F	64 (20 × ⌀)	48 (15 × ⌀)	250

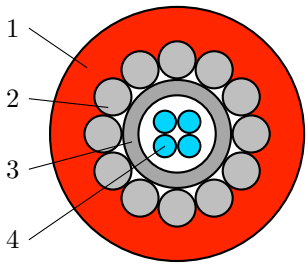

Figure 3.4: Schematic cross-section of *BRUsens temperature* 85 °C ⌀ 4.8 mm (Brugg Kabel, 2013) with: **1** Polyamid outer sheath, **2** Stainless steel wires, 316L, **3** Stainless steel loose tube, 316L **4** Bend insensitive optical fibres with dual layer acrylate coating for increased micro bending performance.

Table 3.3: Technical data *BRUsens temperature* 85 °C (Brugg Kabel, 2013).

Type	Max. no. of fibres [units]	Cable ⌀ [mm]	Weight [kg/km]	Max. crush resistance [N/cm]	Max. tensile strength installation [N]	Max. tensile strength operation [N]
4F	4	4.8	46	800	3000	2000

Type	Min. bending radius with tensile load [mm]	Min. bending radius without tensile load [mm]	Hydrostatic pressure resistance [bar]
4F	20 × ⌀	15 × ⌀	300

3.3 Evaluation of Alternative Measurement Systems

In a pre-study of this project the possible use of a measurement system based on the Electrical Time Domain Reflectometry (ETDR) was investigated. In geotechnics this technology is primarily used to detect potential shear bands along landslides or movements of unstable slopes and monitor their development over time.

The basic working principal is similar to the optical system described above but instead of a light pulse an electric pulse is used. Changes in the impedance of a co-axial cable are recorded to detect any disturbance (shear, kink or crack) along the cable. Generally, very

small movements cause not enough variations in the geometry of the cable to be detected by ETDR. Hence this system is particularly suitable for detecting movements along discrete paths of motion, e.g. shear surfaces (Singer et al., 2011).

With this technology very high accuracy can be achieved at crack detection as Lin et al. (2005) and Lin & Thaduri (2006) have shown under laboratory conditions. Concerning actual field tests an ETDR system was successfully installed by Singer et al. (2009) in the temporary invert of the Lainzer tunnel during regular tunnelling. Although no damage of the lining occurred during the measuring period (three weeks), this system proved its viability for crack detection in tunnel linings. A correlation between the impedance change in the cable and the actual value of occurring strain can only be found by associated laboratory tests comparing the amplitudes of the signals, which is not an easy task according to the authors.

This sensing technology is found not suitable for this project because the intention is to directly measure the strain conditions in the shotcrete lining. The knowledge to do this with a fibre-optic system has already been acquired on the part of IGMS by performing numerous laboratory tests within other projects (Woschitz et al., 2015; Monsberger et al., 2017).

An ETDR system could only be used as a tool for crack detection at highly stressed areas within the lining and work as a control device.

4 Pre-test

To gain required information for the main test, a pre-test is conducted beforehand. A plane, reinforced concrete slab, resembling a segment of lining, is built and equipped with different fibre-optic sensing cable configurations.

4.1 Purpose

The main goal of the pre-test is to answer substantial questions regarding the time consumption of the cable installation, cable handling, fixation methods of different cable types, the influence of hydratation heat during the hardening process of the concrete, the behaviour of the individual cables under the application of an external loading as well as the viability of the measured data. The results are then used to plan the main test.

In particular the answers to the following statements/questions should be found:

1. Time required to install the following on a predefined area:
   a) *Line A* (strain measurement) and *Line B* (temperature measurement) in circumferential direction (straight) on a layer of wire mesh.
   b) *Line A* (strain measurement) and *Line B* (temperature measurement) in longitudinal direction (loops) on a layer of wire mesh.
2. Can the selected fixing method ensure that the cables are not damaged (break) or displaced (change of position, rotation) during the application of shotcrete with maximum spraying performance?
3. Behaviour and handling of different cable types regarding bending radius and stiffness.
4. Is the bond between cable and concrete with the selected fixing method sufficient enough?
5. Is the deformation of the shotcrete slab due to an arbitrarily applied loading clearly visible in the measured data?
6. Can the measured data be correlated with exact positions (x, y) on the predefined area?
7. Is there an observable difference in the measured data due to different cable types?
8. How much do the measured temperatures differ during the hardening process between top and bottom layer and between circumferential and longitudinal direction respectively?
9. Can the change in strain as well as in stress due to hydratation heat clearly be differentiated from the change in strain as well as in stress due to the external loading?

4.2 Measurements Setup

The fibre-optic sensing cables are installed in two different configurations at the pre-test, one for strain measurement (*Line A*) and – parallel to it – one for temperature measurement (*Line B*). Both lines are installed in circumferential and longitudinal direction in respect to a fictional tunnel axis, for the bottom as well as for the top layer of wire mesh. Figure 4.1 shows a schematic sketch of the setup.

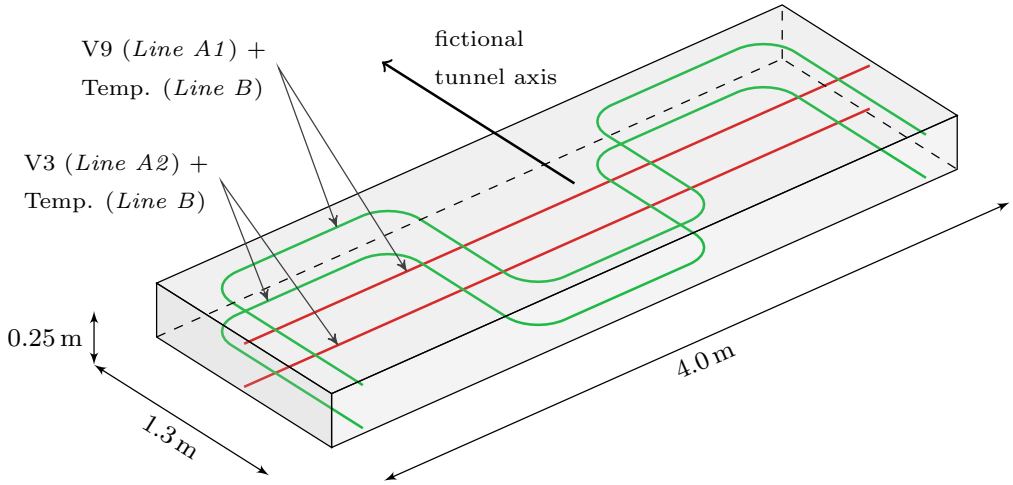

Figure 4.1: Schematic sketch of the cable setup at the pre-test with measurement in circumferential direction (**red**) and in longitudinal direction (**green**).

To find the most suitable fibre-optic sensing cable for the main test, different cable types are installed at the pre-test. Detailed descriptions to the used cables can be found in section 3.2. The robust cable *BRUsens strain V3* is installed at the bottom layer of the test slab to withstand the occurring tensile stresses during the loading test (*Line A2*). The cable *BRUsens strain V9* is installed at the top layer (*Line A1*).

To identify the influence of temperature on the measured strain data the special cable *BRUsens temperature* 85 °C is installed right next to the strain measurement cables in all directions and in both layers (*Line B*).

The measurements are carried out during the hardening phase (continuous) and during the loading test. As the test slab is built inside a tunnel, the OBR has to be protected for the duration of the continuous measurement. Therefore it is set up in a container right next to the test area. It is coupled via a 10 m supply cable with the fibre-optic cables in the concrete slab.

The supply cable itself is protected against negative mechanical influences (e.g. vibrations) inside a plastic tube which is situated alongside the left tunnel wall. An overview of the measurement setup on site can be seen in Figure 4.2.

(a) Alignment of supply cable.

(b) Connectors of supply cable.

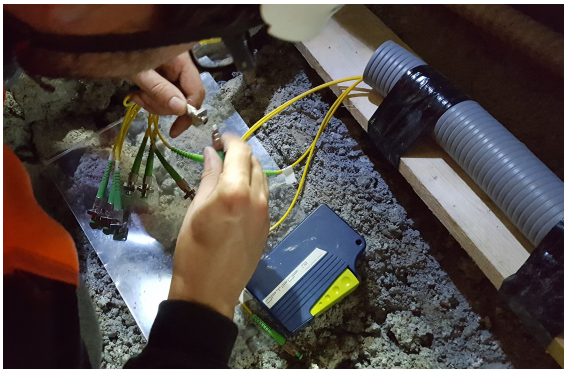

(c) Connection with supply cable.

(d) Measurement system inside the container.

Figure 4.2: Measurements setup at the pre-test.

4.3 Installation

The fabrication of the test slab containing the fibre optic measurement system is conducted on November 17th, 2016 at an already constructed part of the access tunnel Göstritz. The location of the pre-test is chosen so that no interference with the ongoing construction work is guaranteed. After the hardening phase the external loading test is conducted on the next day, November 18th, 2016.

Carrying out the pre-test inside a tunnel has several advantages. On the one hand the hardening process of the concrete can happen at a more or less constant air- temperature and humidity environment and on the other hand the test setup is not influenced by weather or other outer climate conditions. Also the same concrete used for the construction of the access tunnel is used for the test slab to provide optimal results concerning the comparability of the results.

Figure 4.3 displays various phases of the fabrication of the test slab around chainage 135 m of the access tunnel. The strain and temperature cables are fixed with cable ties alongside the wire mesh bars approximately every 20 cm. The installation of the bottom layer of fibre-optic cables consumes 20 minutes in circumferential direction and 25 minutes for the loops in longitudinal direction.

After mounting the cables a first measurement check is performed to guarantee that no cable was damaged during the installation process. After this check the first layer of shotcrete is applied under full spraying performance. Subsequently a second measurement check is done to ensure the complete functionality of the built-in measurement equipment.

The top layer of fibre-optic sensing cables is installed identically as the bottom one. The shotcrete is not applied with full performance for the top layer to prevent damage of the already finished first layer. Before and after the spraying procedure a measurement check is conducted to validate the correct performance of the system and to check for any potential failure of cables. With this, the fabrication of the test slab is finished and the continuous measurement during the hardening process over night is started.

(a) Formwork for test slab.

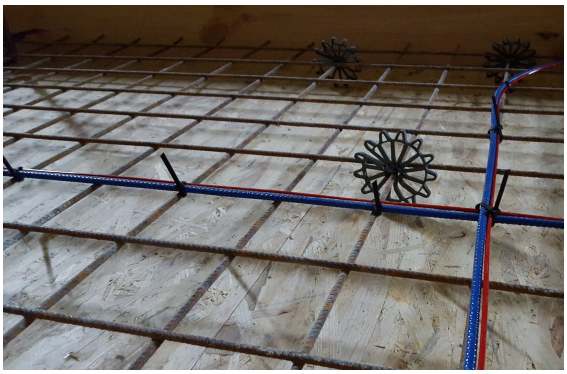

(b) Installed bottom layer of fibre-optic cables.

(c) Spraying of bottom layer shotcrete.

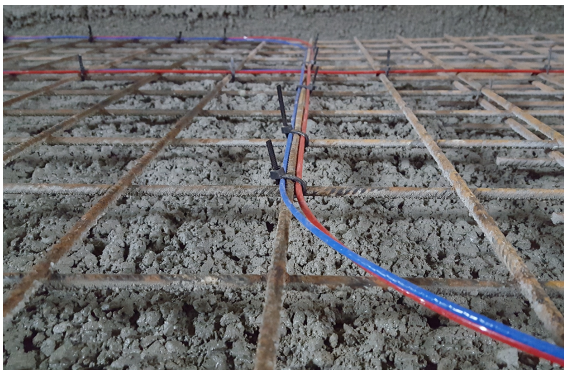

(d) Installed top layer of fibre-optic cables.

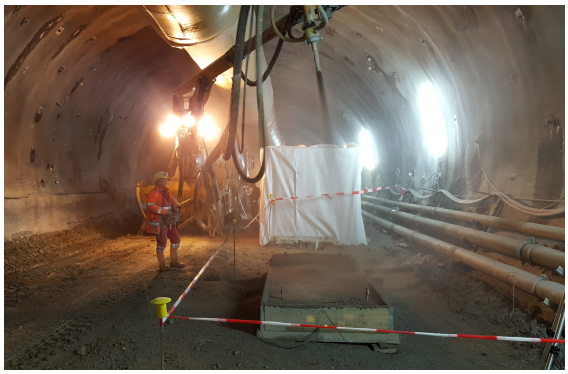

(e) Spraying of top layer shotcrete.

(f) Finished test slab with transport hooks.

Figure 4.3: Fabrication of the test slab in the access tunnel Göstritz.

4.4 Loading Test

The hardened test slab is transported by a wheel loader to the site installation area of the access tunnel for the subsequent loading test (Figure 4.5). There it is set upon two steel

beams and is equipped with three prism targets to geodetically record the deflection during the test. Figure 4.4 shows a schematic sketch of the loading test setup.

An excavator is used to apply a downwards force in the middle of the test slab to determine the reaction of the fibre-optic measurement system to an external loading. For a better load distribution a steel plate is used in between the excavator shovel and the slab.

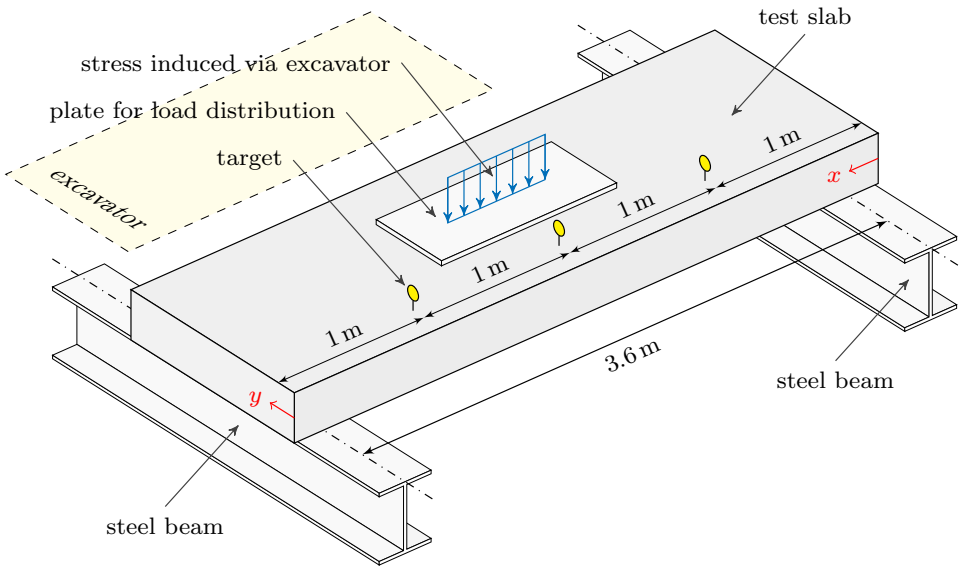

Figure 4.4: Schematic sketch of the loading test setup of the pre-test.

In this test the effective load applied by the excavator is not recorded. Hence no direct correlation of the resulting stress and the strains recorded by the fibre-optic measurement system can be made. The purpose of this loading test is solely to qualitatively evaluate the recorded data of the fibre-optic sensing cables and to identify possible problems.

Different phases are performed regarding the magnitude of the applied load. As mentioned above, the exact load is not recorded, but the attempt is made to keep the load more or less constant during the approximately one minute-long measurement period for each loading phase. Simultaneously the prism targets are measured with a total station.

After the first loading phase the slab is completely unloaded and measured again. After that, the force is steadily increased – the different magnitudes are later derived from the fibre-optic measurements – in several steps (see Table 4.1) until the maximum bearing capacity of the slab is reached and failure occurs.

Table 4.1: Loading regime at the pre-test (magnitude derived from FOS measurements).

Loading phase	Magnitude
1. Loading (first loading)	–
2. Loading (without load)	0
3. Loading	$< 1.$
4. Loading	$< 1.$ and $> 3.$
5. Loading	$< 1.$ and $> 4.$
6. Loading (last before failure)	$> 1.$

(a) Steel plate for load distribution.

(b) First loading phase.

(c) Failure of the test slab.

(d) Exposed failure zone.

(e) Severed fibre-optic cables due to failure.

(f) Exposure of fibre-optic cables after the test.

Figure 4.5: Loading test conducted at the site installation area Göstritz.

All implemented fibre-optic sensing cables are severed (see Figure 4.5(e)) at the point of failure of the test slab. Therefore no further measurements are possible afterwards beyond the breakpoint of the respective cable.

The area in immediate proximity to the failure zone is exposed by hand with hammer and chisel to examine and compare the actual position of the fibre-optic sensing cables within the concrete to their planned position. Also the bond between cable and concrete is investigated to ensure the full compound without any slippage. Note that the strain cable (blue) in Figure 4.5(f) was cut in the process of exposing it, not due to the external loading of the test.

4.5 Results

As mentioned in section 3.1 only relative changes are measured with the installed system. The measured value is always a change of strain and/or temperature with respect to (w.r.t.) a prior carried out reference measurement (= zero measurement) where a positive value indicates tension and a negative value compression along the fibre-optic cable. The reference measurement is conducted separately for both, the continuous measurements and the measurements during the loading test right before the start of the respective tests.

When analysing the following results, note that if blanks are present in the data, either the respective fibre-optic cable is not measured yet, or the data contains serious outliers (e.g. heavy vibrations of the cable during the spraying of shotcrete) and is therefore eliminated from the series.

4.5.1 Continuous Measurement

At the continuous measurement all installed fibre-optic sensing cables are measured autonomously at an interval of two minutes directly after the installation of the test slab. The measurement duration over night is about 10.5 h.

In the following graphs the behaviour during the hardening phase of the concrete is shown for a total of seven points. The points P1 to P4 (Figure 4.6 to Figure 4.13) are located at the intersections of the two directions – circumferential and longitudinal – for the top and bottom layer of fibre-optic sensing cables. The points P5 to P7 (Figure 4.14 to Figure 4.19) are located in between to identify differences in strains of two parallel installed lines.

In each graph certain points of the recorded evolution of strain and temperature are highlighted. Point A represents the measurement check after installation of the bottom layer of fibre-optic sensing cables. This measurement is continued until the first layer of shotcrete is applied (Point B). The temperature change induced by the application of shotcrete can be seen between these two points. Point C is the measurement check after the installation of the top layer of fibre-optic sensing cables which is again continued until the application of the second layer of shotcrete (Point D). After that the continuous measurement is started.

After applying the bottom layer the temperature of the shotcrete slightly decreases until the application of the top layer of shotcrete. It can be seen that the changes in temperature are lower at the points located close to the free surface of the test slab compared to the ones in the centre. The maximum temperature difference until the end of the test is about 5 °C at the central points in the bottom layer. The points located closer to the edges of the test slab show this behaviour only to a minor extent.

This effect is due to the faster cooling of the concrete body at points close to its surface. The top layer shows no significant temperature increases due to the exposed surface area on top. Some points even show a decrease in temperature.

The changes in strain are comparatively small during the hardening phase and lie in the range of ±0.1 mm/m for all points. Since the test slab is only constrained by the formwork this seems reasonable. At some points a slight increase of strain can be detected which most likely arises from internal restraints e.g. a very tight cable tie at this position.

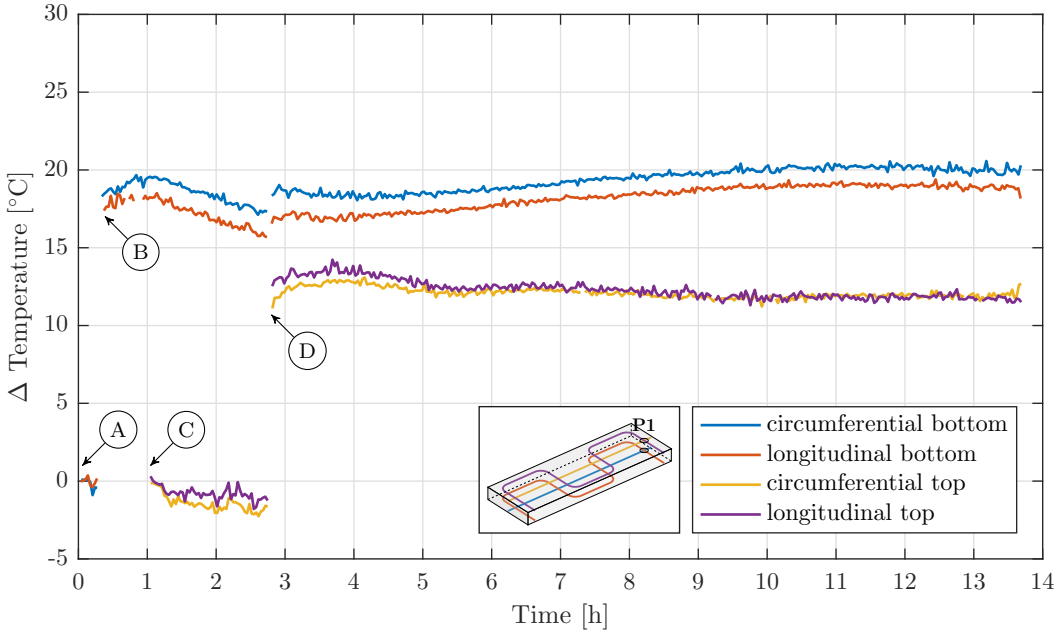

Figure 4.6: Change in temperature of point P1 w.r.t. zero measurement with: **A** measurement check after installation of bottom layer cables; **B** measurement check after applying bottom layer of shotcrete; **C** measurement check after installation of top layer cables; **D** measurement check after applying top layer of shotcrete and start of continuous measurement.

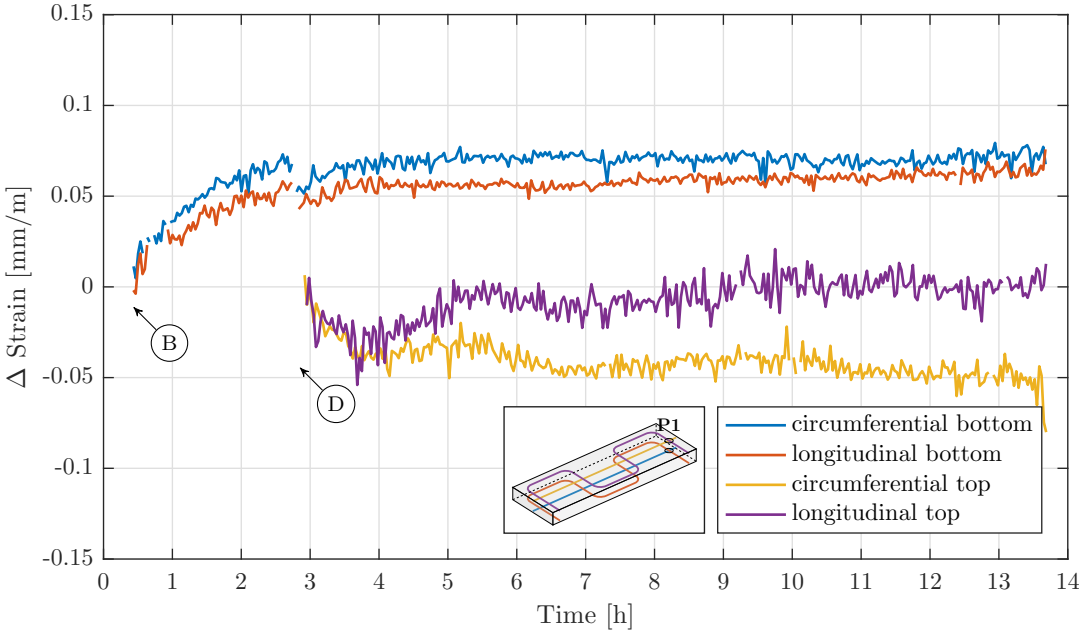

Figure 4.7: Change in strain of point P1 w.r.t. zero measurement with: **B** measurement check after applying bottom layer of shotcrete; **D** measurement check after applying top layer of shotcrete and start of continuous measurement.

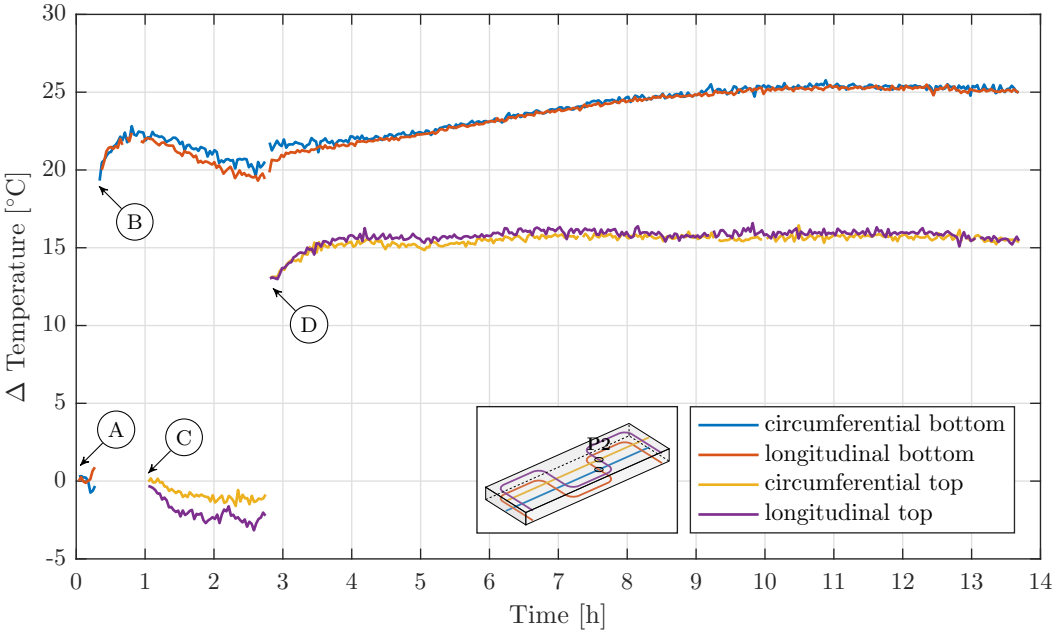

Figure 4.8: Change in temperature of point P2 w.r.t. zero measurement with: **A** measurement check after installation of bottom layer cable; **B** measurement check after applying bottom layer of shotcrete; **C** measurement check after installation of top layer cable; **D** measurement check after applying top layer of shotcrete and start of continuous measurement.

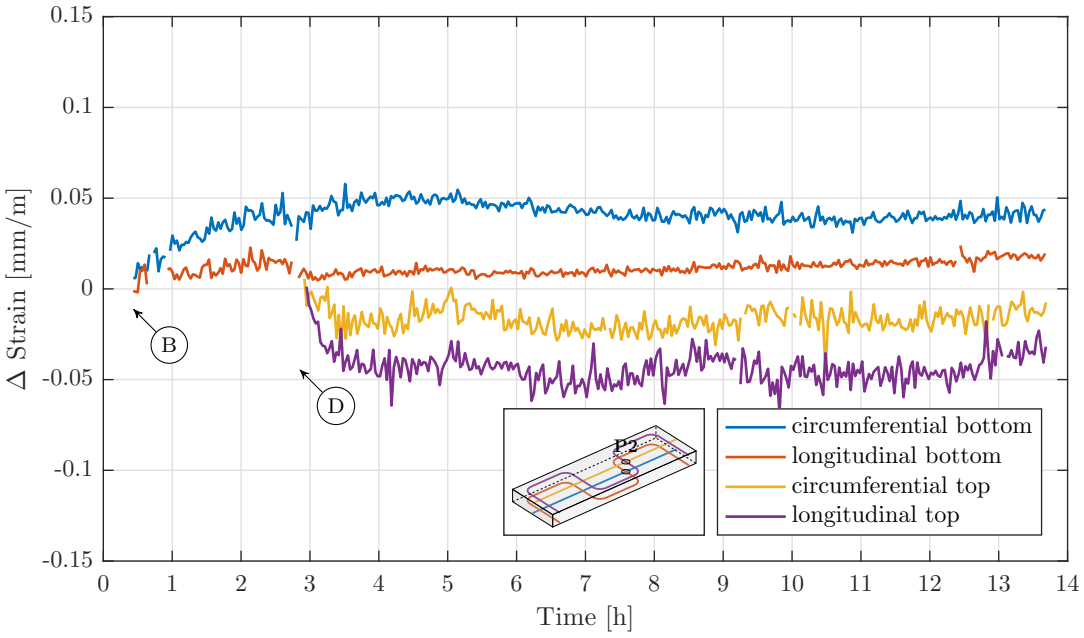

Figure 4.9: Change in strain of point P2 w.r.t. zero measurement with: **B** measurement check after applying bottom layer of shotcrete; **D** measurement check after applying top layer of shotcrete and start of continuous measurement.

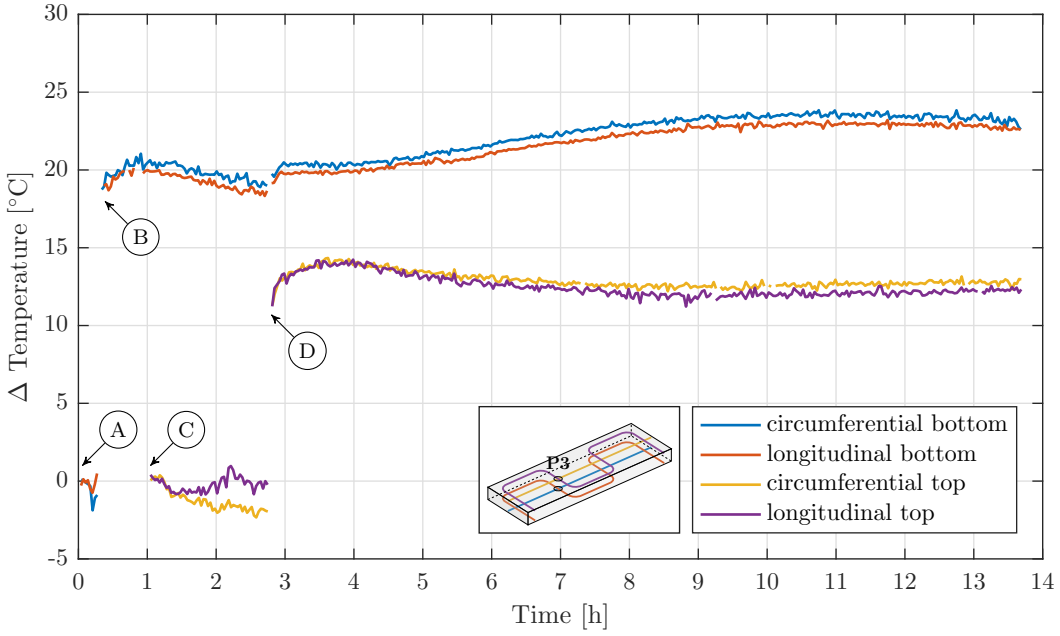

Figure 4.10: Change in temperature of point P3 w.r.t. zero measurement with: **A** measurement check after installation of bottom layer cable; **B** measurement check after applying bottom layer of shotcrete; **C** measurement check after installation of top layer cable; **D** measurement check after applying top layer of shotcrete and start of continuous measurement.

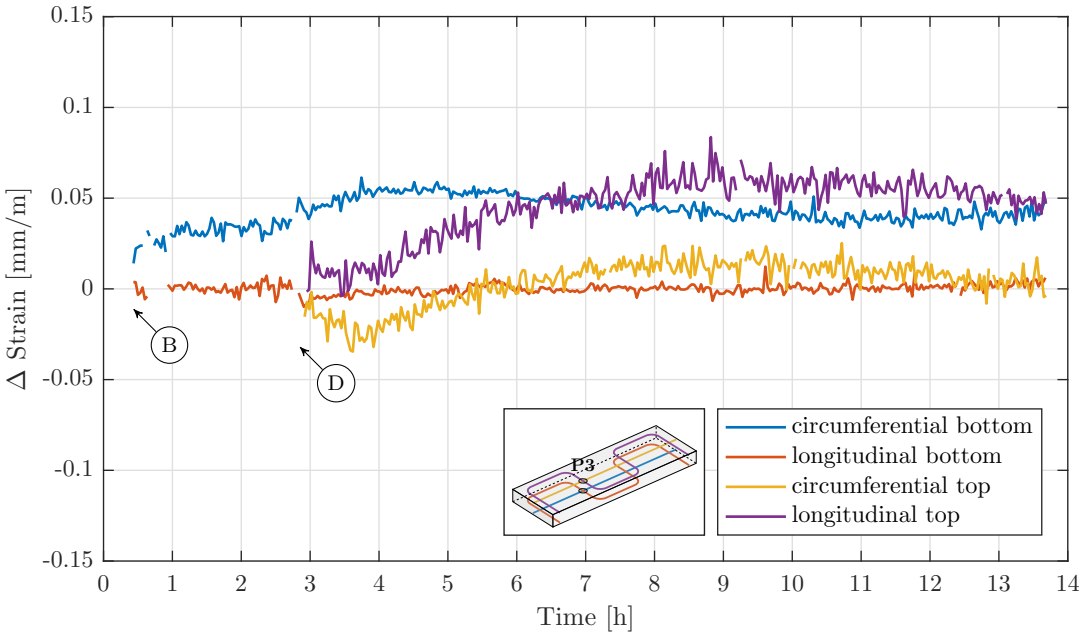

Figure 4.11: Change in strain of point P3 w.r.t. zero measurement with: **B** measurement check after applying bottom layer of shotcrete; **D** measurement check after applying top layer of shotcrete and start of continuous measurement.

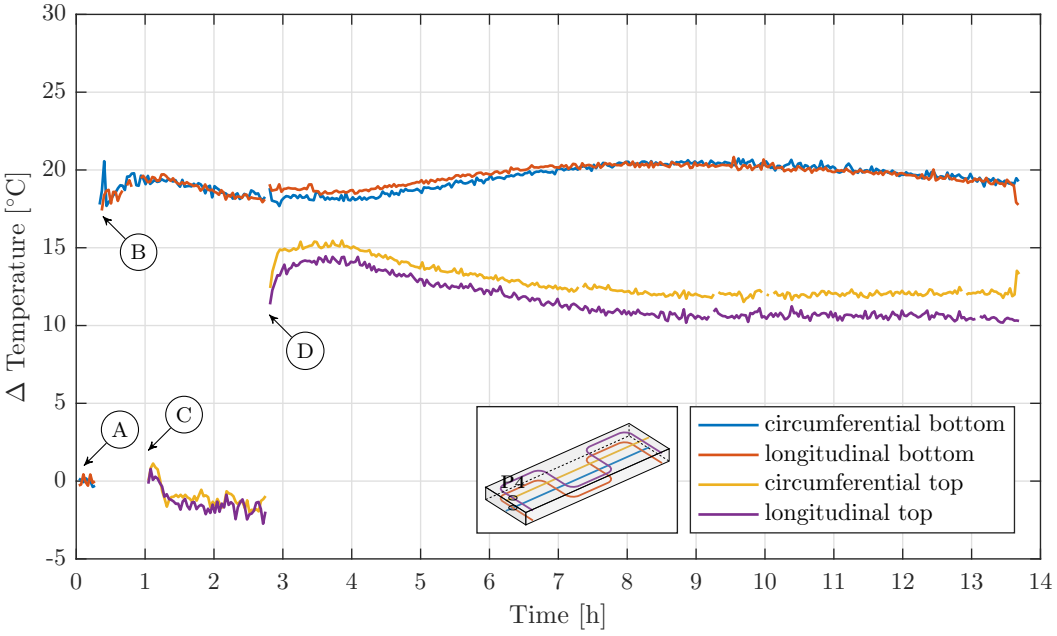

Figure 4.12: Change in temperature of point P4 w.r.t. zero measurement with: **A** measurement check after installation of bottom layer cable; **B** measurement check after applying bottom layer of shotcrete; **C** measurement check after installation of top layer cable; **D** measurement check after applying top layer of shotcrete and start of continuous measurement.

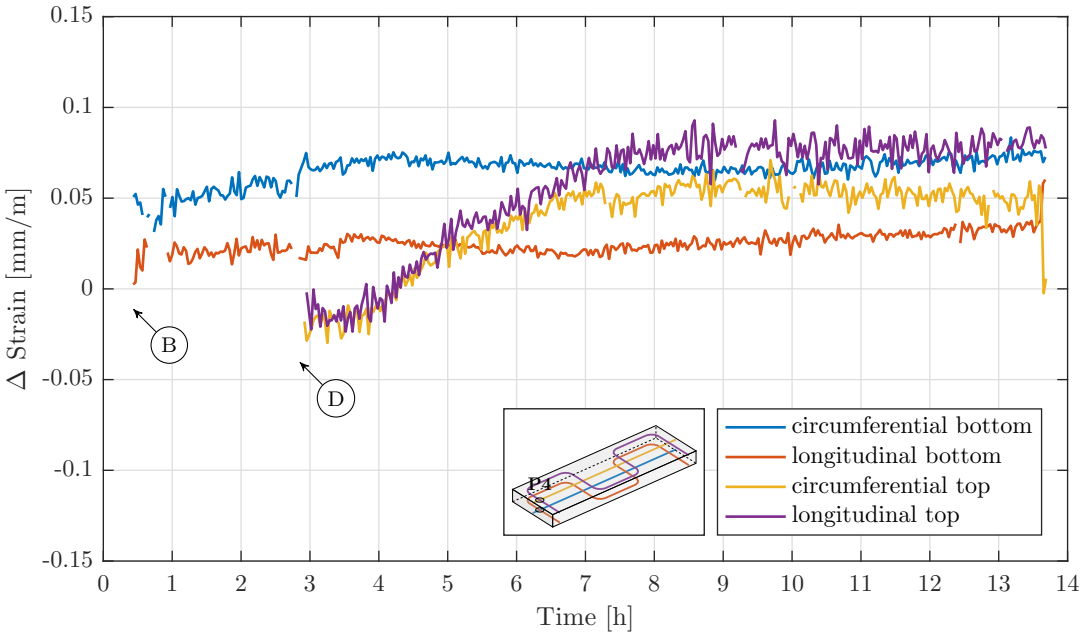

Figure 4.13: Change on strain of point P4 w.r.t. zero measurement with: **B** measurement check after applying bottom layer of shotcrete; **D** measurement check after applying top layer of shotcrete and start of continuous measurement.

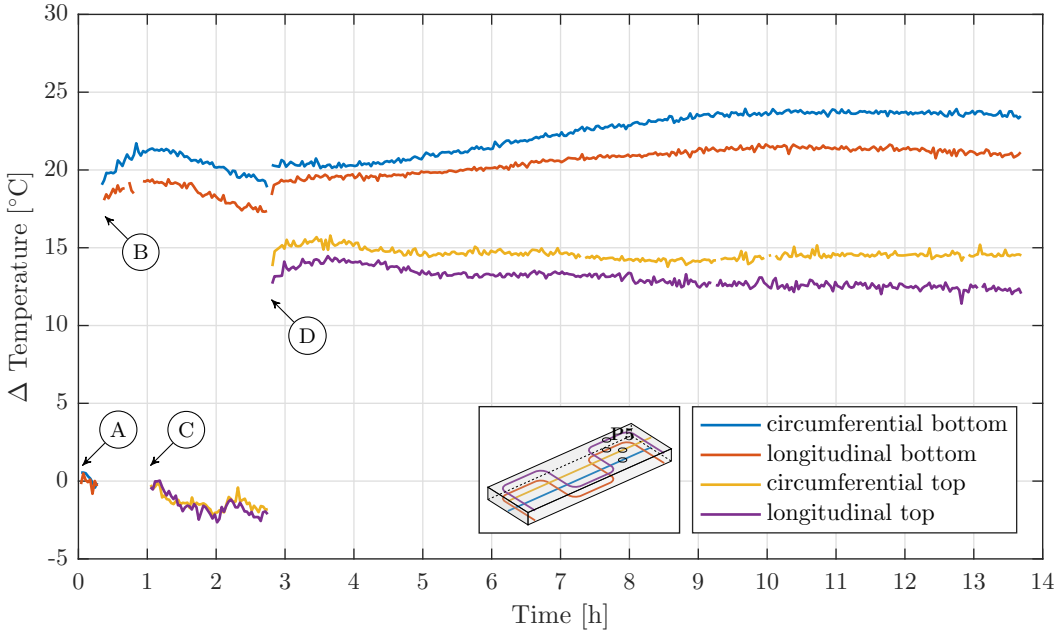

Figure 4.14: Change in temperature of point P5 w.r.t. zero measurement with: **A** measurement check after installation of bottom layer cables; **B** measurement check after applying bottom layer of shotcrete; **C** measurement check after installation of top layer cables; **D** measurement check after applying top layer of shotcrete and start of continuous measurement.

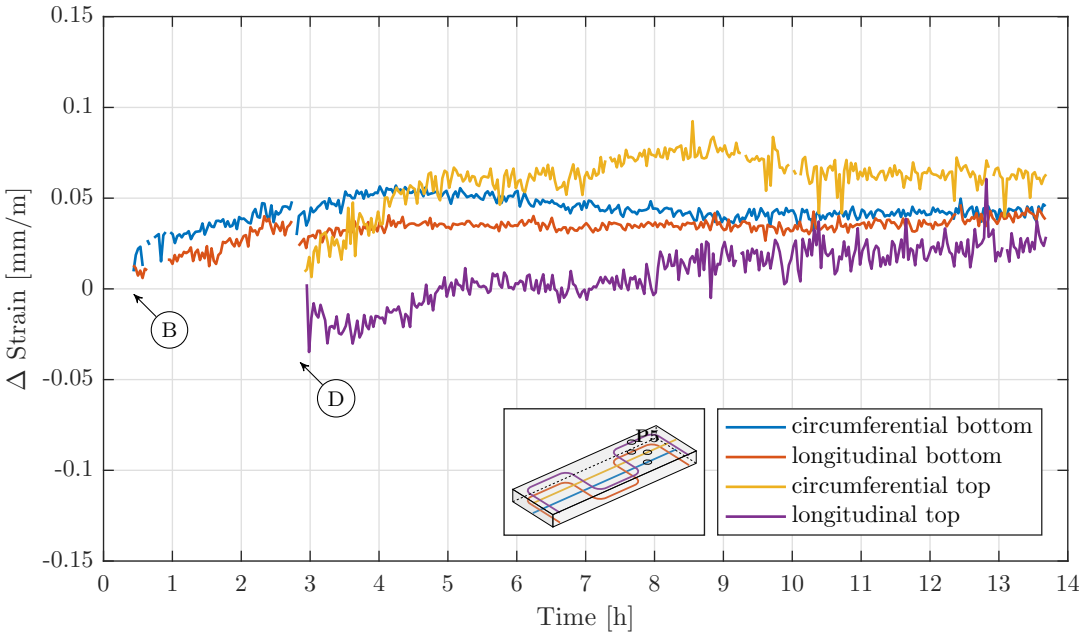

Figure 4.15: Change in strain of point P5 w.r.t. zero measurement with: **B** measurement check after applying bottom layer of shotcrete; **D** measurement check after applying top layer of shotcrete and start of continuous measurement.

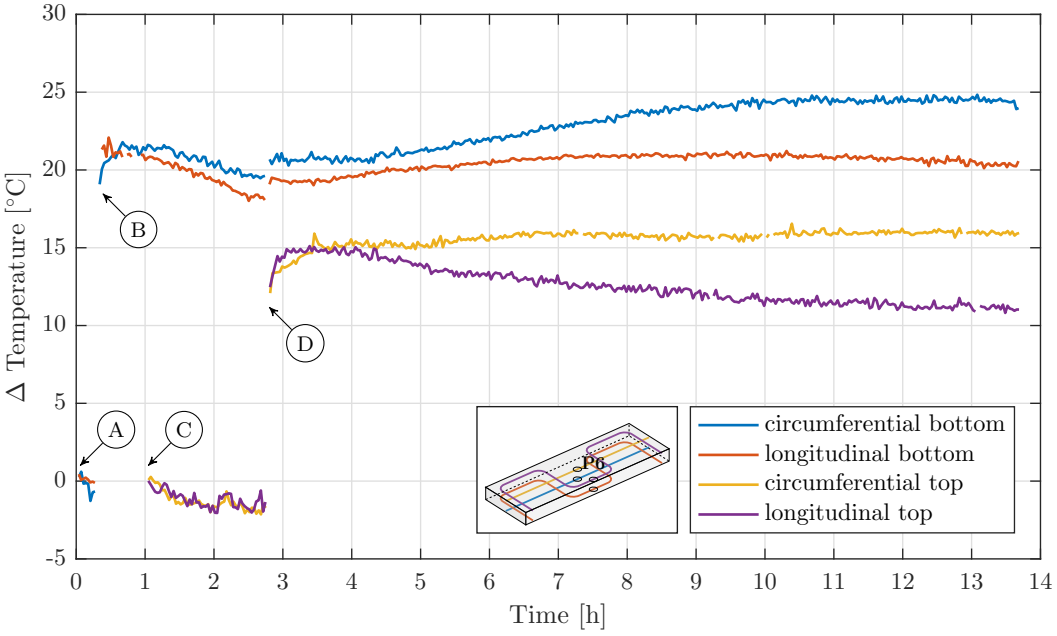

Figure 4.16: Change in temperature of point P6 w.r.t. zero measurement with: **A** measurement check after installation of bottom layer cable; **B** measurement check after applying bottom layer of shotcrete; **C** measurement check after installation of top layer cable; **D** measurement check after applying top layer of shotcrete and start of continuous measurement.

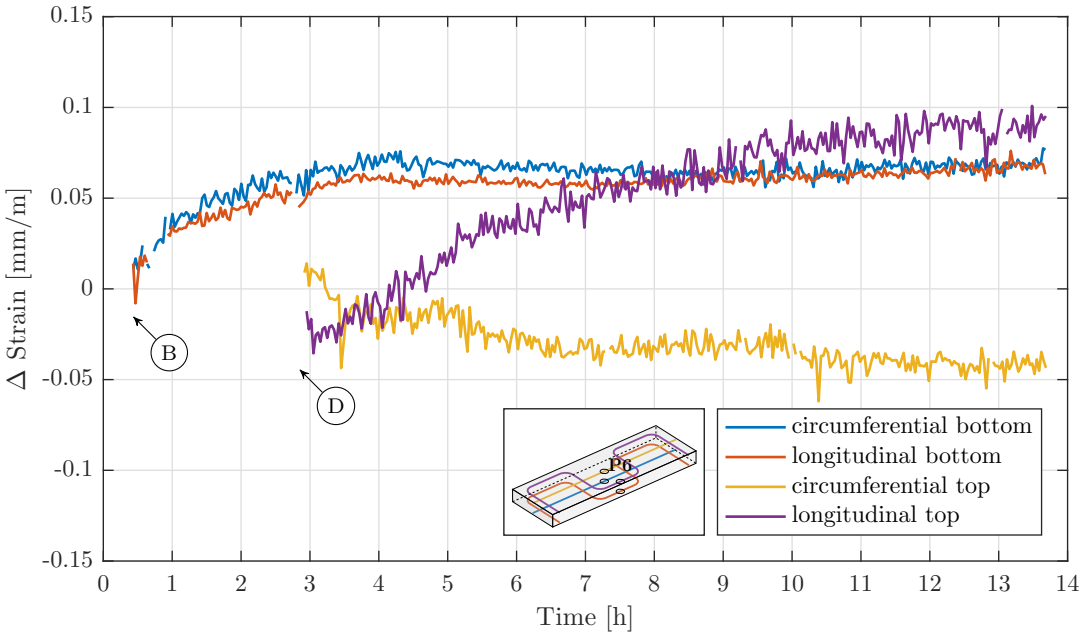

Figure 4.17: Change in strain of point P6 w.r.t. zero measurement with: **B** measurement check after applying bottom layer of shotcrete; **D** measurement check after applying top layer of shotcrete and start of continuous measurement.

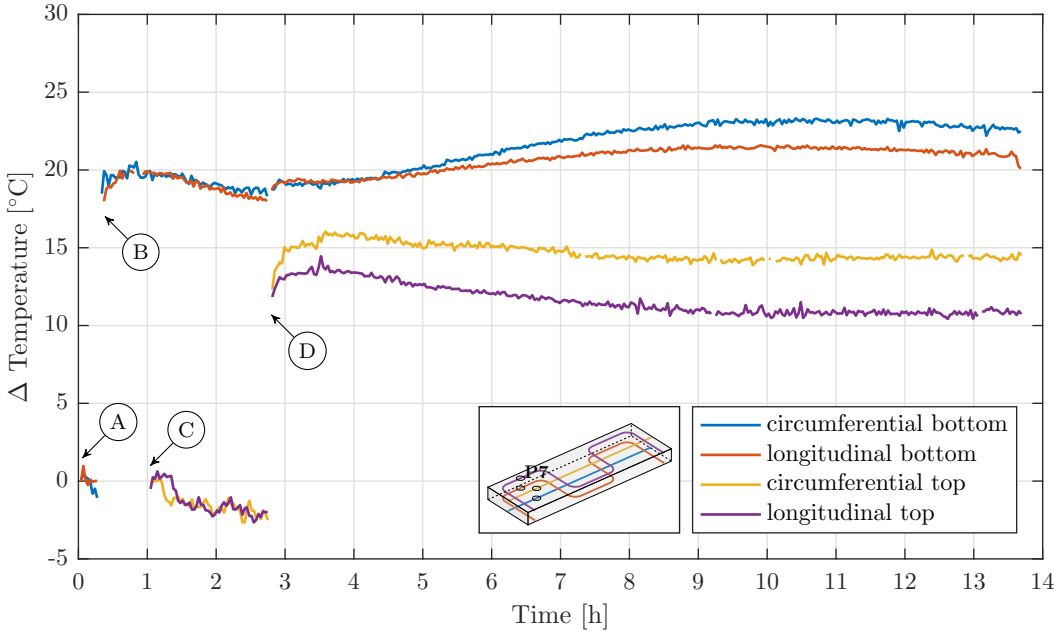

Figure 4.18: Change in temperature of point P7 w.r.t. zero measurement with: **A** measurement check after installation of bottom layer cable; **B** measurement check after applying bottom layer of shotcrete; **C** measurement check after installation of top layer cable; **D** measurement check after applying top layer of shotcrete and start of continuous measurement.

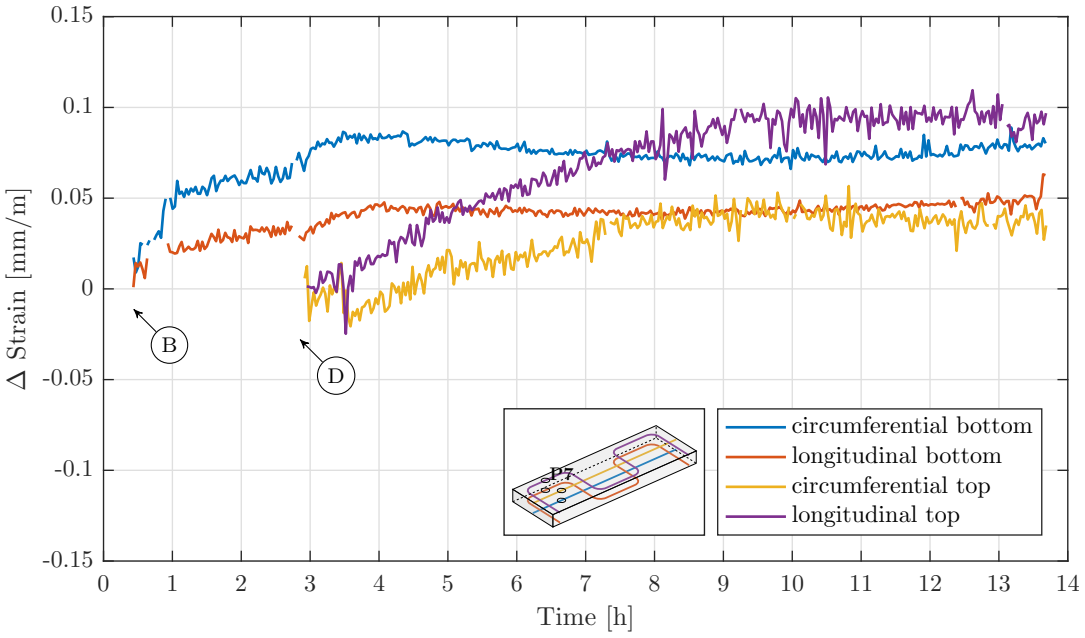

Figure 4.19: Change in strain of point P7 w.r.t. zero measurement with: **B** measurement check after applying bottom layer of shotcrete; **D** measurement check after applying top layer of shotcrete and start of continuous measurement.

4.5.2 Loading Test

For the loading test a total of six loading phases (see Table 4.1) are carried out. In each phase the load is increased. The second phase represents a complete unloading, hence no external load is acting on the test slab.

After the test, the fibre-optic sensing cables are cut right at the surface of the test slab to determine the exact starting point of the cables inside the concrete. These points are offset to all sides by 15 cm because the planned alignment along the wire mesh cannot be guaranteed in the edge areas and therefore the results would not be representative.

To remove peaks in the data and to smoothen the signal, a moving average filter with a window length of 50 mm is applied to all data sets of the recorded strain and temperature changes. The spatial resolution for this test is set to 5 mm. Due to this high density of measurement points only every second value is plotted.

4.5.2.1 Strain Measurement

The following figures show the first, the second and the last loading phase of the pre-test. The intermediate phases are of minor significance, since the results vary only very little and are therefore not displayed.

The graphs show the data of the cables used for strain measurement at the individual loading phases, the axis of the steel beams and the plate used for the load distribution. The zero points of the axis correlate with those in the sketch in Figure 4.4. A positive value represents an elongation, a negative value a compression of the fibre-optic cable.

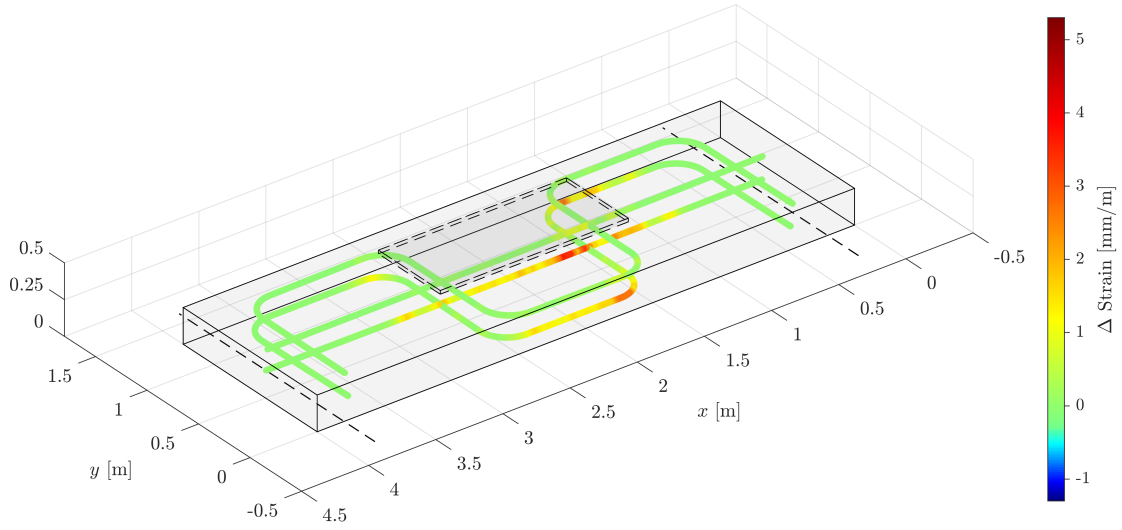

Figure 4.20: Change in strain w.r.t. reference measurement at 1. loading phase.

At the first loading phase (Figure 4.20) a distinct extension of the fibre-optic sensing cables in the bottom layer can be identified. With the given setup this behaviour is expected. The highest values are measured at the bottom, circumferential direction with a maximum absolute value of 3.49 mm/m in change of strain at $x = 1.62$ m. The top layer shows no significant changes in strain compared to the bottom layer.

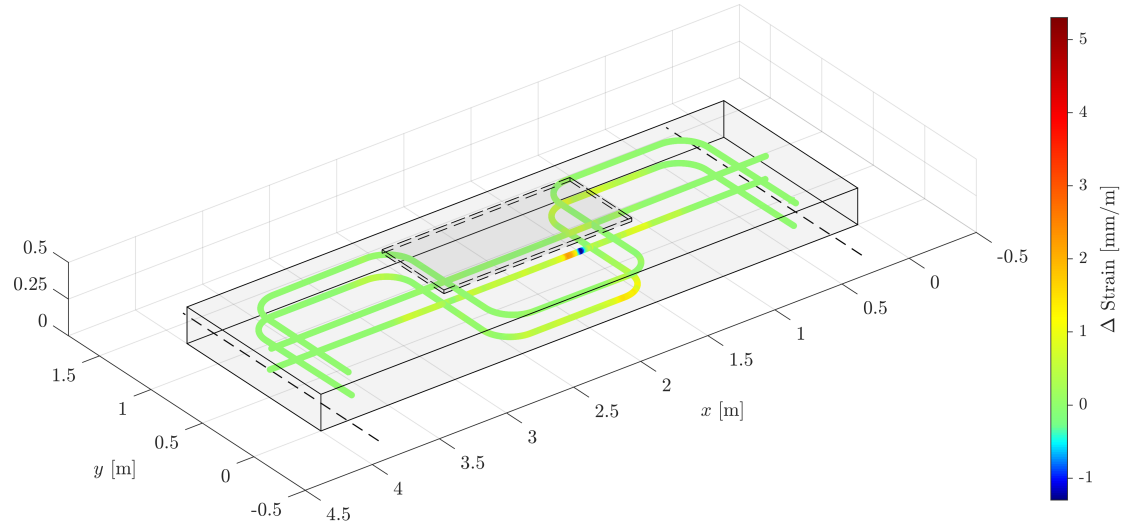

Figure 4.21: Change in strain w.r.t. reference measurement at 2. loading phase.

In the second loading phase (Figure 4.21) no external loads act on the slab. In contrast to the first loading phase, the test slab seems to have experienced plastic deformations (cracks emerging in the slab) since the loading conditions should be the same as at the time of the reference measurement, yet the measurements indicate a change in strain.

The highest values are measured at the bottom, circumferential direction with a maximum value of 2.07 mm/m of change in strain at $x = 1.63\,\text{m}$ and $-1.17\,\text{mm/m}$ at $x = 1.54\,\text{m}$. The top layer shows no significant changes in strain compared to the bottom layer.

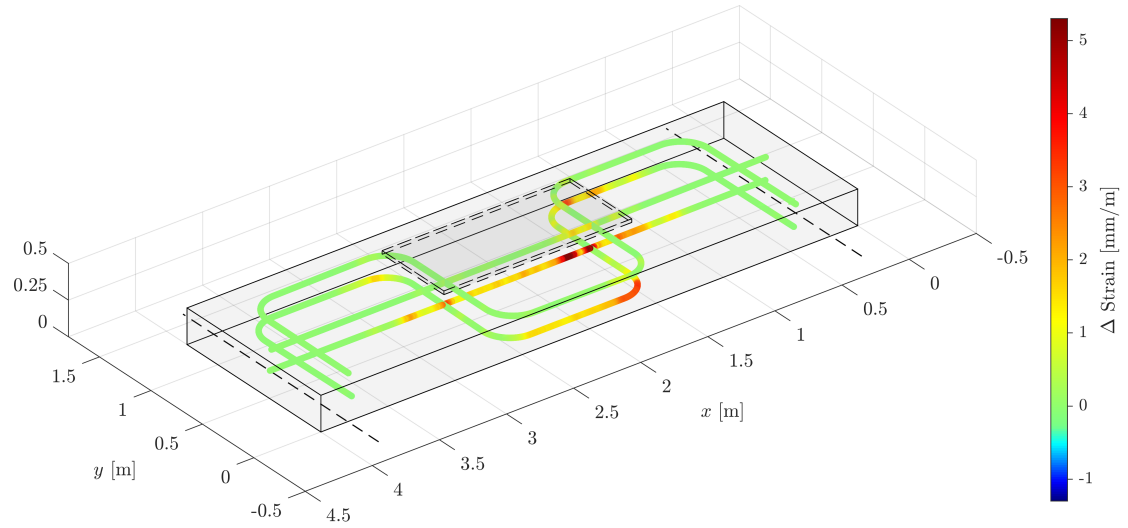

Figure 4.22: Change in strain w.r.t. reference measurement at 6. loading phase.

The sixth and final loading phase before failure shows an extension of the fibre-optic sensing cables at the bottom layer. The highest values are measured at the bottom, circumferential direction with a maximum absolute value of 5.21 mm/m of change in strain at $x = 1.63\,\text{m}$. The top layer shows no significant changes in strain compared to the bottom layer.

At all loading phases a slight, yet abrupt drop in strain (depicted slightly brighter than its surrounding) can be detected in the range of about $x = 1.4\,\mathrm{m}$ to $x = 1.6\,\mathrm{m}$ at the bottom cable in circumferential direction.

Figure 4.23 displays a detailed view of the zone with the highest absolute values of strain changes at the last loading phase where this effect is most prominent. To further illustrate this drop the graph in Figure 4.24 shows the changes in strain of the fibre-optic sensing cables in circumferential direction for the final loading phase.

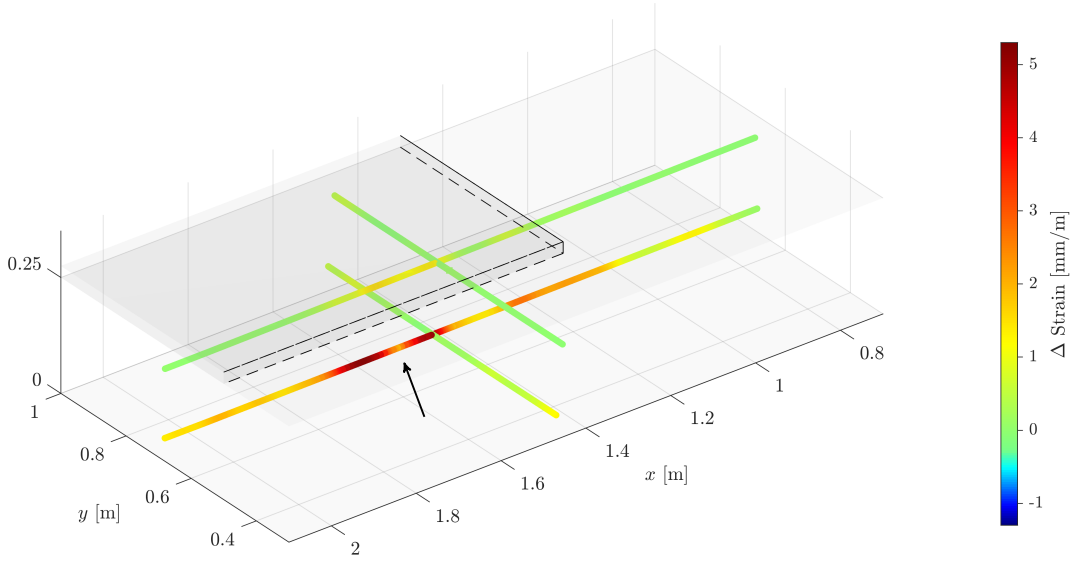

Figure 4.23: Detail view of change in strain w.r.t. reference measurement at 6. loading phase with an abrupt strain drop at the bottom layer.

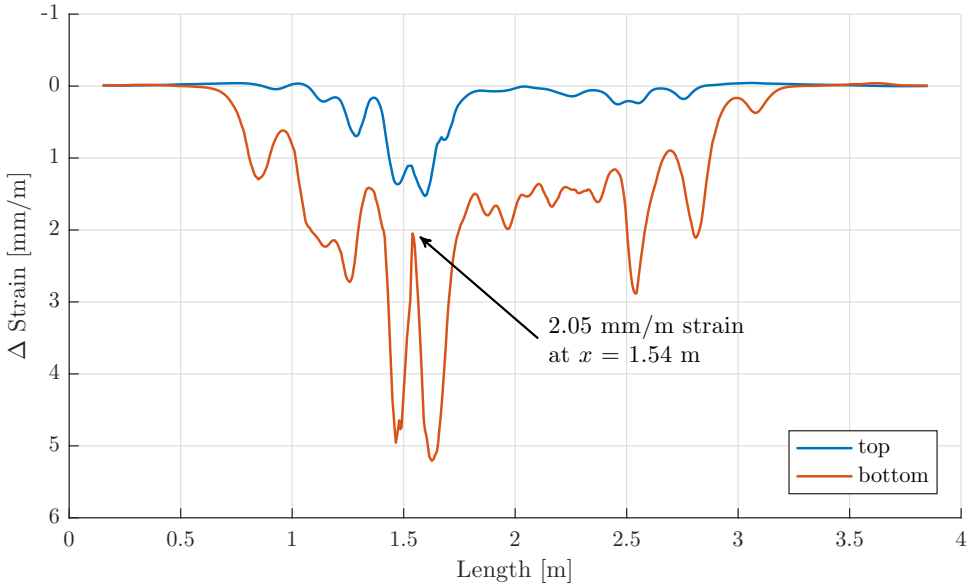

Figure 4.24: Change in strain w.r.t. reference measurement at 6. loading phase of the cables in circumferential direction with an abrupt strain drop at $x = 1.54\,\mathrm{m}$ at the bottom layer.

This drop in strain could potentially be attributed to the fixation method via a very tight attached cable tie at this specific point. As the photo documentary shows a cable tie is situated exactly at the described position (Figure 4.25).

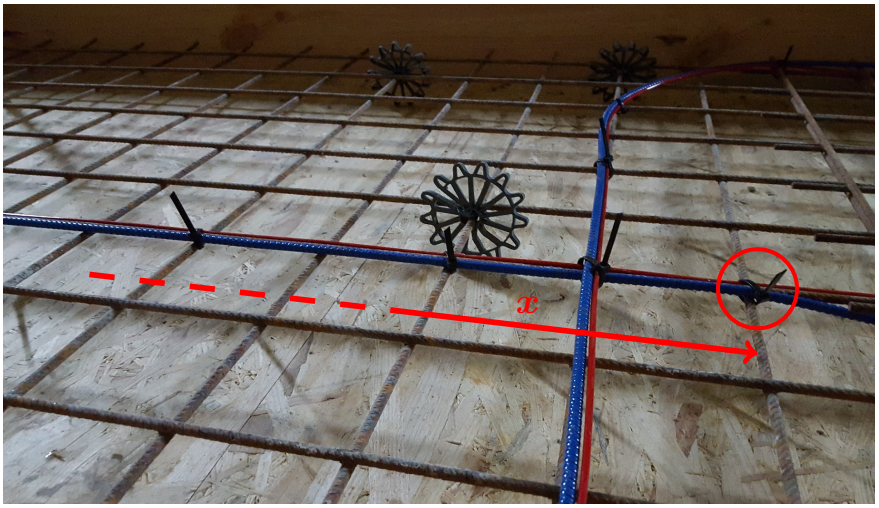

Figure 4.25: Detailed view of the fixation with a cable tie at the described point ($x = 1.54\,\mathrm{m}$) of abrupt strain drop.

A general trend is perceptible in the results, at which the highest changes in strain are concentrated at one point located roughly at $x = 1.5\,\mathrm{m}$ which is not expected at the given test setup with a centric placed loading plate in the middle of the test slab (at $x = 2.0\,\mathrm{m}$).

Due to the rough surface of the sprayed concrete and the not perfectly parallel alignment of the test slab and the shovel, the steel plate for load distribution does not rest planar on the slabs' surface (see Figure 4.26) and therefore a certain eccentric load application is given.

The first contact point of the excavator bucket with the steel plate is approximately at the location with the highest recorded changes in strain. Until the other bucket teeth are in contact with the steel plate, a certain amount of stress is already induced into the test slab creating the off-centered peak.

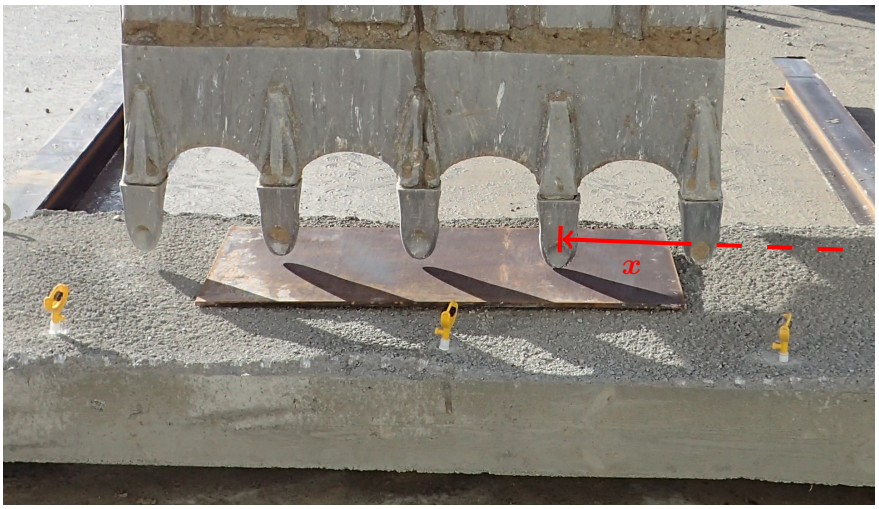

Figure 4.26: Contact point of the second bucket tooth with the load distribution plate at about $x \approx 1.6\,\mathrm{m}$ from the right edge of the test slab.

4.5.2.2 Temperature Measurement

The following figures show the first, the second and the final loading phase of the pre-test. The results of the remaining phases vary only very little and are therefore not displayed.

The graphs show the data of the cables used for temperature measurement at the individual loading phases, the axis of the steel beams and the plate used for the load distribution. The zero points of the axis correlate with the ones in the sketch in Figure 4.4.

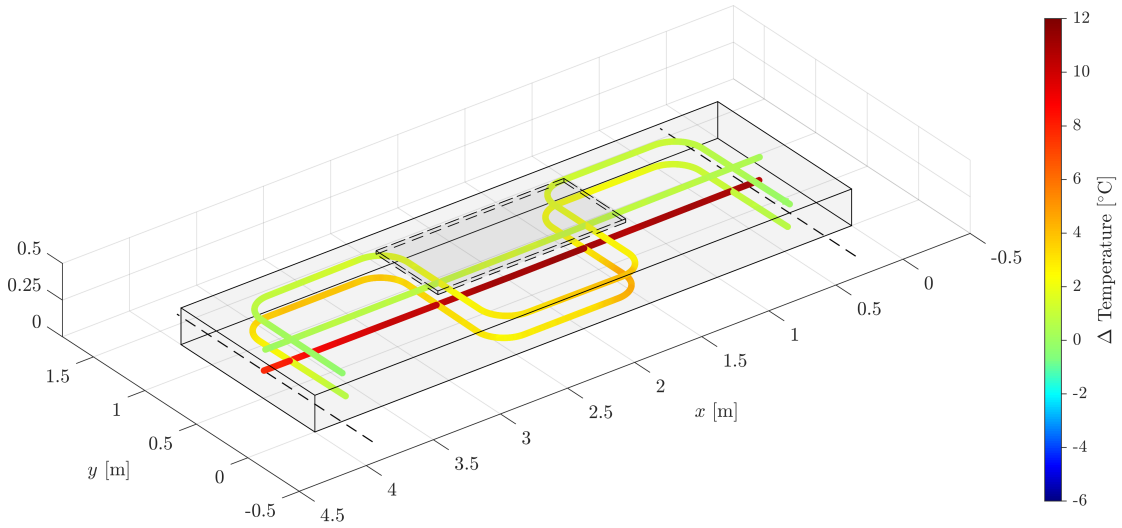

Figure 4.27: Change in temperature w.r.t. reference measurement at 1. loading phase.

At the first loading phase (Figure 4.27) it is apparent that the bottom layer of the fibre-optic sensing cables, especially the cable in circumferential direction, show a distinct change in temperature compared to the reference measurement.

The temperature increases by almost 12 °C along the entire cable length and within a very short time after the reference measurement (test slab without load). This unrealistic increase leads to the conclusion that during the first loading step an impermissible amount of mechanical tension is induced in the cable for temperature measurement which results in this outcome.

It seems that the special temperature cable *BRUsens temperature* 85 °C is not designed to compensate such high mechanical stresses without transferring mechanical stresses from the protective outer layer to the fibre-optic core. Consequently it has to be assumed that the measured change of temperature is not the actual temperature inside the optical fibre, but rather a stress induced distortion of the recorded data.

The fibre-optic sensing cables which are located at lower stressed areas of the test slab also show this behaviour, but to a lesser extent. Nevertheless this trend is present throughout all six performed loading phases and therefore only the result of the first loading phase is discussed here. The second and last loading phase are shown in Figure 4.28 and Figure 4.29 respectively.

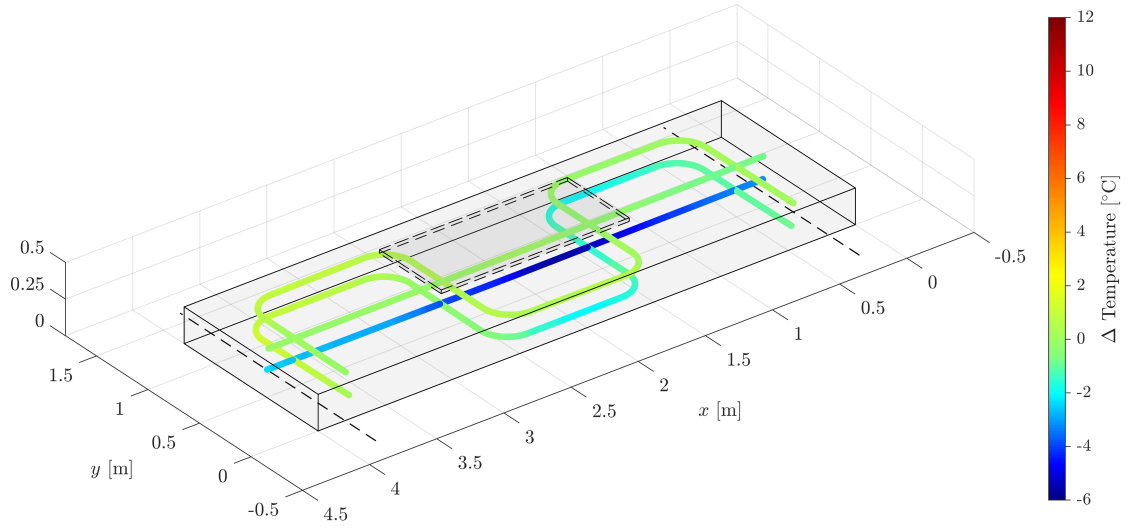

Figure 4.28: Change in temperature w.r.t. reference measurement at 2. loading phase.

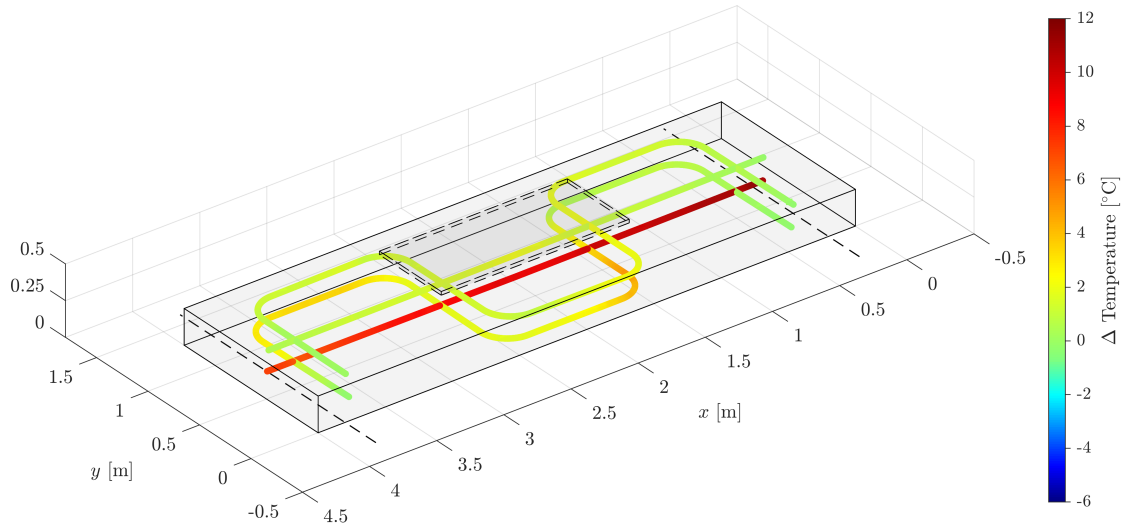

Figure 4.29: Change in temperature w.r.t. reference measurement at 6. loading phase.

4.6 Conclusion

After extensive analysis of all recorded data as well as evaluation of other influencing conditions a conclusion regarding the outcome of the pre-test can be done. The following list summarises the gained insights:

1. With the chosen fixation method the installation of the fibre-optic sensing cables can be realised within a reasonable time.

2. The fixation with cable ties every 20 cm ensures that the cables are not damaged (break) or displaced (change of position, rotation) during the application of shotcrete at maximum spraying performance.

3. No notable disadvantage is observed at the installation process regarding behaviour and handling of the different cables in terms of bending radius and stiffness.

4. Both used fibre-optic sensing cables for strain measurement offered good bonding qualities with the shotcrete due to their structured surfaces.

5. The performed loading test shows that the strain induced by an arbitrary external loading can be allocated precisely in both magnitude and position.

6. All used cable types provide the same quality of data, hence no difference can be stated. (except temperature measurement at the loading test; see point 8.)

7. During the continuous measurement the temperatures between top and bottom layer as well as circumferential and longitudinal direction only differ very little from each other but are still recognised by the system.

8. As the fibre-optic sensing cable used for temperature measurement appears to be not fully independent to mechanical stresses, no distinct statement can be done for the recorded temperatures as the cable was exposed to high tensile forces.

With this information some adjustments are made in the planning of the main test. As described above, the cable *BRUsens temperature* 85 °C used for measuring temperature is not capable of compensating high mechanical strains, thus showing incorrect results in the analysis.
Although the loading situation of the tunnel lining at the main test is different from the one at the pre-test (predominantly compression expected, no very high localised strains), the cable *BRUsens temperature* 85 °C is not used at the main test to avoid a possible failure reason.

As can be seen in Figure 4.24, the top layer of the fibre-optic sensing cable shows mostly zero or close to zero values for the changes in strain inside the test slab. The fact that not much compressional strain can be observed at the top of the test slab (as someone would expect at the given test setup) could be explained with the compressional zone lying slightly above the installed fibre-optic sensing cable and is therefore not showing in the results.

Regarding the temperature compensation from the measurement point of view, it is considered sufficient to install the cables only in circumferential direction for the main test. On the one hand the measured temperature differences between the two directions are so small, that the compensation of one round length can be done with only the cable in circumferential direction while still ensuring the necessary accuracy and on the other hand the effort of installing two separate lines of cables is comparably high to the profit in an even more accurate temperature compensation (using cables in both directions).

5 Main Test

The main test location is situated at the project section SBT 1.1, Tunnel Gloggnitz, track 1 of the Semmering Base Tunnel. The shotcrete lining of the entire cross-section (top-heading and invert) at the monitoring section *MS-1439* is equipped with several fibre-optic sensing cables for a continuous and direct measurement of strain and temperature within the lining.

The fibre-optic measurement system is installed on March 14th, 2017 at the top-heading and five days later on March 19th, 2017 at the invert. The construction phases around the dates of installation can be seen in Figure 5.1. The top-heading round length is constant with 1 m and the invert round length is 2 m.

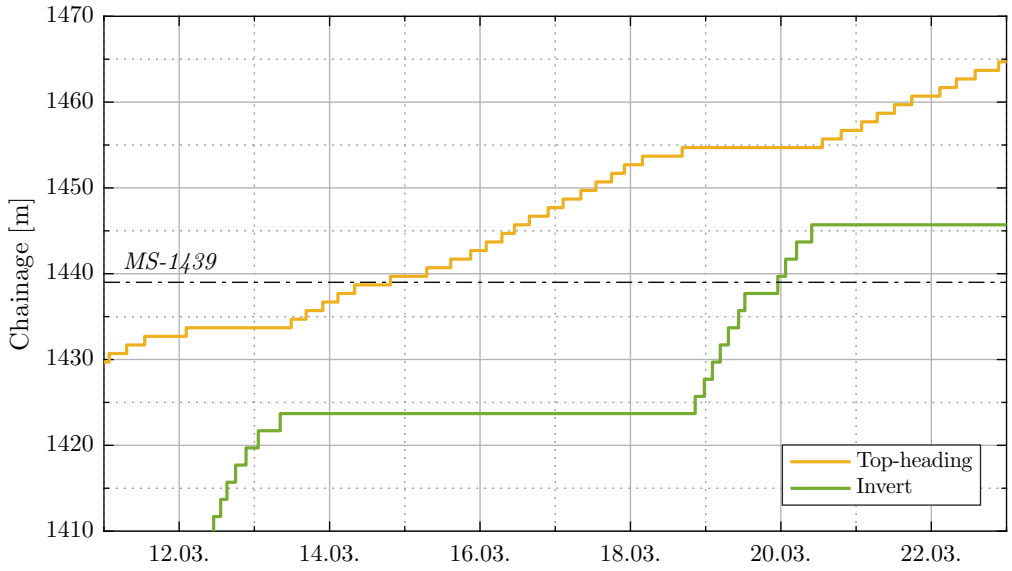

Figure 5.1: Construction phases of top-heading and invert at the time of installation of the fibre-optic measurement system at *MS-1439*.

The continuous measurement starts as soon as the installation process of the FOS system is completed and is carried out for 31 days after the implementation at the invert until April 19th, 2017. After that time no major displacements and hence no significant strain changes in the lining are expected.

However, the measurements concept is designed in a way to allow a reconnection of the OBR at any time in the future to conduct additional measurements if needed (as long as the fibre-optic sensing cables remain intact).

5.1 Measurements Setup

5.1.1 Fibre-optic Instrumentation

The arrangement of the fibre-optic sensing cables is similar to the pre-test. For all strain measurements (*Line A*) the cable type *BRUsens strain V3* (specifications see section 3.2) is

used as it has proven to be the most suitable cable for the main test due to its robustness and durability. It is installed in circumferential direction (perpendicular to the tunnel axis) and in loops (alternately parallel and perpendicular to the tunnel axis) to record strains in longitudinal direction.

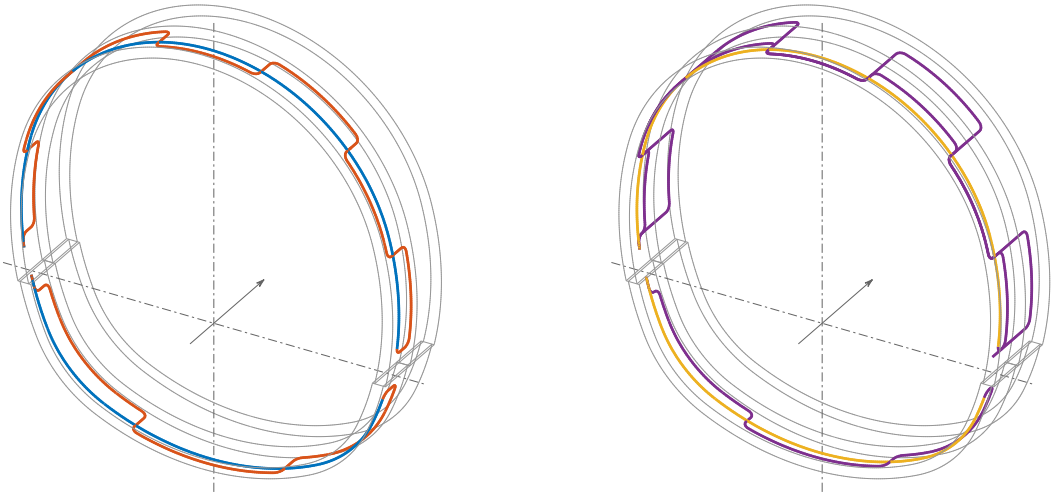

(a) Position of the first/rock side layer of fibre-optic sensing cables.

(b) Position of the second/cavity side layer of fibre-optic sensing cables.

Figure 5.2: Schematic sketch of the fibre-optic measurement system setup at the main test.

The first or rock side layer of the fibre-optic sensing cable in longitudinal direction is installed over one round length with a total of seven loops (Figure 5.2(a)), the second or cavity side layer is implemented in the exact same way as the first layer, but with a supplementary cable which stretches over two round lengths (Figure 5.2(b)).

Figure 5.3 depicts a schematic sketch of a horizontal cross-section of the shotcrete lining showing the locations of the individual lines of fibre-optic sensing cables in reference to the cross-sectional tunnel geometry.

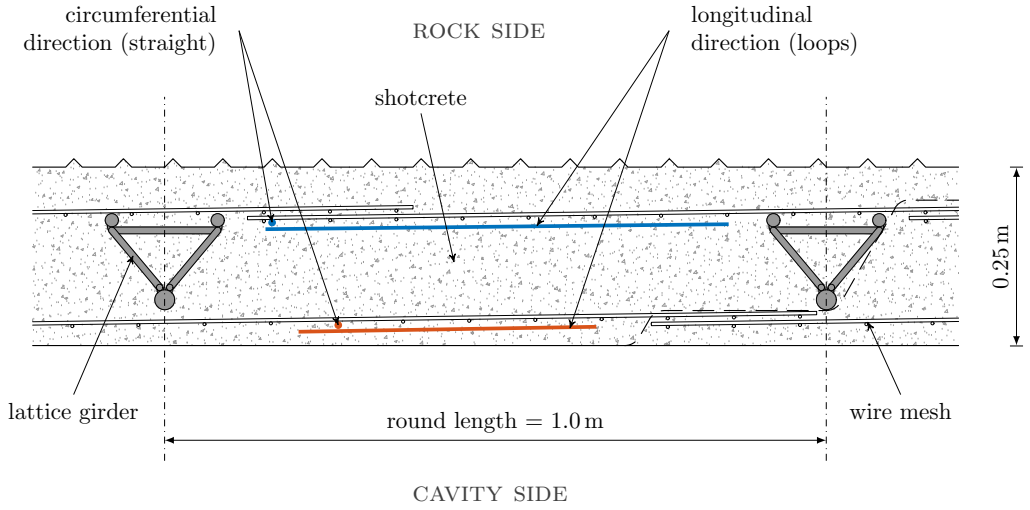

Figure 5.3: Schematic horizontal cross-section of the shotcrete lining including the fibre-optic sensing cables (here only one round length depicted).

Additionally, cables for temperature compensation (*Line B*) are installed parallel to the strain cables in circumferential direction. As the pre-test has shown (see section 4.5.2.2), the cable type *BRUsens temperature* 85 °C originally intended for temperature measurements exhibits a problematic behaviour under high mechanical stress resulting in incorrect data. Instead the cable type *BRUsens strain V3*, inserted in a polyethylene (PE) tube, is used for temperature measurement. The cable can move freely inside this tube which ensures that no external influence other than temperature is altering the results.

The fibre-optic sensing cables for strain measurement are stored on drums at their correct lengths. IGMS already equipped the cables with the necessary connectors when taken on site before installation. The cables for temperature compensation are pre-inserted in the PE-tubes and are also equipped with the required connectors beforehand.

The fibre-optic measurement system (the OBR, the optical switch, an uninterruptible power supply, a laptop and an additional external hard drive for data storage) is set up in a specially built metal box (see Figure 5.4(a)) which is mounted approximately 60 m behind the face at the left tunnel wall to protect it for the duration of the continuous measurement.

The supply cable is protected against negative mechanical influences (e.g. heavy vibrations) inside a plastic tube which is placed alongside the left tunnel wall. The connections between the supply cable and the fibre-optic cables at the monitoring section are housed in a second metal box (see Figure 5.4(d)) in the left side wall.

Due to the construction sequence of the tunnel, it is not possible to connect the cables of the top-heading and the invert at the right side wall. An overview of the measurements setup on site can be seen in Figure 5.4 below.

(a) Installed instrument box.

(b) Alignment of the supply cable.

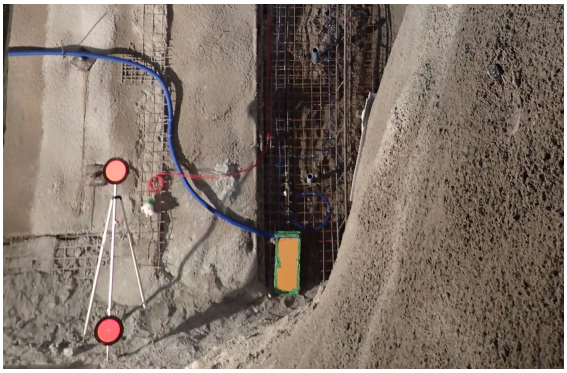

(c) Connection box at the monitoring section.

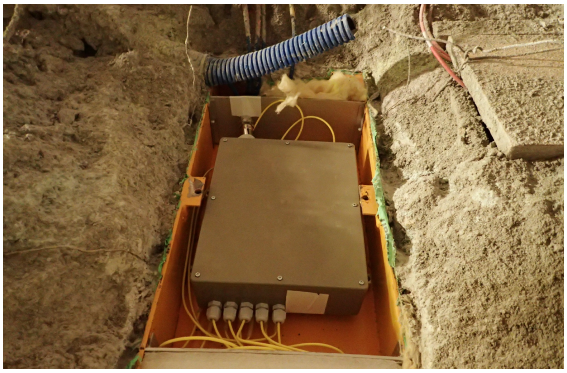

(d) Detailed view of the connection box.

Figure 5.4: Measurements setup at the main test.

5.1.2 Additional Measurement Equipment

Besides the standard geodetic measurement via prism targets, vibrating wire strain gages and pressure cells are installed to obtain further data to get comparable results for the FOS measurements. Figure 5.5 shows the positions of the installed additional measurement equipment.

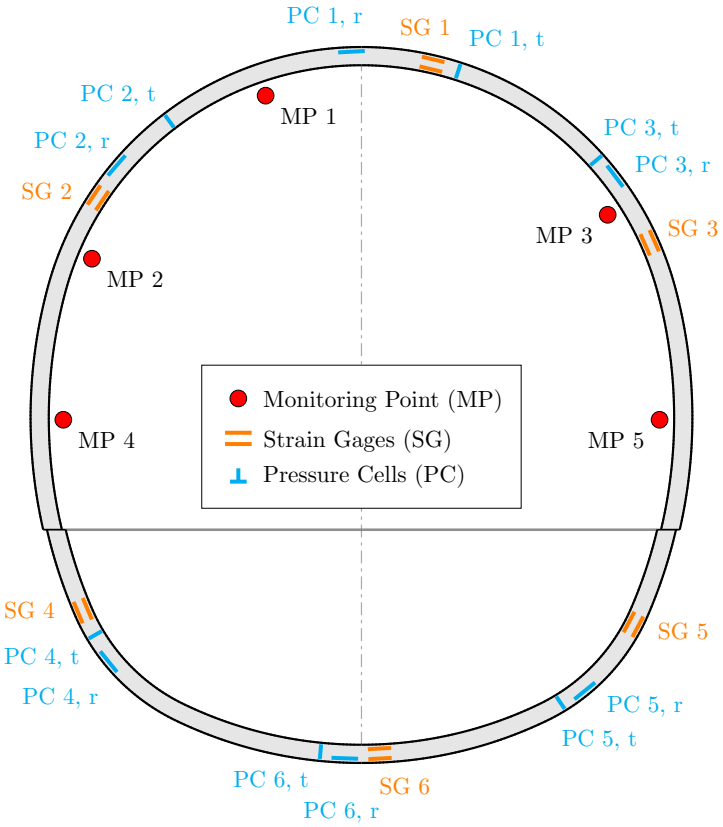

Figure 5.5: Positions of the additional measurement equipment installed at *MS-1439* for the main test.

Five standard geodetic measurement bi-reflex targets are mounted on the shotcrete lining of the top-heading to record the absolute displacements.

For both top-heading and invert pairwise vibrating wire strain gages of the type 4200ER from the company Geokon, Incorporated are used. The manufacturer specifies a measurement range of up to 10 000 µε with a resolution of 2–5 µε at an accuracy of ±0.5 % F.S. at laboratory conditions (Geokon, 2016).

They are attached to the respective layers of wire mesh (see Figure 5.6(a)) in tangential direction to record relative changes in strain. With the used strain gages also the local temperature can be calculated with the measured temperature depended resistance of the instrument.

For top-heading as well as invert pressure cells of the model 4850 from the company Geokon, Incorporated are used. The manufacturer specifies a measurement range of up to 20 MPa in tangential and 3 MPa in radial direction. The resolution for both directions lies at ±0.025 % F.S. at an accuracy of 0.1 % F.S. at laboratory conditions (Geokon, 2017).

The pressure cells are installed in tangential as well as in radial direction (Figure 5.6(b)) in order to measure the tangential pressure within the lining and the radial pressure resulting from the ground pressure acting on the lining.

(a) Pairwise installed strain gages.

(b) Radial and tangential installed pressure cells.

Figure 5.6: Additional measurement equipment installed at *MS-1439* for the main test.

5.2 Installation

As explained in chapter 3, only relative changes of strain and temperature to a prior performed reference measurement can be recorded. To obtain absolute values for the temperature, a starting value at the time of installation is required.

Therefore the air temperature (and the air humidity) at the respective times of installations for top-heading and invert are recorded. These measurements are further carried out inside the tunnel over the entire course of the one-month-long continuous monitoring period (see Figure 5.7) in close vicinity to the monitoring section *MS-1439*. This measurement was not carried out for all days by the technician on site, explaining the gap in the graph below.

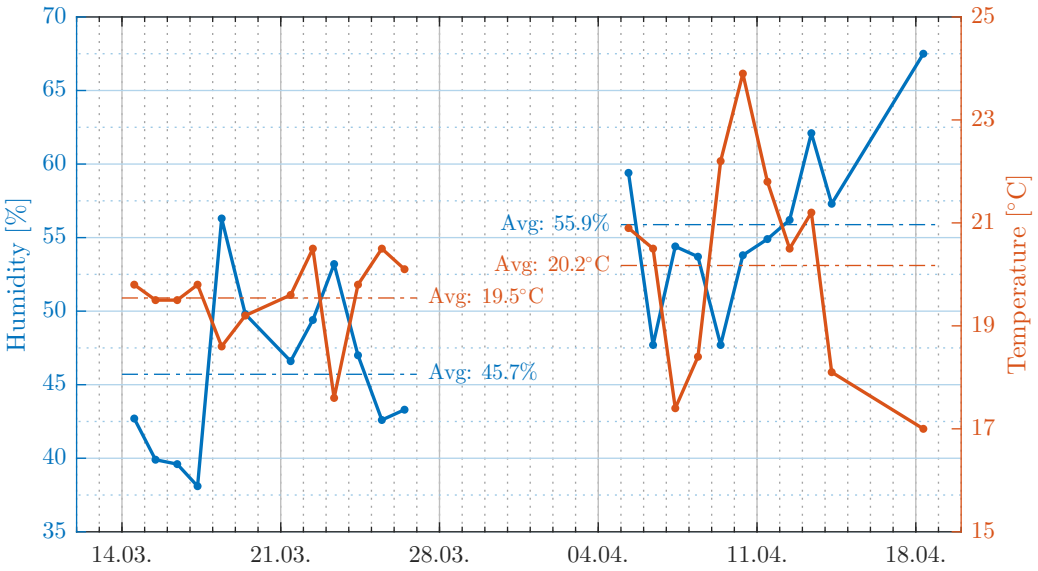

Figure 5.7: Recorded air- humidity and temperature during the continuous monitoring period.

At the time of installation at the top-heading the mean air temperature is 19.8 °C with an average air humidity of 42.7 %. The mean temperature at the time of installation at the invert is 19.6 °C with an average air humidity of 56.3 %. The apparent divergence at the end of the continuous monitoring period with a relative high humidity and low temperature can be explained by the construction stop at Easter (April 14th to April 18th) this year.

5.2.1 Top-heading

On March 14th, 2017 the fibre-optic measurement system is implemented at the top-heading. First the connection box is set at the left top-heading foot and is connected with the supply cable coming from the instrument box. Consecutively the individual lines of fibre-optic sensing cables are installed by the workers on site at the rock side layer of wire mesh, fixed with cable ties.

After an initial measurement check is performed, the first layer of shotcrete is applied. A second measurement check afterwards ensures the full functionality of the installed cables. This procedure is then repeated for the second layer in the exact same manner.

In total the installation of the fibre-optic sensing cables at the top-heading takes about 1 h for the rock side layer and 1 h 50 min for the cavity side layer. An overview of the installation works can be seen in Figure 5.8 with the fibre-optic sensing cables for strain measurement in blue, the PE-tube containing the fibre-optic sensing cable for temperature compensation in black and the cables of the strain gages in red.

(a) Installation of first layer, left side wall.

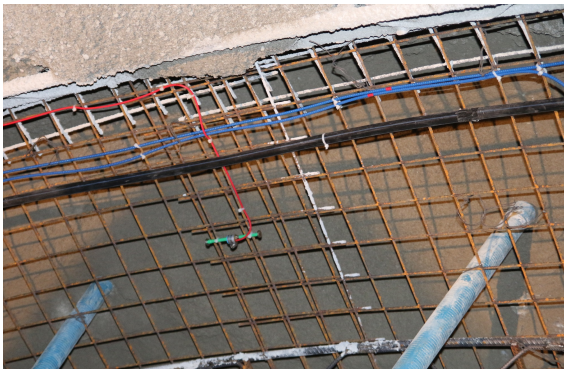

(b) First layer (with strain gage), crown.

(c) Installed second layer, left side wall.

(d) Spraying of second layer shotcrete.

Figure 5.8: Installation of the fibre-optic sensing cables at the top-heading.

To avoid damaging the cables during the borehole drilling for the support with grouted bolts, plastic tubes (light blue in Figure 5.8(b)) indicating the future positions for the drill holes are placed along the excavation profile for both round lengths.

Due to the tight time schedule and the very small working area at a round length of 1 m some cables are not installed exactly according to their planned positions. This deviation is documented and considered in the analysis of the recorded data.

5.2.2 Invert

The implementation of the fibre-optic measurement system at the invert is done on March 19th, 2017. All fibre-optic sensing cables are connected with the supply cable at the already installed connection box. A first measurement check is conducted after fixing the individual lines of the first layer of cables onto the bottom layer of wire mesh with cable ties by the workers on site. Then the first layer of shotcrete is applied followed by a second measurement check. This process is repeated for the second layer.

It takes about 2 h 20 min to install the fibre-optic sensing cables at the invert for the rock side layer and 1 h 30 min for the cavity side layer. Figure 5.9 shows the installation works at the invert with the fibre-optic sensing cables for strain measurement in blue, the PE-tube containing the fibre-optic sensing cable for temperature compensation in black, the cables of the strain gages in red and the cables for the pressure cells in yellow.

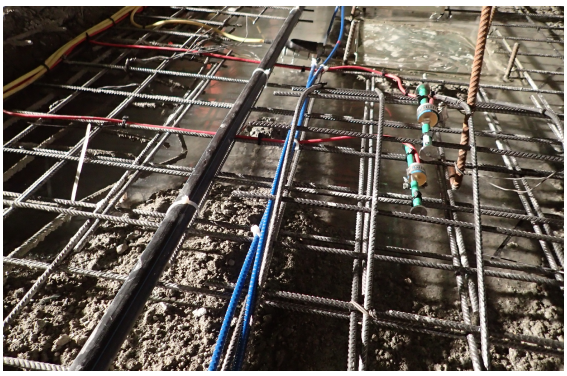

(a) First layer (with strain gages), bottom.

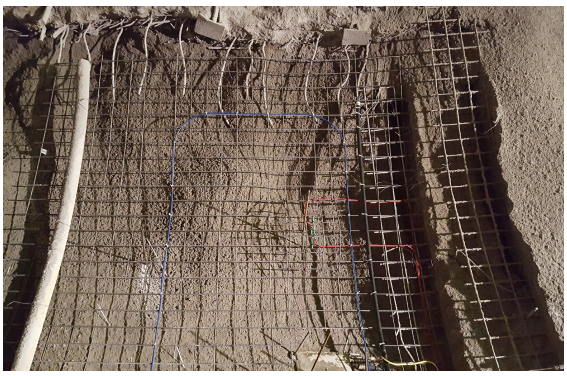

(b) First layer, right bench.

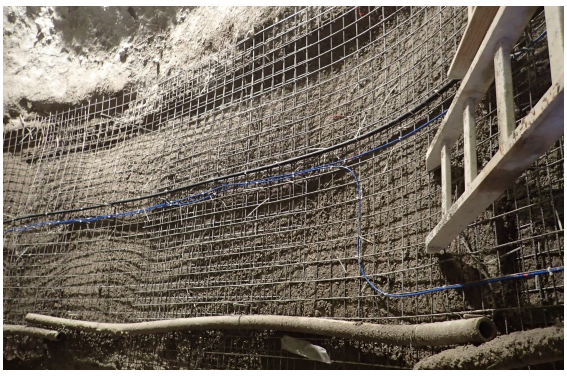

(c) Second layer, left bench.

(d) Spraying of second layer shotcrete.

Figure 5.9: Instalment of the fibre-optic sensing cables at the invert.

For still unknown reasons the top layer of the fibre-optic sensing cables at the invert (both cables for strain measurement as well as temperature compensation) cannot be accessed by the OBR after the second layer of shotcrete has been applied. As a consequence the complete recording of data for those specific cable lines is not possible.

Potential reasons could be a kink of the connector cables inside the connection box or a damage (break) of the fibre-optic sensing cables due to the application of the final layer of shotcrete.

Attempts to investigate this issue by opening the connection box have been discarded, since the possible risk of damaging the other functioning cable lines is valued greater than the additional data gain of the lost cables.

6 Results

This chapter displays and describes the results of the fibre-optic measurements carried out at the monitoring cross-section *MS-1439* of track 1 at Tunnel Gloggnitz over the course of the planned one-month-long measurement duration.

To adequately present the results, different forms of depiction are used. The evolution of strain change for particular points in the lining is displayed in several time plots. The distribution of change in strain in sense of a cross-sectional view is plotted perpendicular to the tunnel surface. For displaying the fibre-optic sensing cables in longitudinal direction a full three-dimensional view is used.

The recorded measurements are always relative changes in strain with respect to a prior carried out reference measurement (= zero measurement) which is conducted for every line of installed fibre-optic sensing cables separately after the initial application of shotcrete at the respective layer.

All following results are displayed as change in strain normalised to the distance of one meter ($1\,\mathrm{mm/m} = 1000\,\mu\mathrm{m/m} = 0.1\,\% = 1\,‰$) where a positive value indicates tension and a negative value compression along the fibre-optic sensing cable. All shown results are temperature compensated, meaning absolute changes in strain due to external loading. A resolution of 2 cm can be achieved for all conducted measurements.

Since the temperature values determined from the fibre-optic measurements have shown unrealistic results during data evaluation, IGMS performed individual temperature calibrations of the sensing cables under laboratory conditions. These calibrations demonstrate that the linear standard coefficient is not sufficient to calculate temperature values from the recorded data. However, further investigations will be carried out by IGMS to handle these effects in the future.

The recording starts right after spraying the respective layer of shotcrete with the OBR measuring autonomously at an interval of one minute over the entire observation period. Due to this tremendous amount of data, one epoch every hour for the first week and after that one epoch every twelve hours is considered for all further evaluations.

If blanks are present in the data, either the respective fibre-optic sensing cable is not measured yet, or the data at that point contains serious outliers (e.g. heavy vibrations of the cable during the spraying of shotcrete) and is therefore eliminated from the series. Unfortunately, at some very rare cases also system failures occurred over a short period of time resulting in a minor data loss.

6.1 Evolution of Strain for Single Points

The following graphs show the evolution of change in strain for both installed layers of fibre-optic sensing cables at the positions of the five 3D geodetic targets at the top-heading. Since no 3D targets are available at the invert, the positions of the installed tangential strain gages are used for evaluation. For the exact positions see Figure 5.5.

As the recorded data is not a smooth function, a single data point at the exact position

of the desired location would not represent an appropriate strain value. Therefore the mean value of 30 cm of fibre-optic sensing cable around the desired location is used for the evaluation of changes in strain at single points (see Figure 6.1).

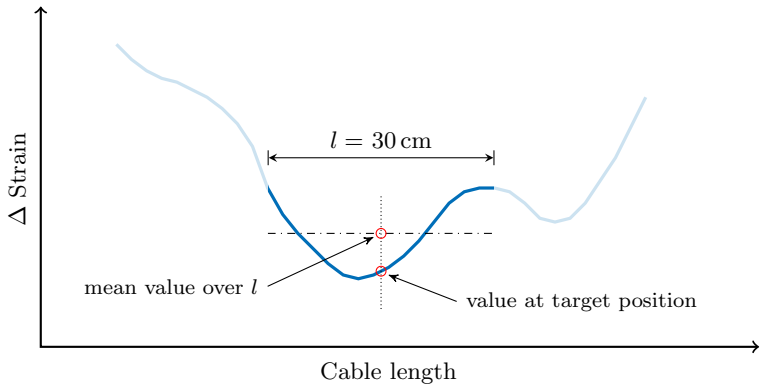

Figure 6.1: Mean value of the measured changes in strain around target position used for the evaluation of single points.

To get an impression of the changes in strain of the first layer in relation to the second layer, the dash-dotted line in the graphs show the changes in strain of the first layer relative to the moment of installation of the second layer. Due to the different times of installation, the already induced strain within the shotcrete of the first layer is subtracted as a static offset with zero at the time of installation of the second layer.

6.1.1 Top-heading

For the crown point (Figure 6.2) the highest increases of change in strain can be observed in the first days after excavation. The data of the second layer of fibre-optic sensing cables show a lower amount of change in strain than the first layer over the total monitoring period with also a lower end level of relative strain. The subsequent excavation of the invert from March 18th to March 20th has hardly any observable influence at the crown.

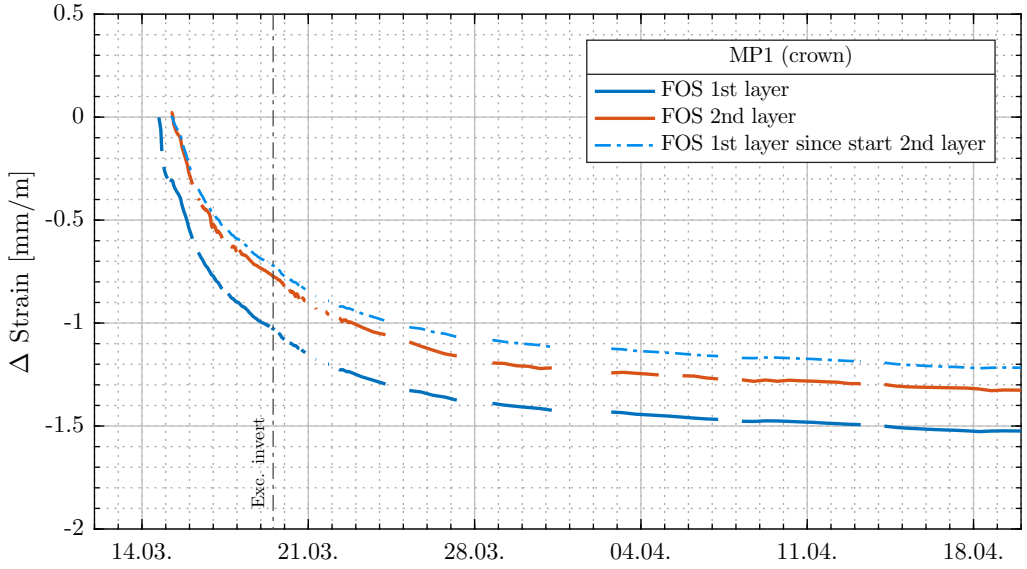

Figure 6.2: Evolution of change in strain of the fibre-optic sensing cables in circumferential direction during the continuous monitoring period at MP1 (crown).

At the shoulder points of the top-heading (Figure 6.3 and Figure 6.4) the largest increases of change in strain occur at the beginning of the observation period. The end level of relative strain is higher at the right shoulder. It is notable that in contrast to the crown point, both shoulder points experience a crossing of the graphs regarding the individual recorded layers in terms of the total accumulated change in strain.

The second layer of fibre-optic sensing cables experiences a higher change in strain than the first layer after a certain point in time. This happens for the left shoulder point approximately 10 days and for the right shoulder point about 3 days after starting the measurements.

The excavation of the invert causes a slight decrease of change in strain which is visible at the graph for the right shoulder point. The left shoulder point does not explicitly show this behaviour.

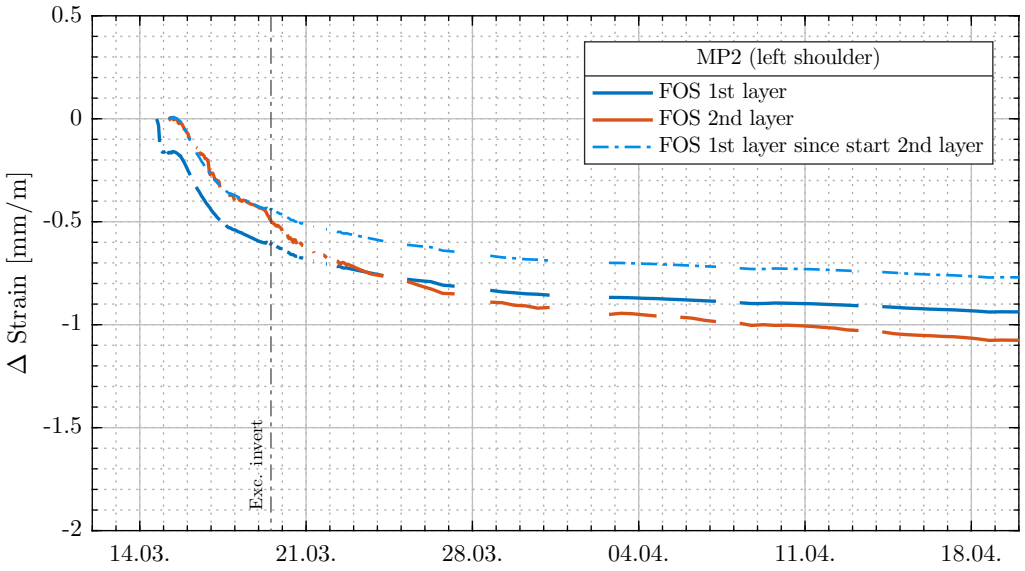

Figure 6.3: Evolution of change in strain of the fibre-optic sensing cables in circumferential direction during the continuous monitoring period at MP2 (left shoulder).

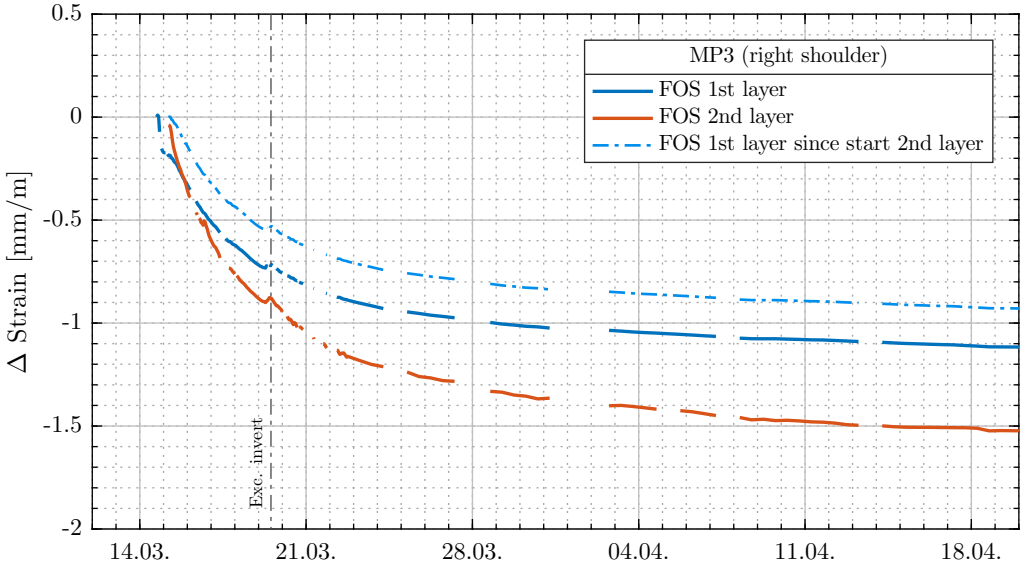

Figure 6.4: Evolution of change in strain of the fibre-optic sensing cables in circumferential direction during the continuous monitoring period at MP3 (right shoulder).

At the side walls of the tunnel (Figure 6.5 and Figure 6.6) the changes in strain are generally at a lower level compared to the previously described points. For either points the excavation of the invert is visible as a decrease in strain change.

The overall level of increase of change in strain for the left side wall is the lowest of all five points, especially the second layer seems not to increase much past the initial drop after installation.

For the considered point at the right side wall, tension is observable for the first layer about one day after installation. A further decrease of change in strain at the same layer is apparent at the time of excavation of the invert. Beyond that point the second layer shows a higher magnitude in strain change than the first one.

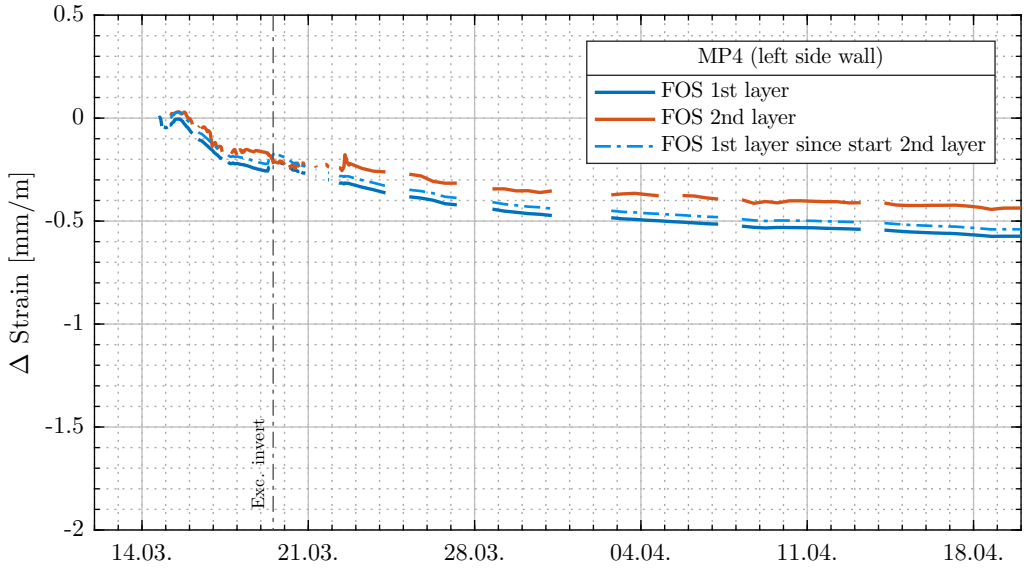

Figure 6.5: Evolution of change in strain of the fibre-optic sensing cables in circumferential direction during the continuous monitoring period at MP4 (left side wall).

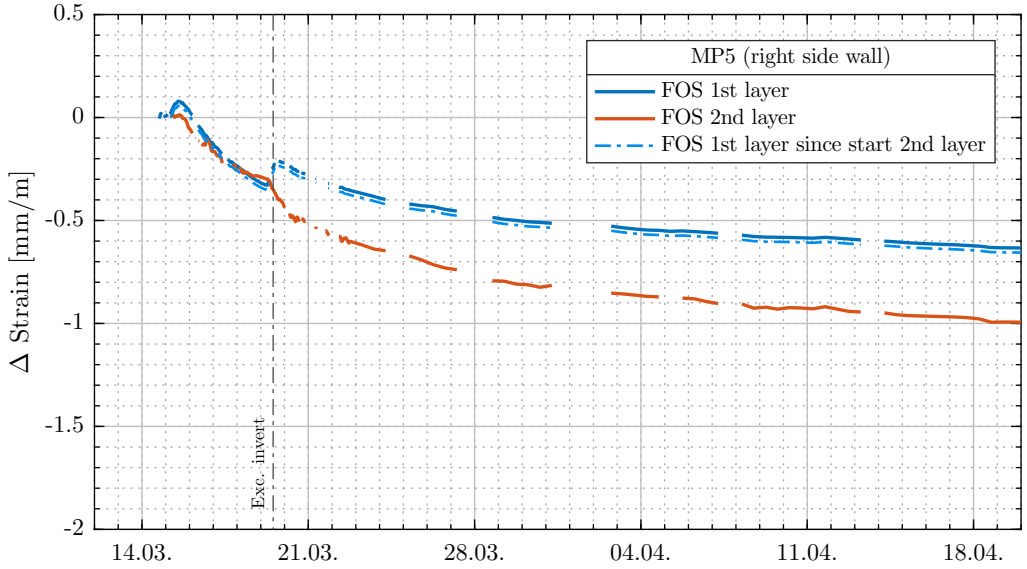

Figure 6.6: Evolution of change in strain of the fibre-optic sensing cables in circumferential direction during the continuous monitoring period at MP5 (right side wall).

The evolution of change in strain at the very early stages after construction is of great interest, since the young shotcrete has the highest incremental gain in strength in this phase. Therefore a detailed view of these early stages is displayed in Figure 6.7 for the positions of all five geodetic targets of the top-heading.

The crown point experiences the highest accumulation in strain for both layers of fibre-optic sensing cables compared to the other points. The rock side first layer already exhibits 0.4 mm/m in compression before the second layer is even installed. The further rate of growth afterwards is about the same for both layers (parallel slope of curves).

The two shoulder points tend to show the same behaviour as the crown point, however, at a smaller magnitude. The first layer exhibits approximately 0.13 mm/m for MP2 (left shoulder) and 0.23 mm/m for MP3 (right shoulder) in compression at the time of spraying the second layer of shotcrete.

The side wall points show almost no increase of change in strain for the first day. After that, only a small increase is observable. The right point (MP5) even shows slight tension at the rock side layer for about one day after construction.

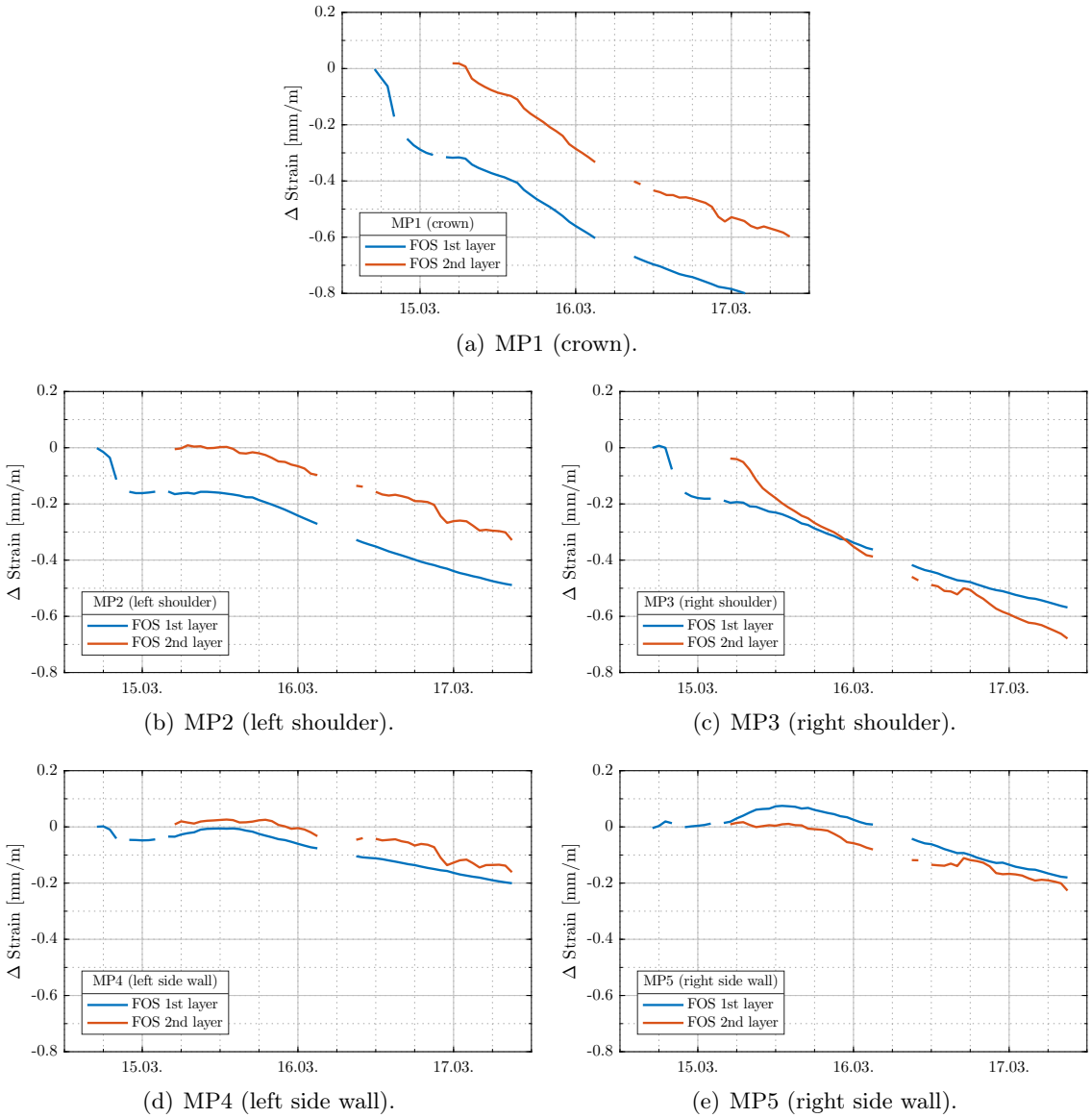

(a) MP1 (crown).

(b) MP2 (left shoulder).

(c) MP3 (right shoulder).

(d) MP4 (left side wall).

(e) MP5 (right side wall).

Figure 6.7: Early changes in strain in the first two days after installation at *MS-1439*.

As observed in the results above, the construction of the invert has a major influence on the strain evolution within the entire lining. A decrease of the already induced strain is especially observable at the rock side layers of fibre-optic sensing cables. This behaviour is more distinct, the closer the observed point is to the bottom of the top-heading. It is also notable that this decrease starts already before the invert is excavated at the monitoring section (for exact advance rate see Figure 5.1). Figure 6.8 shows the points MP2 to MP5 around the time of the invert construction. Note the different limits of the ordinates (yet same scale for all figures).

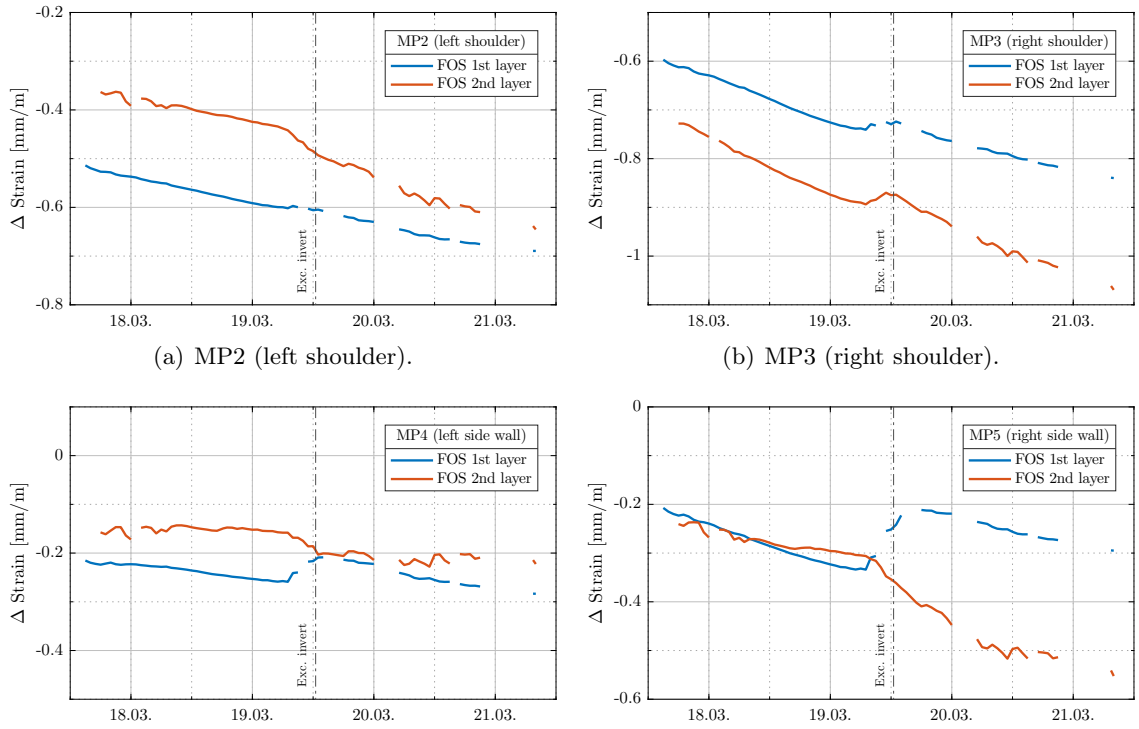

(a) MP2 (left shoulder).

(b) MP3 (right shoulder).

(c) MP4 (left side wall).

(d) MP5 (right side wall).

Figure 6.8: Changes in strain at the time of invert construction at *MS-1439*.

6.1.2 Invert

As stated before, for the evaluation of changes in strain at the invert, the positions of the built-in tangential strain gages are used. Due to the data unavailability of the fibre-optic sensing cables at the second layer of the invert, Figure 6.9 shows all three points of the rock side layer at once.

It can be seen that the invert point experiences a very steep increase in compressive strain of up to 0.5 mm/m at the early stages after installation, whereas the other two points do not show this behaviour in such a distinct manner.

This steep increase begins to stagnate after the excavation sequences is switched back to top-heading drive on March 20th at 9:50am. Afterwards, the overall evolution of the three observed points is roughly the same, however, on different magnitude levels, where the end level of change in strain is the highest for the invert point and the lowest for the point on the right-hand side. This point even shows tension for the early stages (see Figure 6.10).

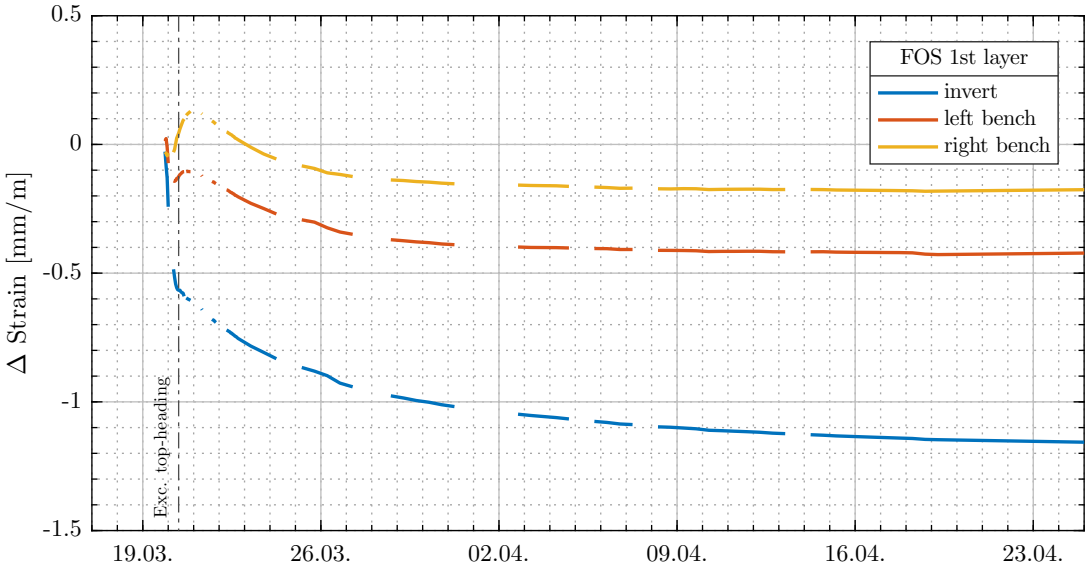

Figure 6.9: Evolution of change in strain of the fibre-optic sensing cable in circumferential direction during the continuous monitoring period at the invert.

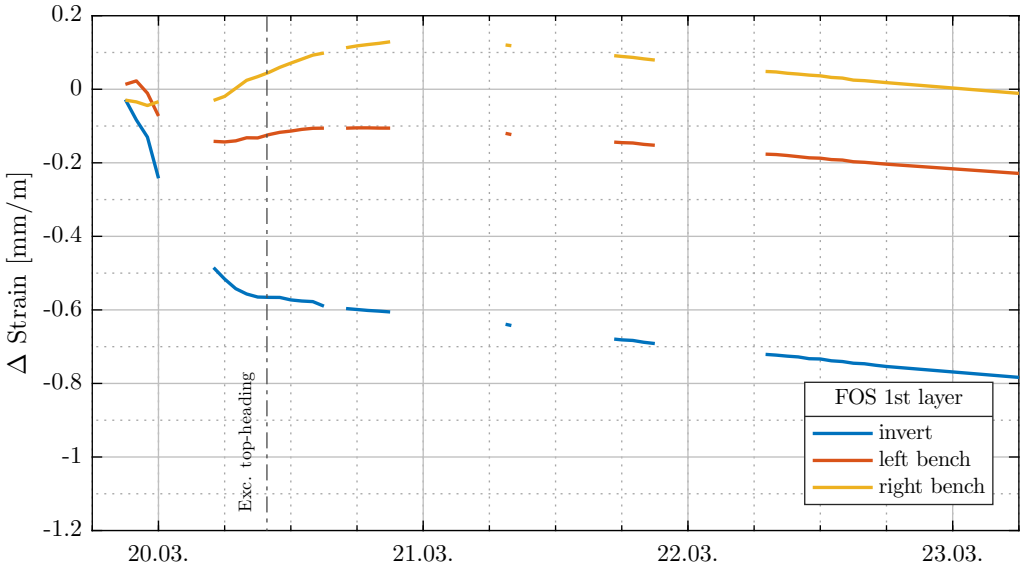

Figure 6.10: Early changes in strain for three days after installation at the invert at *MS-1439*.

6.1.3 Follow-up Measurement

As explained in chapter 5, the fibre-optic measurement setup is designed in a way allowing future measurements at any point in time by simply reconnecting the OBR. Such a follow-up measurement is conducted two months after the end of the continuous monitoring period on June 14th, 2017. The results of this additional reading are displayed here in two time plots for the top-heading and the invert.

Figure 6.11 shows the evolution of change in strain for both layers of fibre-optic sensing cables in circumferential direction at the top-heading at the location of all five monitoring targets. Note that for better display reasons gaps in the data are not graphed.

The data of this follow-up measurement shows that the changes in compressional strain are still increasing at almost every point and layer. Only at the left side wall (MP4) a slight decrease in strain is observable for both layers since the end of the continuous monitoring period.

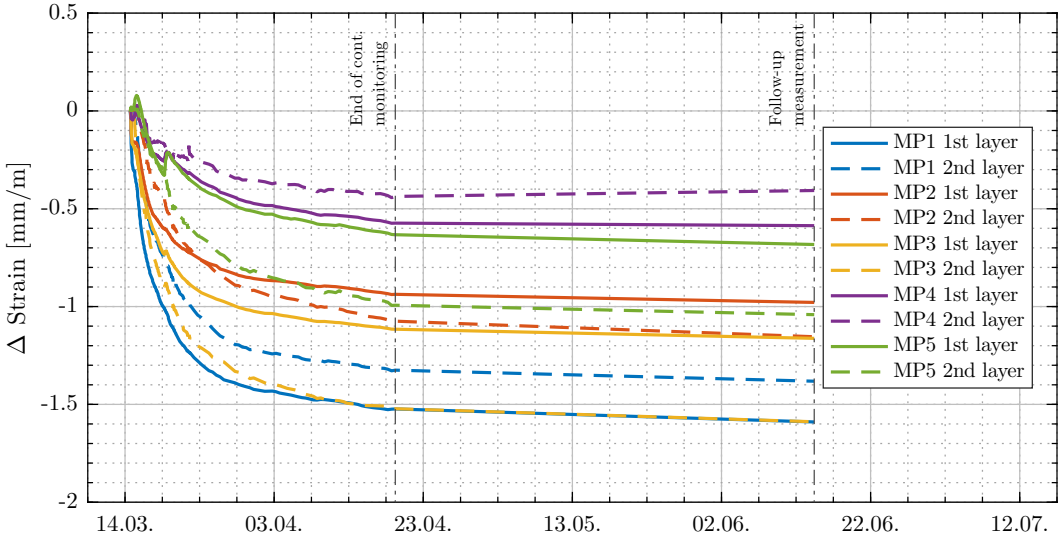

Figure 6.11: Evolution of change in strain of the fibre-optic sensing cables in circumferential direction over the course of the continuous monitoring period including a follow-up measurement at the points of all five monitoring targets.

Figure 6.12 shows the evolution of change in strain for the rock side layer of fibre-optic sensing cables in circumferential direction at the invert. Note that for better display reasons gaps in the data are not shown.

The change in strain clearly increases at the invert point, whereas the two points at the benches show a small decrease in compressional strain since the end of the continuous monitoring period.

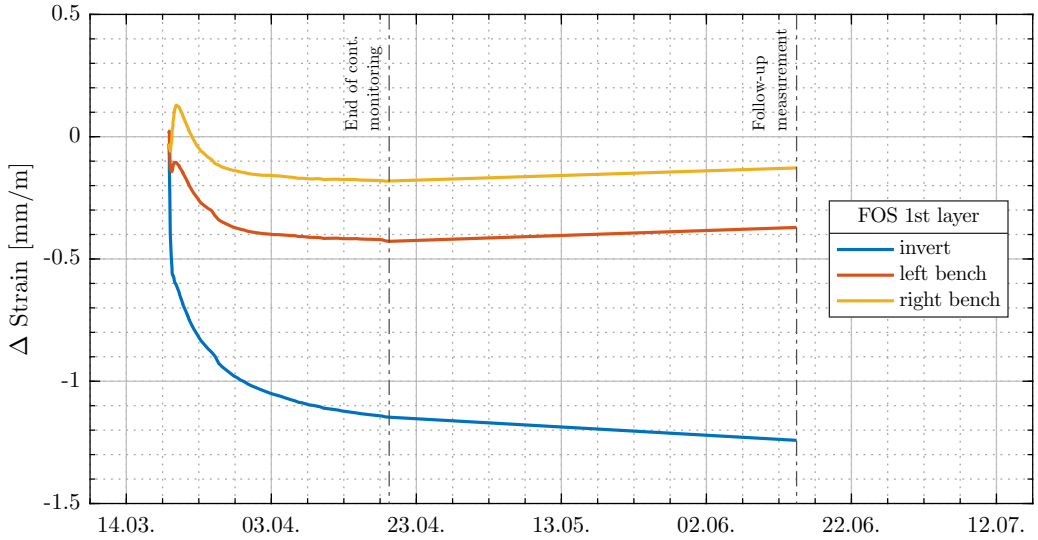

Figure 6.12: Evolution of change in strain of the fibre-optic sensing cables in circumferential direction over the course of the continuous monitoring period including a follow-up measurement at the invert.

6.2 Cross-sectional Distribution of Strain

6.2.1 Circumferential Direction

This section shows the results of the fibre-optic sensing cables installed in circumferential direction at both layers within the shotcrete lining. The change in strain w.r.t. the reference measurement is plotted orthogonal to the tunnel perimeter with yellow indicating a contraction of the cable (= compression) and green an elongation (= tension). All graphs show the specific time at which the measurement is conducted, the time since the application of shotcrete as well as the distance to the face of the respective heading.

Looking at the early stages of the rock side layer (Figure 6.13(a)), compression peaks develop at the crown and both shoulders of the tunnel. The top-heading side walls and footing show slight tensile strains rather than compression. The second layer of shotcrete (Figure 6.13(c)) at the same time shows a lower level of strain compared to the first one, but also with higher values at the shoulders and low compression at the side walls.

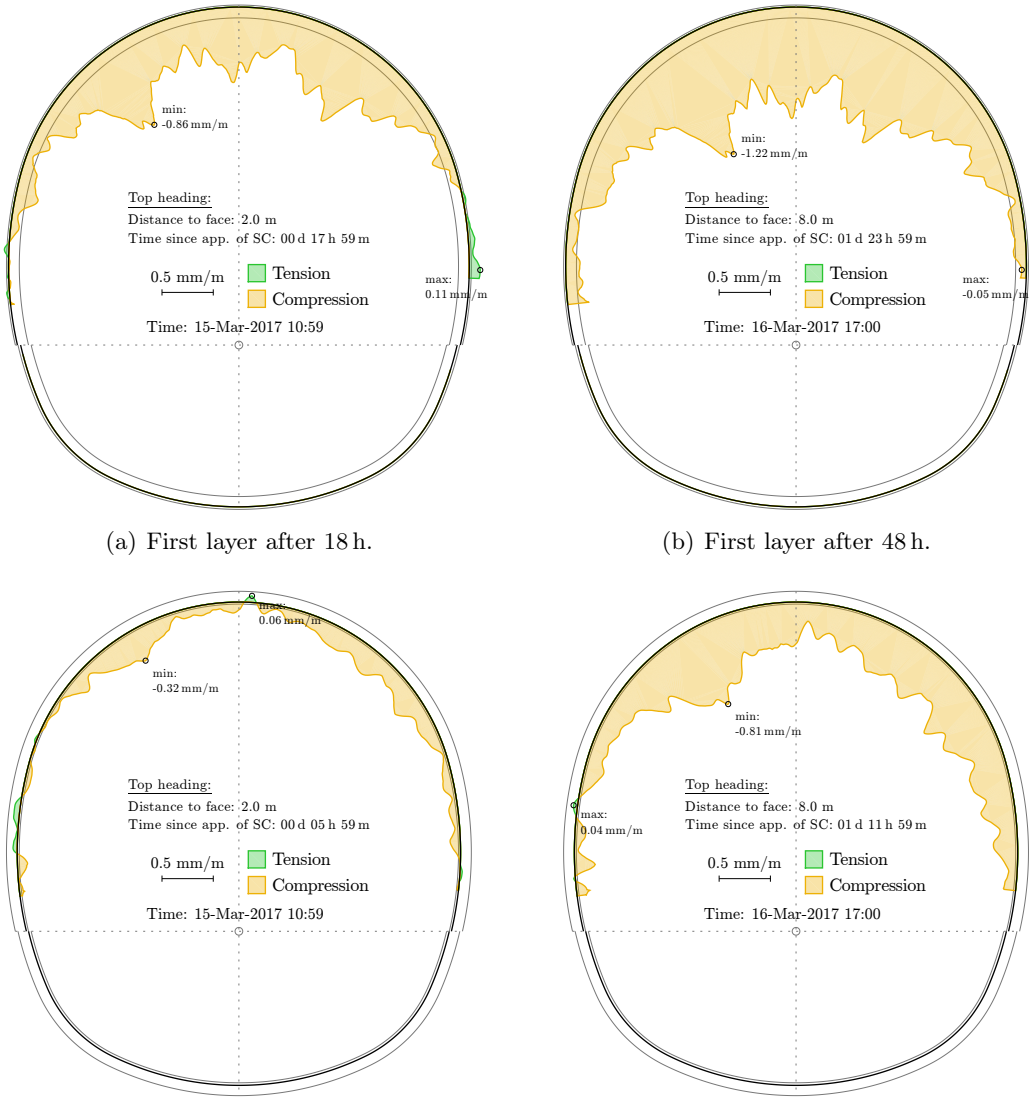

(a) First layer after 18 h.

(b) First layer after 48 h.

(c) Second layer after 6 h.

(d) Second layer after 36 h.

Figure 6.13: Circumferential distribution in strain of first and second layer at the early stages after installation at the top-heading.

This circumstance can be explained in the relative time difference of 12 h between the respective applications of shotcrete and the excavation of the next round in this timespan. The rock side layer of shotcrete has more time to harden and therefore a certain level of strain can already develop.

For the first layer a continuous increase in compressive strain at the entire circumference is observable 30 h later (Figure 6.13(b)). The major peaks are located again at the shoulders and the crown. The later measurement of the second layer (Figure 6.13(d)) shows a larger incremental increase in strain in contrast to the rock side layer. The strain growth is distributed more evenly around the whole circumference with no particular peaks, however, the left side wall shows smaller strains compared to the right side wall.

Note that the scale in Figure 6.14 is different to the scale in Figure 6.13. This is due to the fact that at earlier stages the strains are smaller and hence it is easier to identify variations in the evolution of change in strain on a bigger scale. For comparisons at a time basis, the graphs in section 6.1 are more adequate.

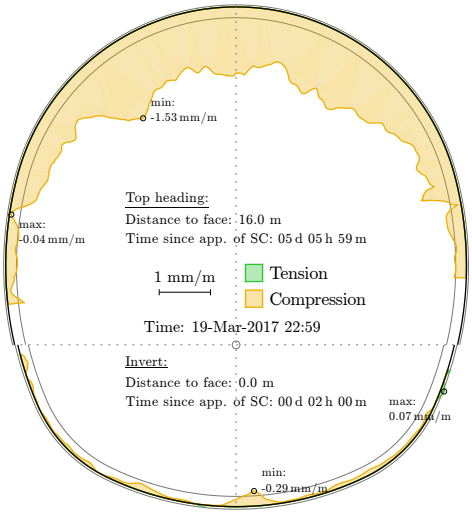

(a) First layer after 2 h (invert).

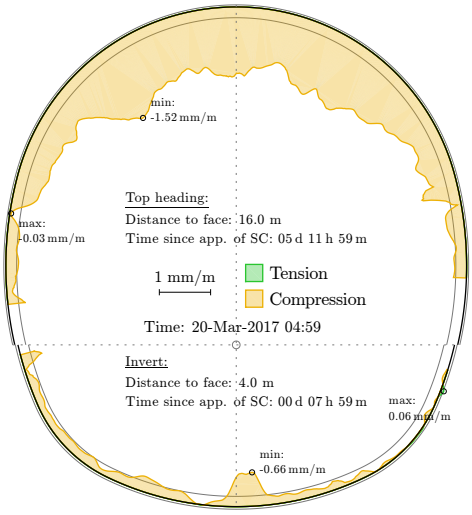

(b) First layer after 8 h (invert).

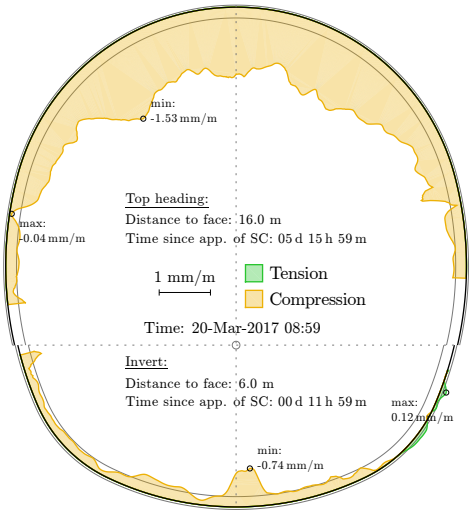

(c) First layer after 12 h (invert).

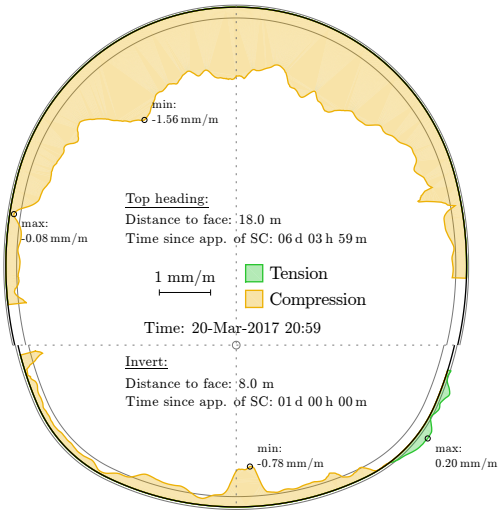

(d) First layer after 24 h (invert).

Figure 6.14: Circumferential distribution in strain of first layer after excavation of the invert for top-heading and invert.

Two hours after spraying the first layer of shotcrete at the invert, a peak in compressive strain starts to develop right at the invert point (Figure 6.14(a)). This peak increases further as time advances. To the right-hand side of the invert, very little to almost zero strain values are measured after eight hours (Figure 6.14(b)) compared to the left side. After twelve hours (Figure 6.14(c)) slight tensile strain develops at the right side of the invert which is even more prominent after a full day (Figure 6.14(d)).

During and after the excavation of the invert, the changes in strain at the first layer of the top-heading show a more or less constant increase. The strain changes at the second layer of the top-heading show a similar behaviour and are therefore not displayed here.

Figure 6.15 displays the distribution of the recorded strain of the first layer at the last conducted measurement at the end of the continuous monitoring period. No tensile strain is recorded in this epoch.

The largest values for the top-heading occur around the crown and the shoulders. The highest compressional strain value w.r.t. the reference measurement is 1.88 mm/m located at the right shoulder, the lowest 0.53 mm/m measured at the left side wall.

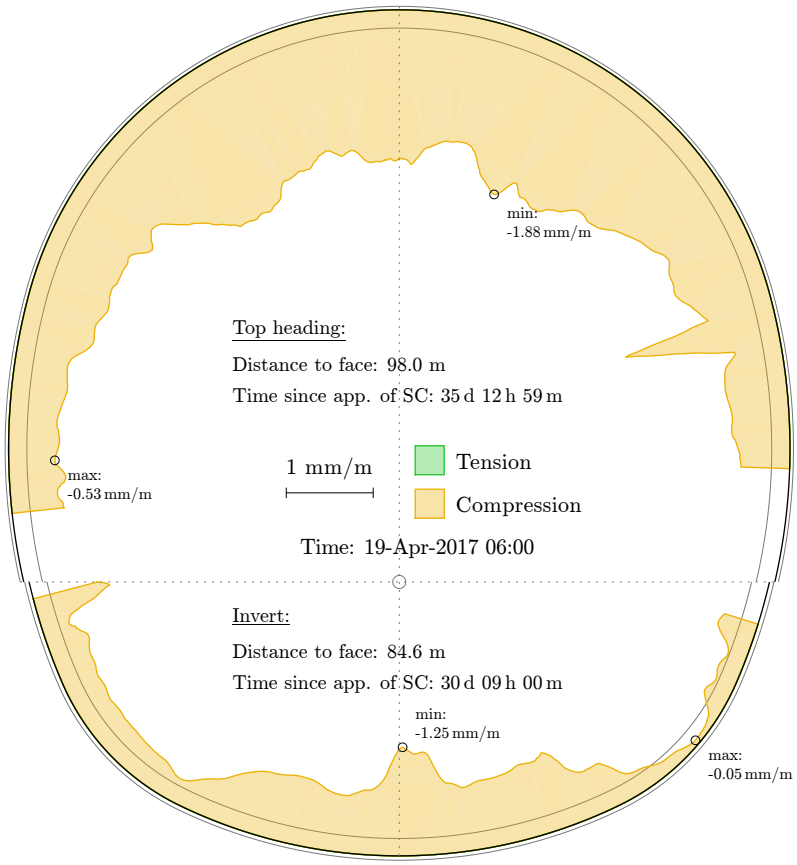

Figure 6.15: Circumferential distribution in strain of the first layer at the last measurement of the continuous monitoring period.

In the invert the maximum change in strain w.r.t. the reference measurement is 1.25 mm/m in compression at the invert point. The strain values become smaller to the sides left and right of the invert with the lowest value of 0.05 mm/m measured at the right side.

In Figure 6.16 the distribution of the recorded strain of the second layer at the last conducted

measurement at the end of the continuous monitoring period is depicted. The maximum compressional strain value w.r.t. the reference measurement is 1.87 mm/m located at the left shoulder. At the left side wall tension with 0.09 mm/m is recorded.

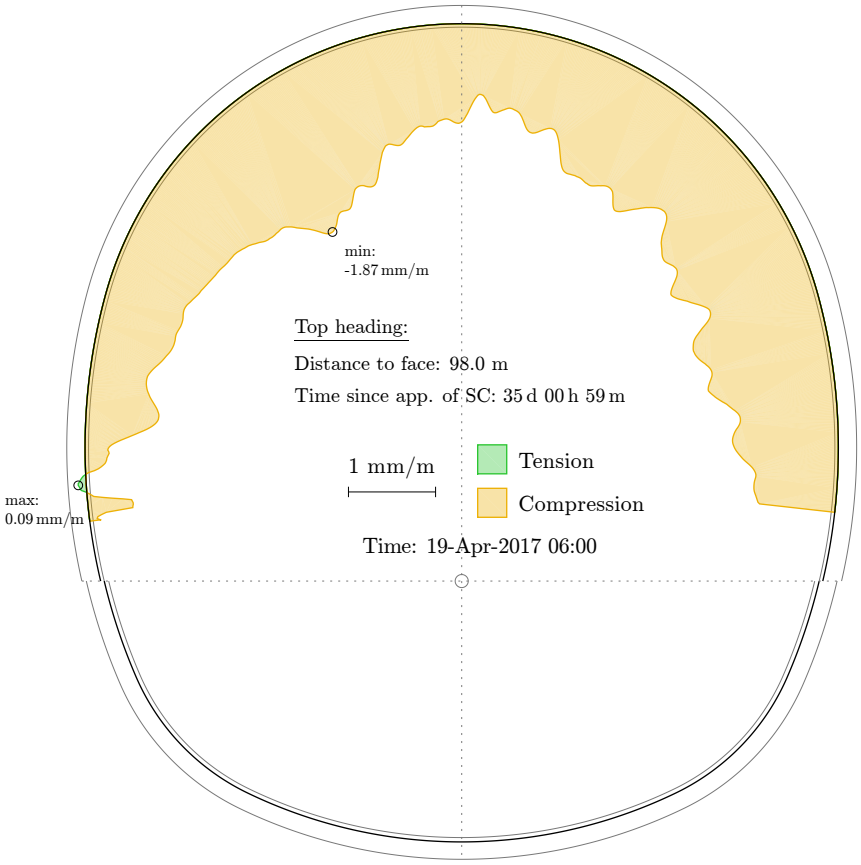

Figure 6.16: Circumferential distribution in strain of the second layer at the last measurement of the continuous monitoring period.

6.2.2 Longitudinal Direction

This section shows the results for the fibre-optic sensing cables installed in longitudinal direction at both layers within the shotcrete lining. The changes in strain w.r.t. the reference measurement are plotted in a colour scale. All graphs show the specific time at which the measurement is conducted, the time since the application of shotcrete as well as the distance to the face of the respective heading.

In the early stages after installation at the top-heading (Figure 6.17(a)), the rock side layer shows tensile strain at a magnitude around 0.5 mm/m at the longitudinal sections of the fibre-optic sensing cable. 30 h later (Figure 6.17(b)) the values have not changed considerably.

The longitudinal sections at the second layer do not show a significant change in strain in the early stages after excavation for the cable installed at the initial round and the cable that stretches over the initial and the next round. The recorded changes in strain since the reference measurement are around zero after 6 h (Figure 6.17(c)) and slight compression 30 h later (Figure 6.17(d)).

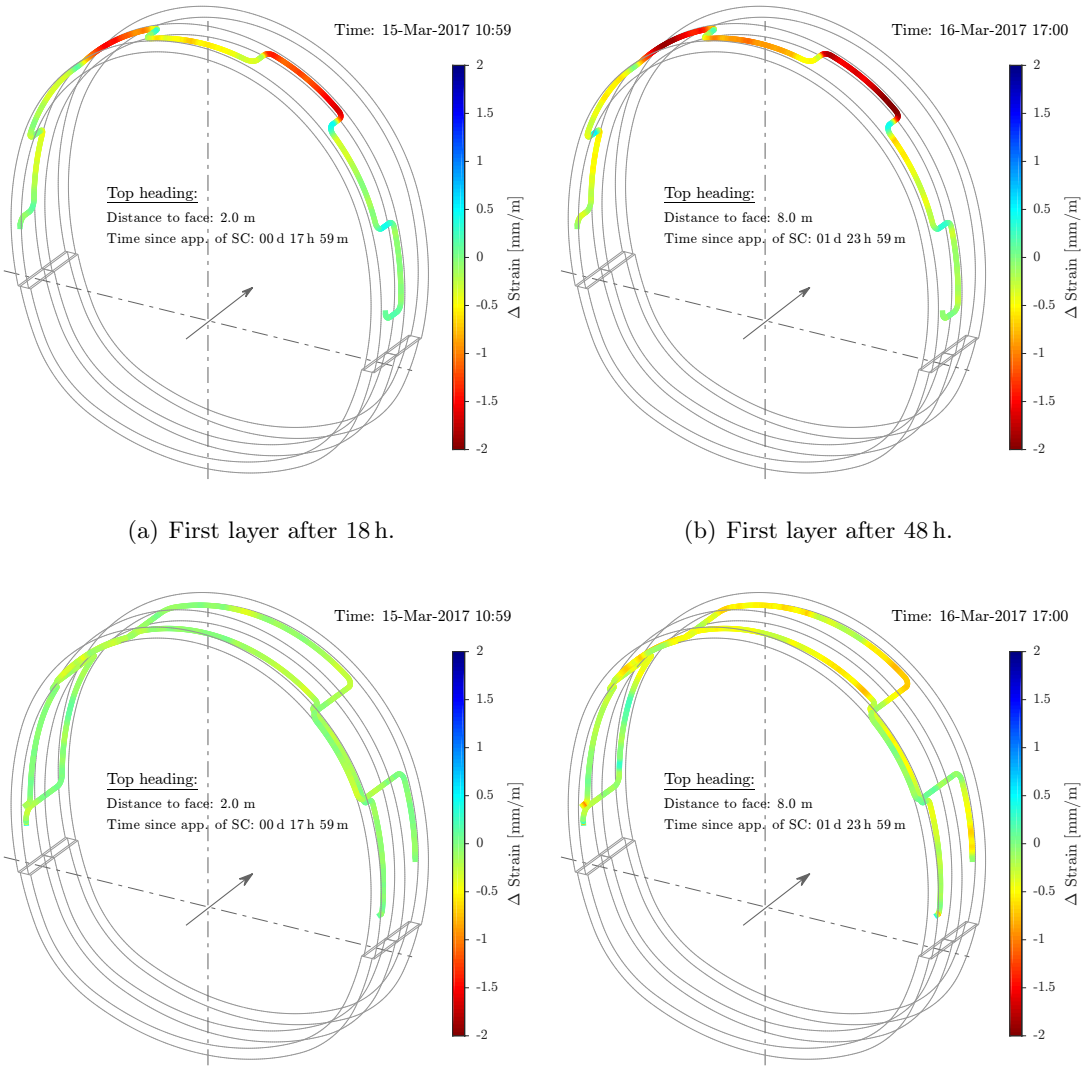

(a) First layer after 18 h.

(b) First layer after 48 h.

(c) Second layer after 6 h.

(d) Second layer after 36 h.

Figure 6.17: Longitudinal distribution in strain of first and second layer at the early stages after installation at the top-heading.

Looking at the circumferential strain of the first layer, it can be seen that compression at the shoulders develops faster at the cable segments which are located closer to the face. This trend continues after further advance. The second layer does not show this behaviour in such a distinct manner.

Figure 6.18 shows the longitudinal distribution in strain at the last measurement of the continuous monitoring period for the rock side layer. At the top-heading the longitudinal sections of the fibre-optic sensing cable show strain in the form of compression up to about 0.5 mm/m at the upper side walls. At the longitudinal sections for the shoulders and the crown, the strain values are not showing a consistent behaviour, hence making it difficult to display one expressive numerical strain value for the respective section.

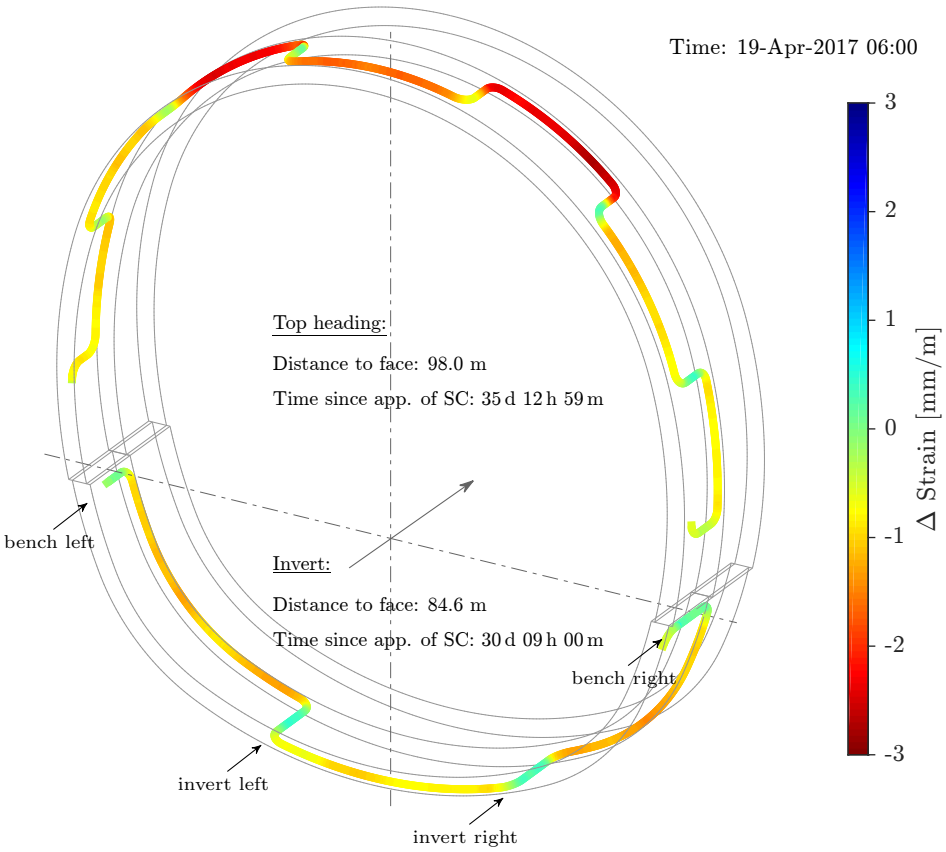

Figure 6.18: Longitudinal distribution in strain of the first layer at the last measurement of the continuous monitoring period.

At the invert the longitudinal strain behaviour is different compared to the top-heading. The changes in strain show the opposite sign meaning tension acting within the invert lining in advance direction.

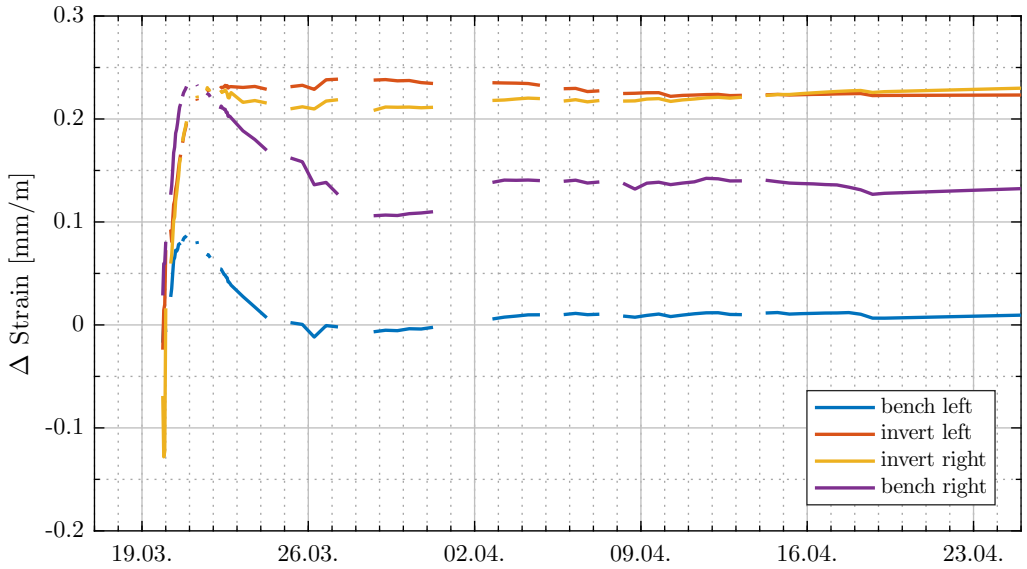

Figure 6.19: Averaged changes in strain of the longitudinal fibre-optic sensing cable sections at the invert over the course of the continuous monitoring period.

To see and understand the development of this behaviour over time better, the recorded values of changes in strain at the longitudinal sections of the fibre-optic cable installed at the invert are averaged and plotted over the course of the continuous monitoring period (see Figure 6.19).

The changes in strain left and right of the invert are increasing quickly after excavation. Both reach a value of about 0.23 mm/m in tension after only one day and remain constant around this magnitude afterwards. The longitudinal section at the right bench also shows this drastic growth in strain, but drops afterwards over the period of one week to a constant strain level of approximately 0.14 mm/m.

The peak after excavation is also observable at the left bench, however, smaller in magnitude. During one week the strain level decreases to an end level of zero strain in longitudinal direction.

Figure 6.20 shows the longitudinal distribution in strain at the last measurement of the continuous monitoring period for the cavity side layer. The longitudinal sections of both lines of fibre-optic sensing cables show a rather inconsistent behaviour, hence making it difficult to display one expressive numerical strain value for the respective section.

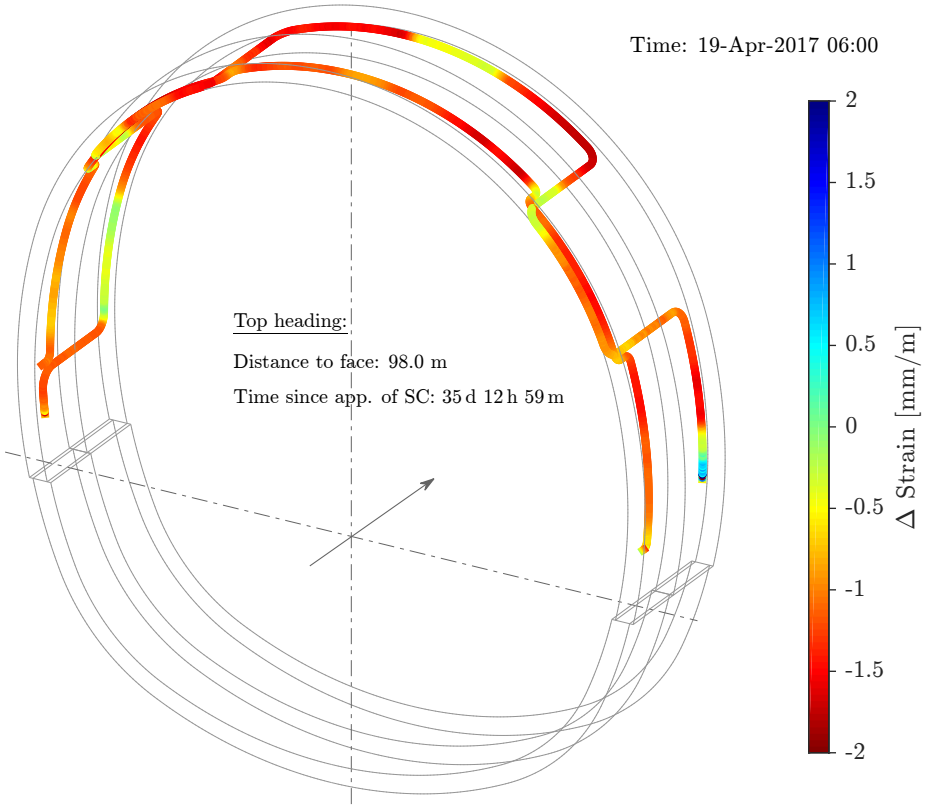

Figure 6.20: Longitudinal distribution in strain of the second layer at the last measurement of the continuous monitoring period.

6.3 Results of Additional Measurements

As mentioned in section 5.1.2, additional measurement equipment is installed at both top-heading and invert of monitoring cross-section *MS-1439* (for exact positions see Figure 5.5) to compare and verify the results of the fibre-optic instrumentation. The installation and the data acquisition of these additional measurements is not part of this thesis, however, their results are presented here.

Data is read out once a day beginning with the installation of the fibre-optic measurement system until the end of the continuous monitoring period (during the Easter break no readings were done). After that, readings are done on a weekly basis.

6.3.1 Strain Gages

6.3.1.1 Strain Measurement

Figure 6.21 displays the recorded data of the tangential, pairwise installed strain gages at the top-heading. Two series particularly stand out in this graph. On the one hand, the outer gage of the left pair (SG2) shows a relatively low level of change in strain compared to the other points and on the other hand, the outer point of the right pair (SG3) shows a much higher level of change in strain compared to the other points.

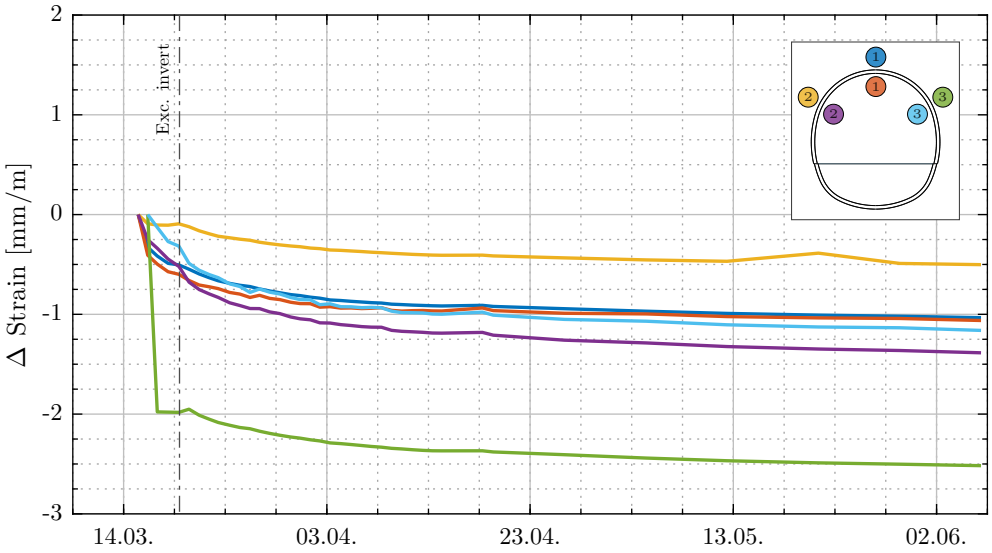

Figure 6.21: Change in strain recorded by strain gages at the top-heading of *MS-1439*.

The remaining points at the top-heading show a more or less similar behaviour with about the same incremental increase of strain change at the beginning and an end level in change of strain around 0.9–1.2 mm/m.

Figure 6.22 depicts the changes in strain for the pairwise, tangentially installed strain gages at the invert. It can be seen that both invert points show a different behaviour in the sense of accumulating strain over time. Their increase happens over a longer period of time compared to the very steep trends of the points to the right and left after installation. The two spikes around April 8th are most likely artefacts in the data and not actual values in terms of change in strain within the lining.

The end level of strain change is the same for all points with one exception with about 0.9–1.4 mm/m. The outer gage of the left pair (SG4) shows an overall lower course with a lower end level around 0.45 mm/m.

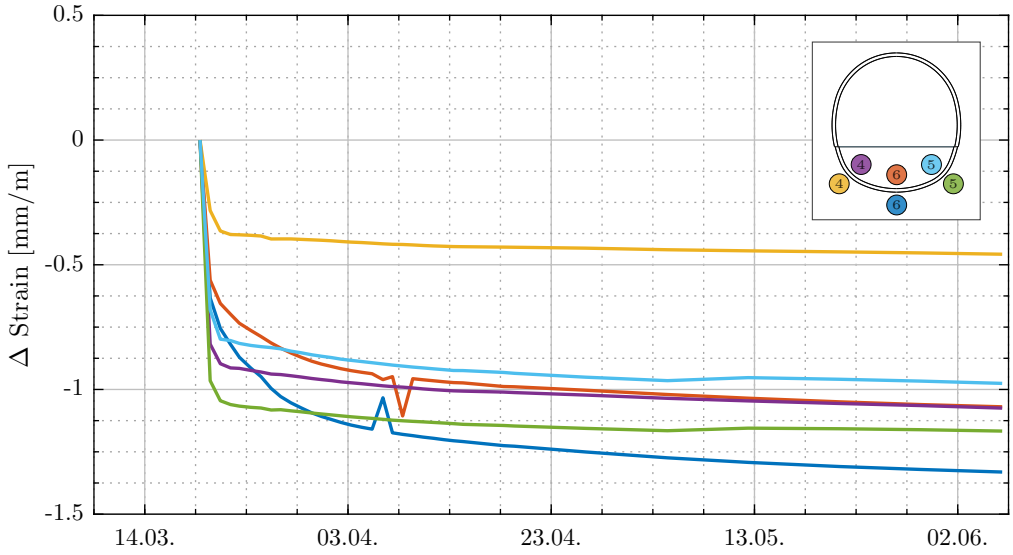

Figure 6.22: Change in strain recorded by strain gages at the invert of *MS-1439*.

6.3.1.2 Temperature Measurement

Figure 6.23 shows the evolution of temperature within the lining of the top-heading. The first measurement is conducted after spraying the initial layer of shotcrete and thus missing the 'zero-measurement' before the application of shotcrete.

With the highest temperatures after the days of installation, the end level of approximately 20 °C for all points is reached after about 15 days. As mentioned in section 5.2, the decrease in temperature due to the construction stop at Easter (April 14th to April 18th) is not only visible in the recorded air temperature (see Figure 5.7) inside the tunnel at *MS-1439*, but even noticeable in the temperature inside the concrete itself.

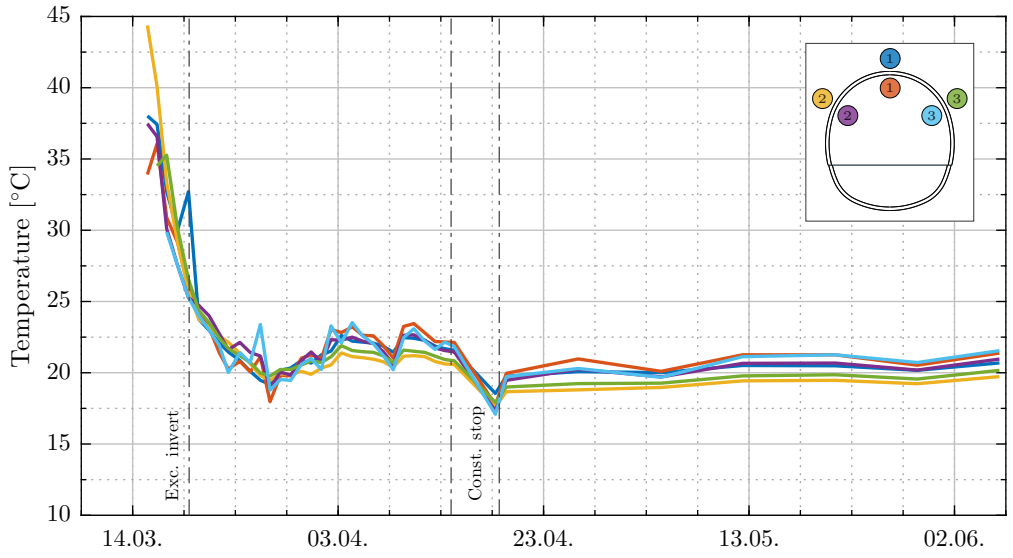

Figure 6.23: Change in temperature recorded by strain gages at the top-heading of *MS-1439*.

At the invert (Figure 6.24) the end level temperatures are about 5 °C lower compared to the top-heading. This circumstance can probably be attributed to the backfill material resting on the invert lining and thereby preventing it from getting warmer due to the increased air

temperature caused by the construction vehicles inside the tunnel. After April 26th, a slight, yet constant increase of the points left and right to the invert is observable.

The temperature of the shotcrete right after construction is significantly lower (difference approximately 12.5 °C) for both invert points. The other measuring points show a temperature about the same level as for the top-heading points after the application of shotcrete.

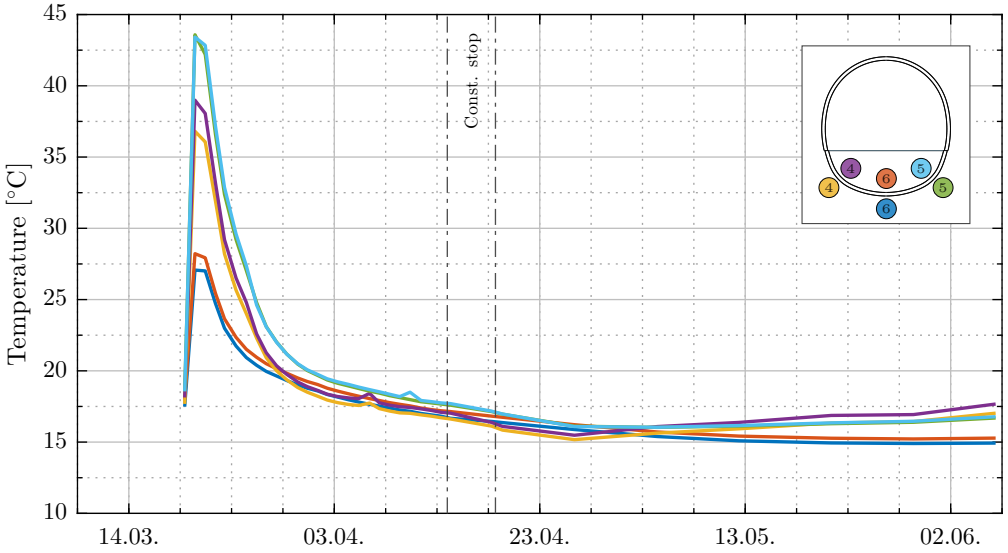

Figure 6.24: Change in temperature recorded by strain gages at the invert of *MS-1439*.

6.3.2 Pressure Cells

6.3.2.1 Radial

The graph in Figure 6.25 displays the pressure recorded by the radially installed pressure cells at the top-heading. At the early days after installation the pressure rises at the crown and the right shoulder of the tunnel until it drops at the time of excavating the invert.

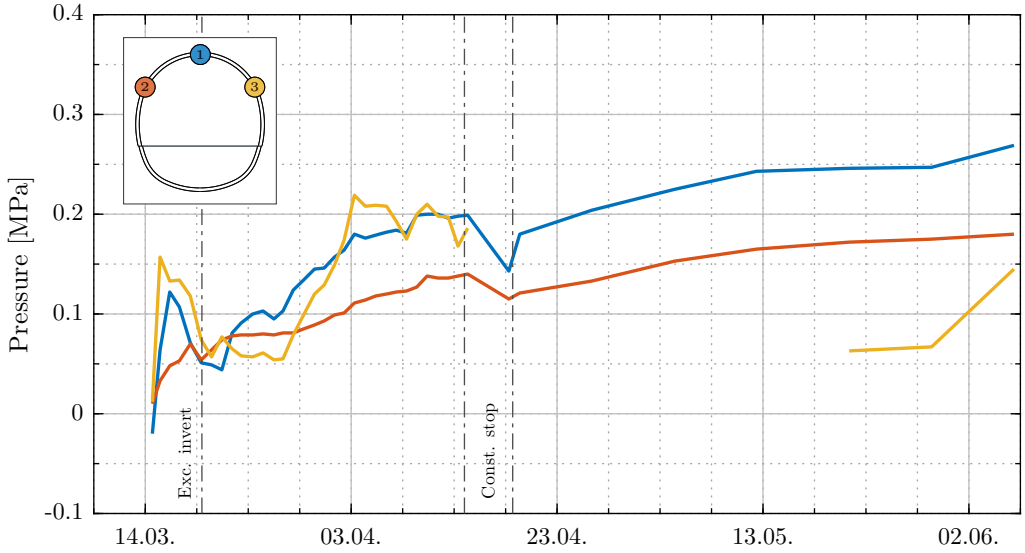

Figure 6.25: Radial pressure recorded by pressure cells at the top-heading of *MS-1439*.

Afterwards it increases again for both points to about 0.2 MPa until April 12th. The left shoulder point shows a more constant, yet lower increase compared to the other ones. As the

readings are out of range for the right shoulder point (PC3,r) after April 14th, a gap is present in the graph.

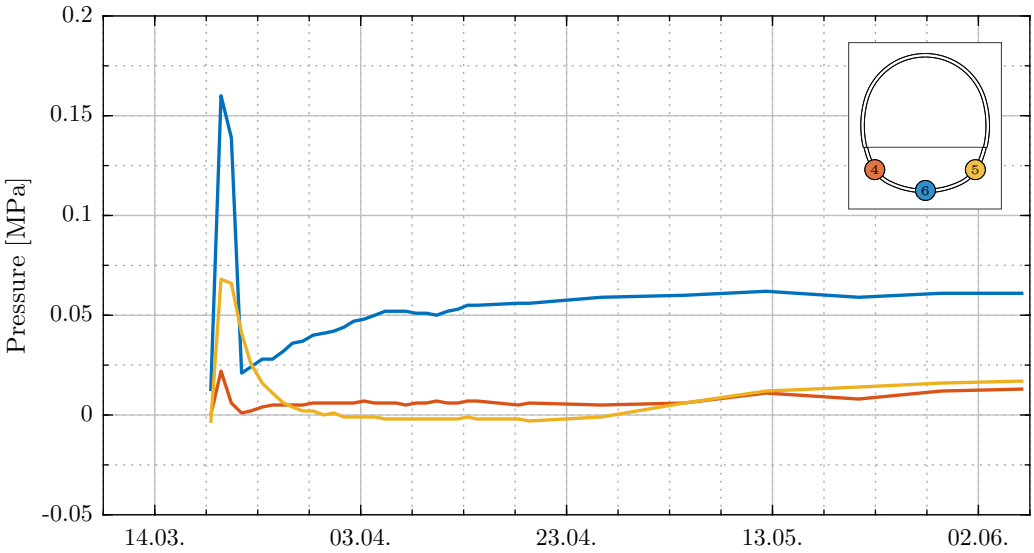

Figure 6.26: Radial pressure recorded by pressure cells at the invert of *MS-1439*.

For the invert the recorded radial pressure is plotted in Figure 6.26. For the first three days after installation all three points show a rapid increase of radial pressure followed by a drop to almost the initially recorded value. The invert point (PC6,r) has the most pronounced gain in pressure, whereas the side points, especially the left one (PC4,r), show this behaviour in a way smaller magnitude.

After these first three days the radial pressure at the invert point increases again to about 0.06 MPa. Both points left and right of the invert stay around zero radial pressure after ten days.

6.3.2.2 Tangential

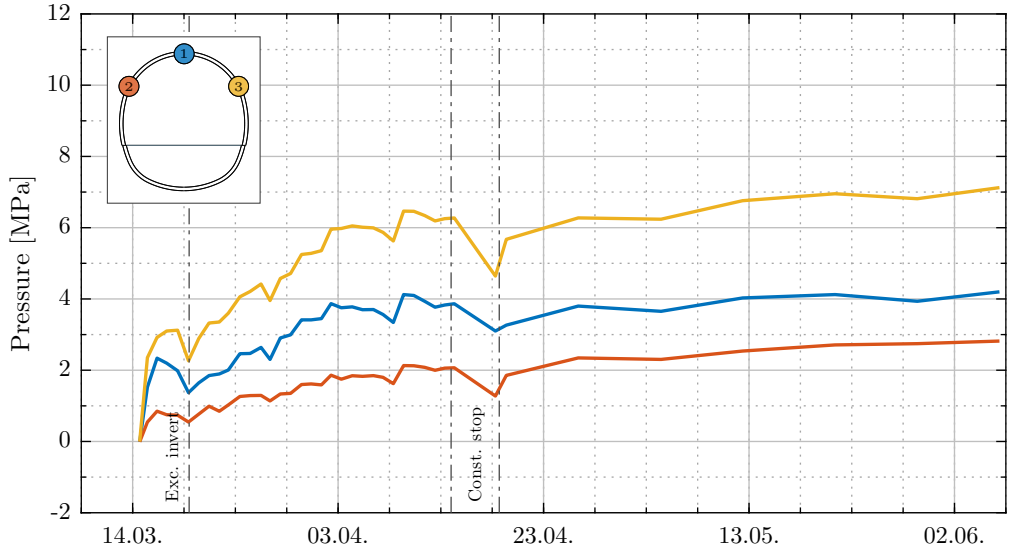

Figure 6.27: Tangential pressure recorded by pressure cells at the top-heading of *MS-1439*.

Figure 6.27 displays the tangential pressure recorded at the top-heading. All three points almost show an identical evolution of the tangential pressure although on different levels of magnitude with the right shoulder (PC3,t) being the highest, the crown (PC1,t) in the middle and the left shoulder (PC2,t) the lowest.

The excavation of the invert is observable as a slight drop in the graph. The decrease in tangential pressure around April 18th may be due to the construction stop at Easter.

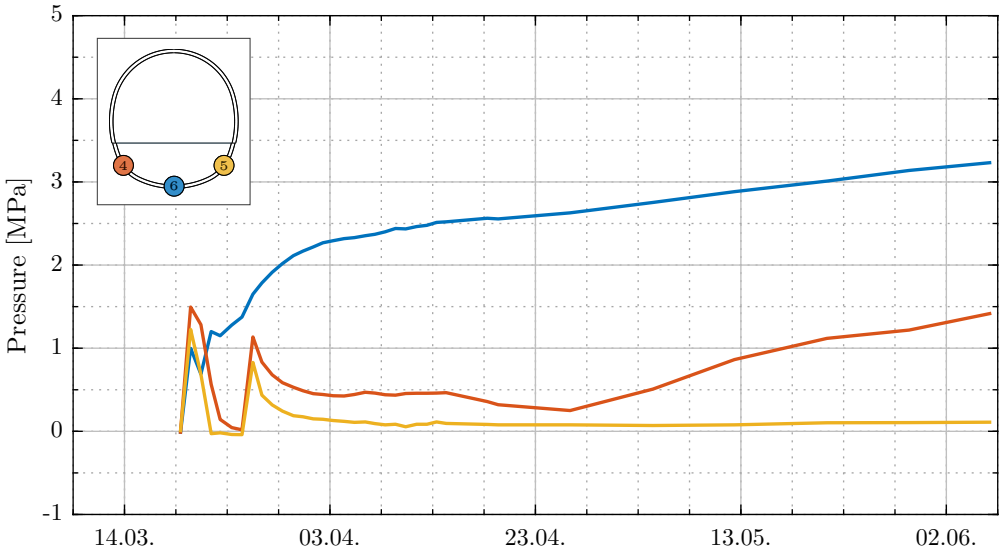

Figure 6.28: Tangential pressure recorded by pressure cells at the invert of *MS-1439*.

The tangential pressure for the invert (Figure 6.28) shows a clearly visible increase for the invert point (PC6,t). The other points show an increase only for the first day after installation followed by a drop to zero afterwards. The cells PC4,t and PC5,t are re-pressurised on March 25th but the pressure falls off to zero again. After one month the cell situated at the left side starts recording an increase of tangential pressure in the lining.

As the results of the measured changes in strain neither by the fibre-optic system nor by the strain gages indicate any decrease during the mentioned construction stop, the given circumstances suggest that a possible temperature dependency of the used pressure cells is present. Both radial and tangential installed pressure cells show this decrease in pressure at the time of the construction stop where also the temperatures inside the concrete decreases (see section 6.3.1.2).

7 Interpretation

The following sections cover the interpretations of the results presented in chapter 6 of the fibre-optic measurements at *MS-1439* in coherence with the given geologic situation (see chapter 2) as well as an interpretation of the deformations considering the recorded displacement data of the conventional monitoring targets.

In addition, a comparison of the fibre-optic measurement data with the recorded changes in strain of the installed strain gages and a comparison with back-calculated strains of the software TUNNEL:SUITE is conducted.

7.1 Deformations

Looking at the deformation of monitoring section *MS-1439*, an asymmetric behaviour is observable (see Figure 7.1 to Figure 7.3). The left part of the tunnel profile deforms to a greater extent than the right part. This is the case for the deformation in vertical direction (downwards), in horizontal direction (towards the excavation) and in longitudinal direction (against the direction of the drive).

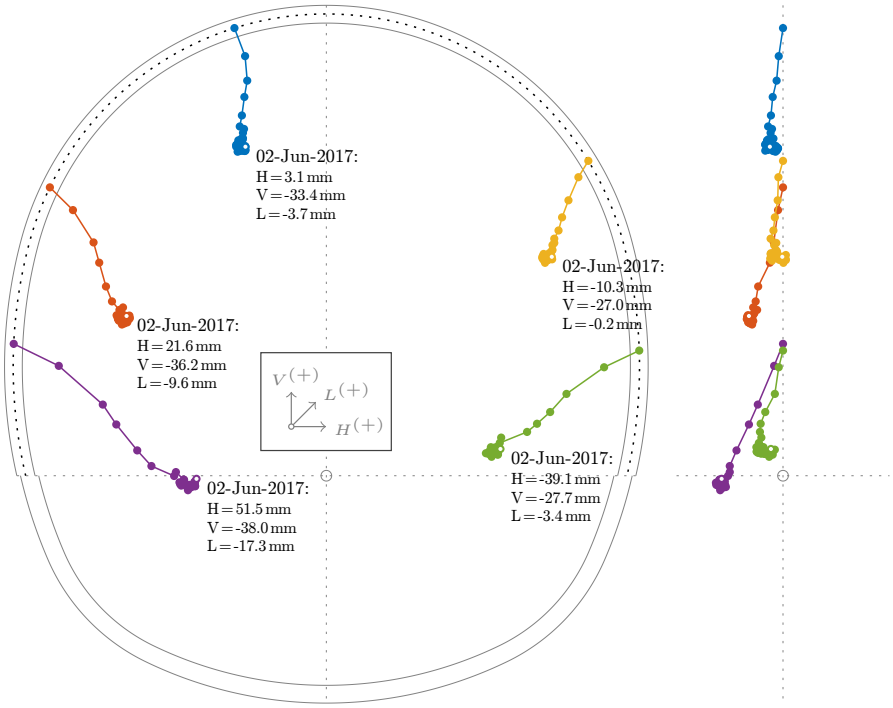

Figure 7.1: Recorded displacements of monitoring targets at *MS-1439*, cross-sectional view on the left side, longitudinal view on the right (display up-scale factor = 50).

As the foliation is not well-defied (mechanically less/not effective) due to the tectonic overprinting (for geology see chapter 2), it is assumed that discrete faults parallel to the foliation cause the asymmetry of the deformation in longitudinal direction.

Several faults cross the rock mass next to the monitoring section *MS-1439* (see Figure 2.2 and Figure 2.3(c)), striking the tunnel face in an acute angle, most of them dipping vertically. With a sub-vertical to vertical alignment of mechanically effective discontinuities – in this case faults – the cross-section deforms asymmetrically as long as the orientation of the discontinuities' strike deviates from the one of the tunnel face (see Figure 7.4). This phenomenon is independent whether the discontinuity dips in or against the direction of the drive.

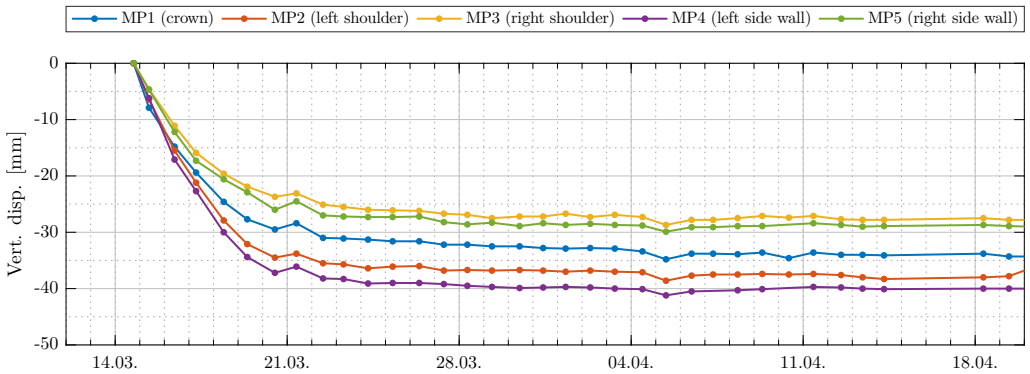

(a) Evolution of vertical displacements of monitoring targets at *MS-1439*.

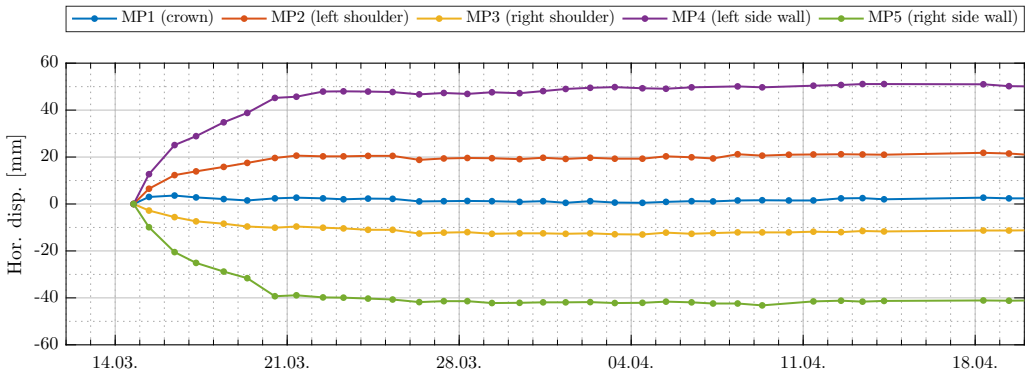

(b) Evolution of horizontal displacements of monitoring targets at *MS-1439*.

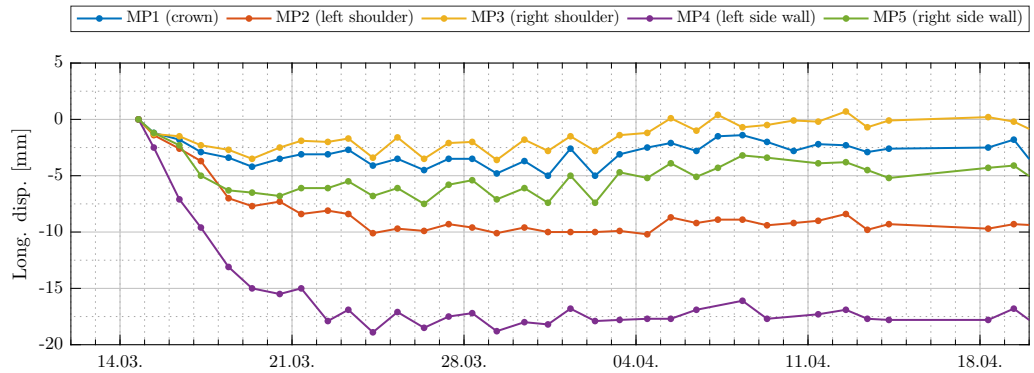

(c) Evolution of longitudinal displacements of monitoring targets at *MS-1439*.

Figure 7.2: Recorded displacements of monitoring targets at *MS-1439* (the sign of the ordinates correspond with the definition in Figure 7.1).

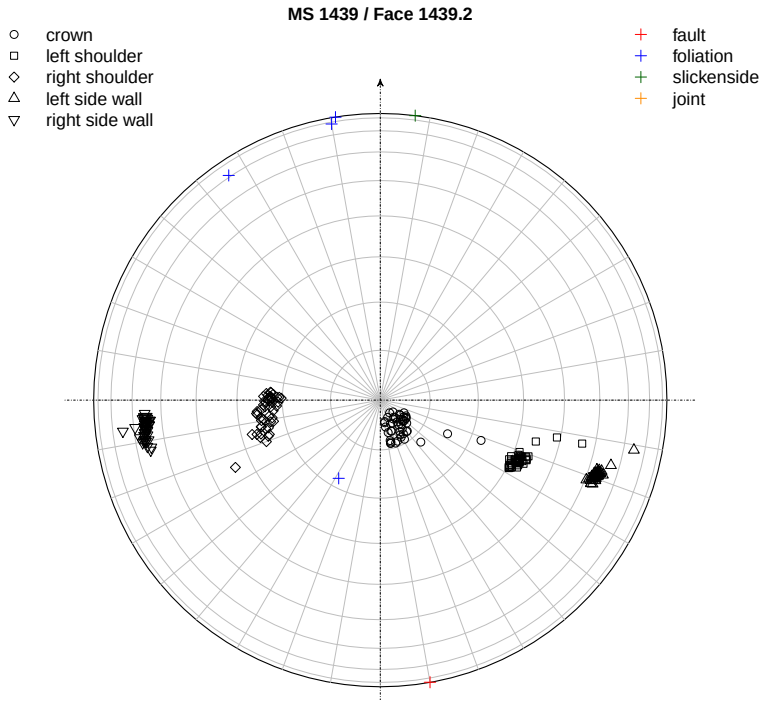

Figure 7.3: Stereographic plot of the recorded deformations at *MS-1439* including the major geological features mapped of the tunnel face at chainage 1439.2 m.

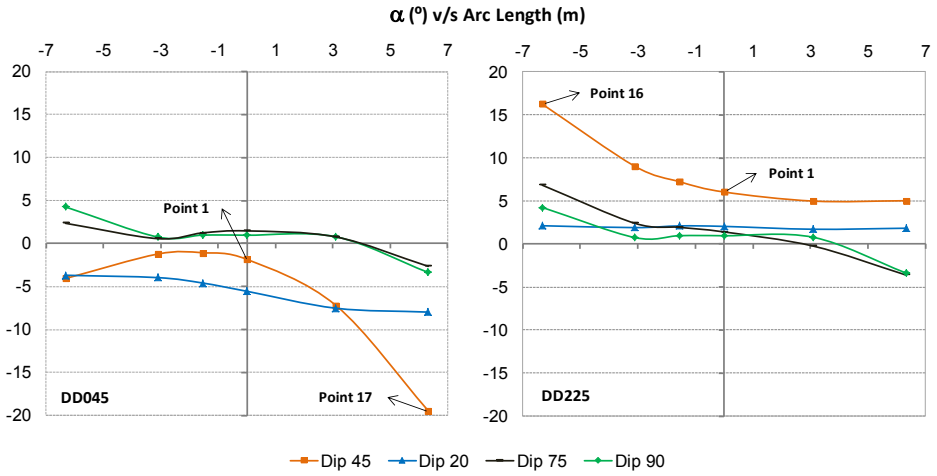

Figure 7.4: Comparison of resulting vector orientations α (i.e. ratio of longitudinal to vertical displacement) of numerically analysed headings trough a transversally isotropic rock mass (planes of weakness with specific dip and dip direction. Tunnel axis strikes N-S) after Davila Mendez (2016). Note that the author uses a reversed sign convention for α. Point 1 at crown, point 16 at left shoulder, Point 17 at right shoulder.

Because of kinematic restrictions, failure of discontinuities (sliding along discontinuity, opening of discontinuity) is more likely to occur at the left side of the tunnel section than at the right side.

Within bigger fault zones isotropic conditions (lateral pressure coefficient $k_0 \approx 1$) regarding the primary stress state are predicted (ÖBB-Infrastruktur, 2014), preferably because of the

high tectonic overprinting. Hence, the major difference in magnitude between the horizontal displacements at the side walls (left: 52.5 mm, right: −39.1 mm) and the vertical displacements at the crown (−33.4 mm) is probably not caused by the stress state.

A 2D numerical calculation confirms that under isotropic stress conditions an excavation profile with relatively high side walls and a short roof arch – as it is the case for the study at hand – larger deformations occur at the side walls than at the crown.

For a circular excavation profile the deformations at the side walls and at the crown are more or less the same. The characteristic of this phenomenon, however, certainly depends on several conditions (e.g. location and orientation of anchors relative to the primary orientation of discontinuities, which determine their efficiency significantly).

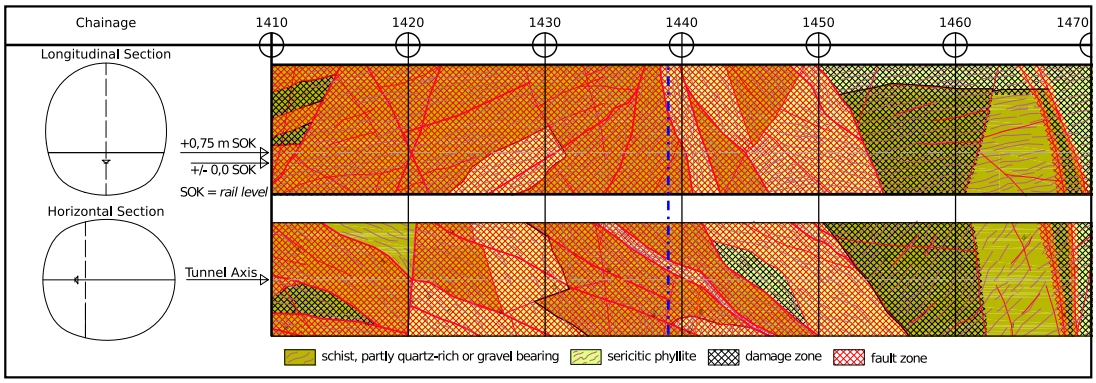

Figure 7.5: Longitudinal section (top) and horizontal section (bottom) of Tunnel Gloggnitz, track 1 including the major geological features. The vertical blue line shows the location of the monitoring section *MS-1439*.

Figure 7.5 shows the longitudinal section view (top) and the horizontal section view (bottom) of tunnel Gloggnitz, track 1 from chainage 1410 m to 1470 m including the geology and main rock mass features.

Assuming that the stronger schist layer mapped at the face at chainage 1423.2 m (see Figure 2.3(a), area A) passes the monitoring section *MS-1439* close to the right, and considering the stronger schist layer mapped at the face at chainage 1441.2 m (see Figure 2.3(e), area B) situated ahead of the right part of the tunnel face at chainage 1439 m, both conditions might explain the difference between the deformation of the left side wall and the deformation of the right side wall, the latter deforming less due to the stronger rock mass zones in the vicinity.

The major part of the displacements (approximately 80 %) develop within the first ten days (see Figure 7.2). The magnitude of the displacements in longitudinal direction is in the range of the measurement accuracy being the reason for alternating changes of the displacement trend even after one month.

7.2 Fibre-optic Measurement

In this section certain significantly observed behaviours, effects or circumstances present in the results of the fibre-optic measurements are explained and interpreted. Note that the presented interpretation is only valid for the observed chainage. Also not every minor alteration of the changes in strain can be explained entirely, as there are many influencing factors. An attempt to describe and explain the major observed behaviours is made.

As presented in section 6.1.1, the changes in strain of the first layer of fibre-optic cables for

points close to the crown experience a high level of incremental change at the very early stages (≈ 12 h). Figure 7.6 displays changes in strains at MP1 (crown) for the first two days after installation where the described effect is most prominent including the construction sequence for the top-heading.

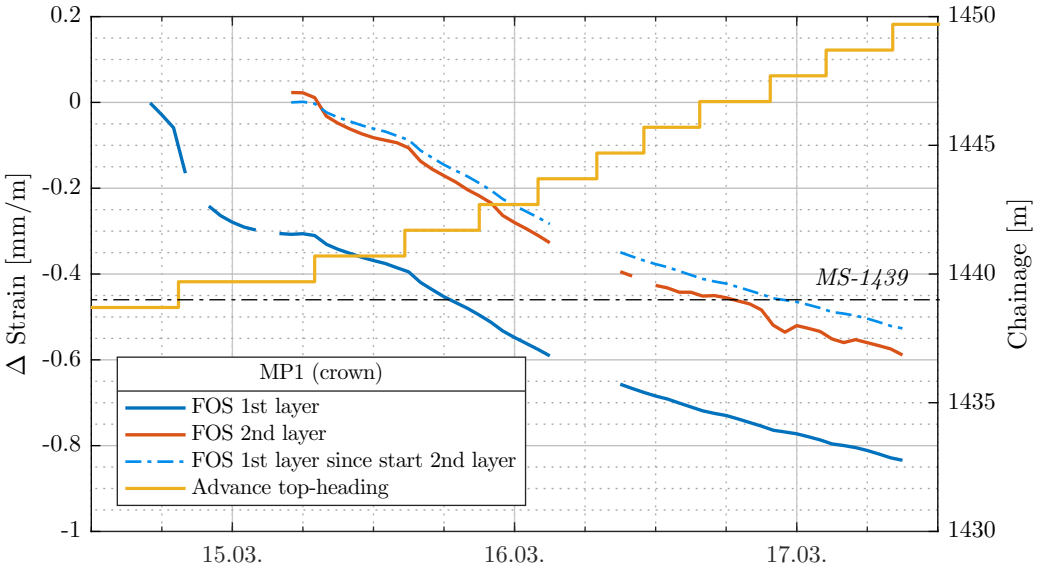

Figure 7.6: Changes in strain in the first two days after installation at MP1 (crown) including the advance of the top-heading.

This behaviour can be explained looking at the given construction sequence between March 14th at 6:00pm and March 15th at 12:00 Noon. As the first layer of shotcrete for the round length, which comprises the main part of the fibre-optic instrumentation, is completed, the continuous measurement starts for the first layer of cable lines in this round. Afterwards the next round is excavated before the application of the second layer of shotcrete and installation of the second layer of fibre-optic cables in the first round.

In other words, the recorded steep increase of changes in strain in the first layer is caused by the excavation of the next round. As soon as the excavation of this second round is finished, the second layer of shotcrete (including the installation of the second layer of fibre-optic cables) is applied at the first and second round in one working step. This also explains the decrease in the gradient of the recorded data of the first layer of fibre-optic cables after March 15th 6:00am, since now both layers of shotcrete are effective.

The excavation of the invert has major influence on the strain development in the lining of the top-heading. As presented in section 6.1.1, especially the first layer of fibre-optic cables at the side walls of the top-heading (points closest to the invert) indicate a notable decrease around the time of the invert construction.

As it can be seen in Figure 7.7 for the point at the left side wall (MP4), this decrease starts about four rounds (≈ 8 m) before the monitoring section and stops (respectively continues to increase again) as soon as the invert is installed at *MS-1439* (ring closure).

In contrast, the second layer indicates a slight increase in the gradient of the changes in strain four rounds before the invert is excavated at *MS-1439*. Figure 7.8 shows the evolution of changes in strain at the right side wall (MP5) where this increase of changes in strain of the second layer is even more striking.

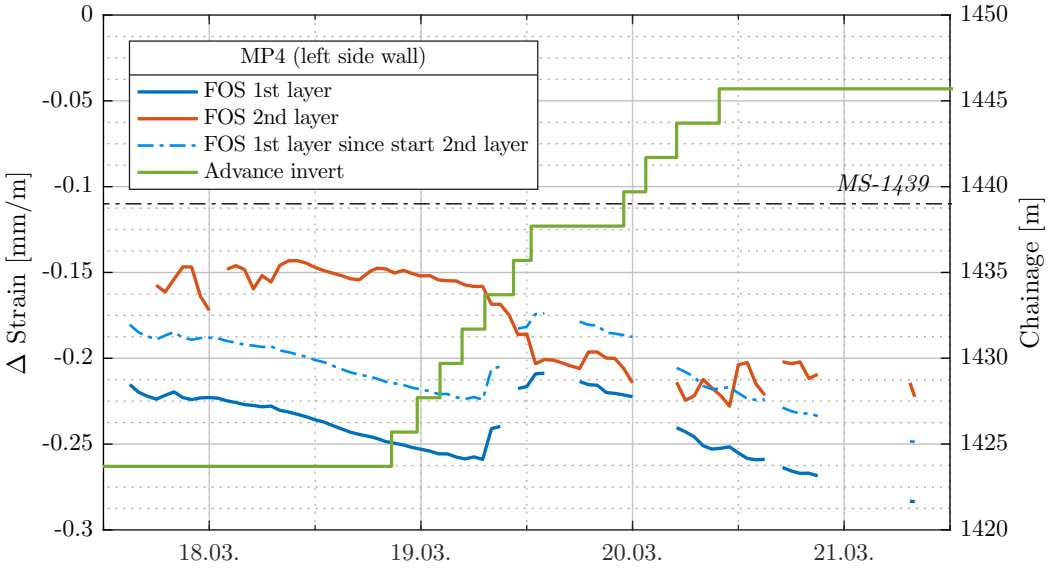

Figure 7.7: Changes in strain at the time of invert excavation at MP4 (left side wall) including the advance of the invert.

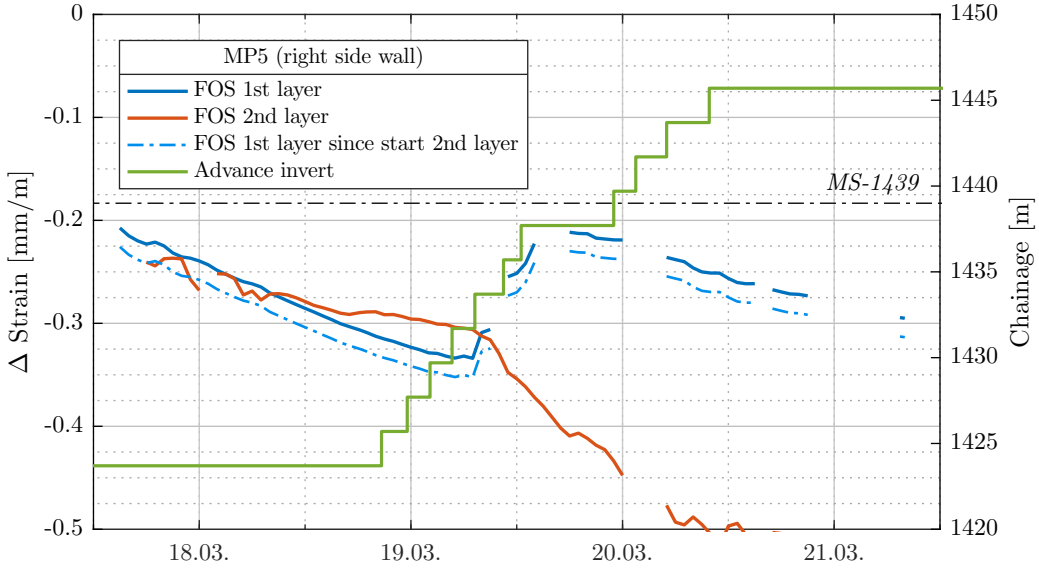

Figure 7.8: Changes in strain at the time of invert excavation at MP5 (right side wall) including the advance of the invert.

The above stated behaviour suggests that the excavation of the invert causes a reduction of compressional strain – and therefore stress – at the rock side layer of shotcrete with a simultaneous growth of compression at the cavity side area of the lining at the top-heading side walls.

As a consequence of the observed strain difference of the rock and cavity side area of the lining, it might be the case that a counter clockwise bending moment forces the top-heading foots to move slightly horizontally in the direction of the cavity (and maybe even upwards) shortly before the excavation of the invert at *MS-1439*.

7.3 Comparison FOS with Strains Recorded by Strain Gages

This section compares the results of the installed pairwise strain gages (see section 6.3) with the recorded data of both layers of fibre-optic sensing cables in circumferential direction, plotted relatively to the times of the first reading of the respective strain gages.

7.3.1 Top-heading

It can be seen that for the crown and the left shoulder point (Figure 7.9 and Figure 7.10), the cavity side second layer of strain gages and the corresponding layer of fibre-optic sensing cables almost show a congruent strain history (particularly the left shoulder point).

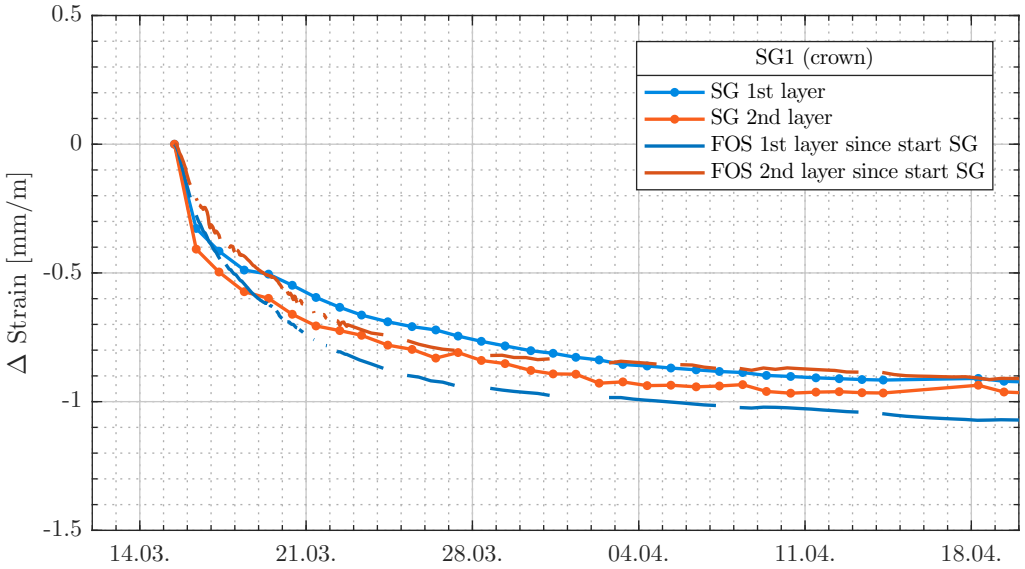

Figure 7.9: Comparison of the evolution of change in strain of the fibre-optic sensing cables in circumferential direction with the strain gages at SG1 (crown).

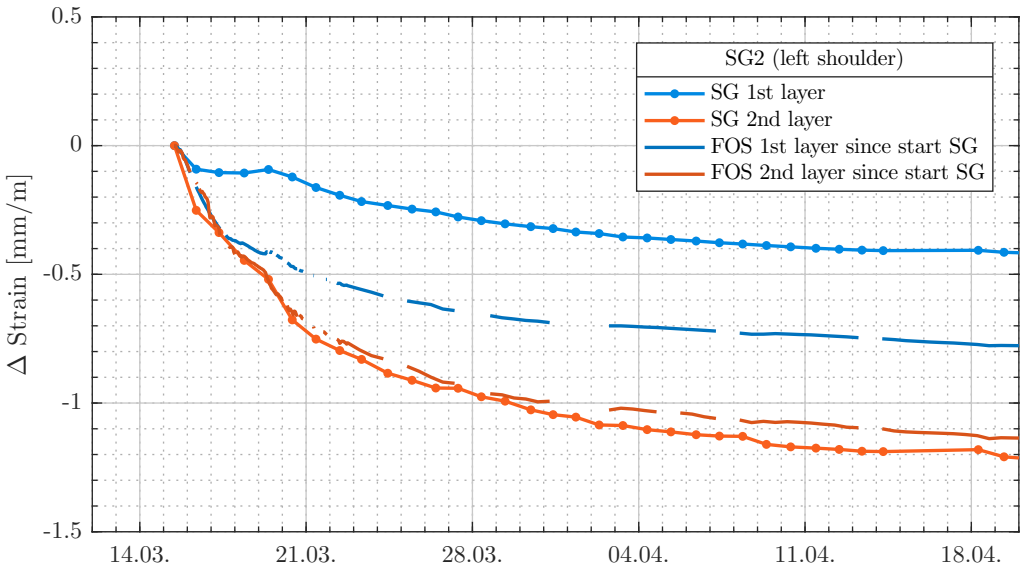

Figure 7.10: Comparison of the evolution of change in strain of the fibre-optic sensing cables in circumferential direction with the strain gages at SG2 (left shoulder).

The data of the rock side first layer does also show a good agreement. However, the end levels of change in strain at the crown are about 0.2 mm/m and at the left shoulder roughly 0.35 mm/m off the strains measured by the strain gages.

For the right shoulder point (Figure 7.11) a good agreement can also be observed for the data of the second layer as specific points in time like the excavation of the invert are visible at both curves (fibre-optic and strain gage). The data of the rock side strain gage shows an unrealistic high level of magnitude and can therefore be neglected. Most likely a random error occurred during the zero reading.

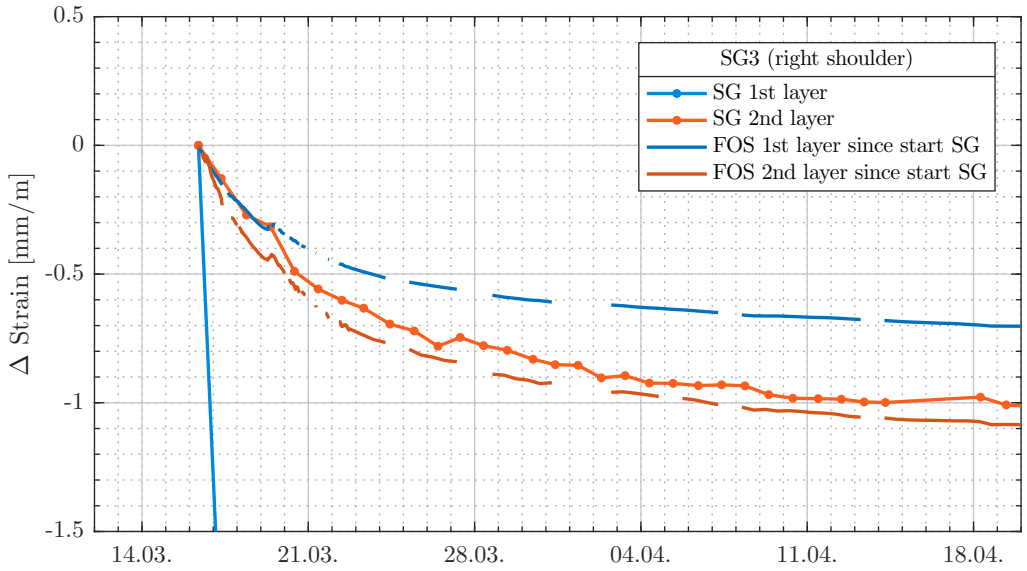

Figure 7.11: Comparison of the evolution of change in strain of the fibre-optic sensing cables in circumferential direction with the strain gages at SG3 (right shoulder).

The reason for the deviations between the strain measured by the fibre-optic system and the strain gages might be the different positions of the sensors in relation to each other in longitudinal direction (direction of the drive). The strain gages are situated in the middle of the round, whereas the fibre-optic sensing cables are installed behind with an offset of about 20 cm for the second layer and 45 cm for the first layer (measured against direction of the drive). Therefore it can be said that the presented results of the fibre-optic measurements show overall a very good agreement with the data from the strain gages.

7.3.2 Invert

At the point located left of the invert the data of the fibre-optic measurements show good accordance with the data of the strain gages (Figure 7.12). At the early stages, the data of the strain gages show a rather rapid increase of change in strain compared to the fibre-optic data, which show a more steady increase over time after an initial drop on the first day of measurement.

The measurement point situated to the right of the invert (Figure 7.13) shows a deviation of nearly 0.5 mm/m amongst the two different measurement systems. Also the tensional strain at the beginning recorded by the fibre-optic sensing cable is not present in any way in the data recorded by the strain gage.

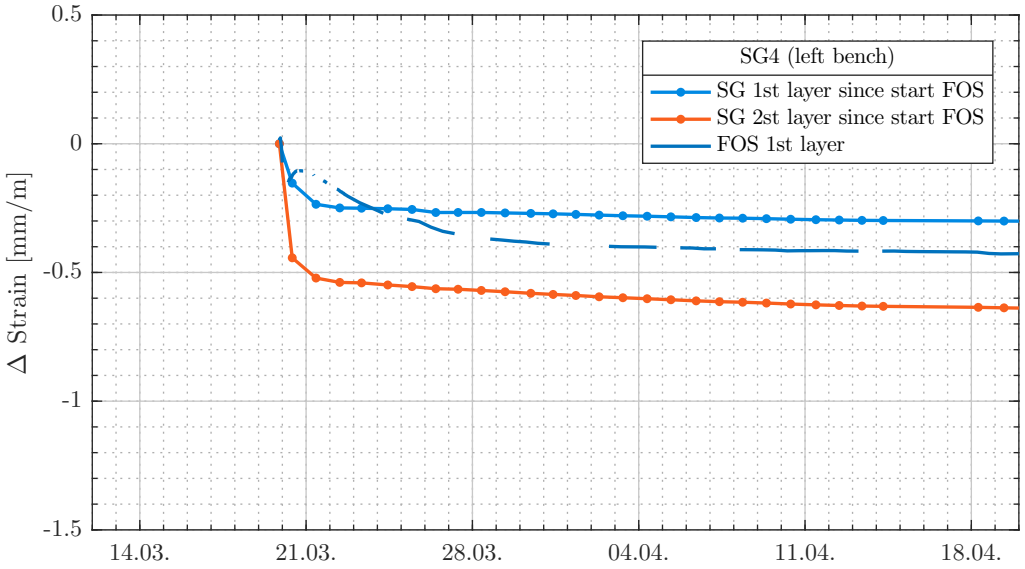

Figure 7.12: Comparison of the evolution of change in strain of the fibre-optic sensing cables in circumferential direction with the strain gages at SG4 (here called left bench).

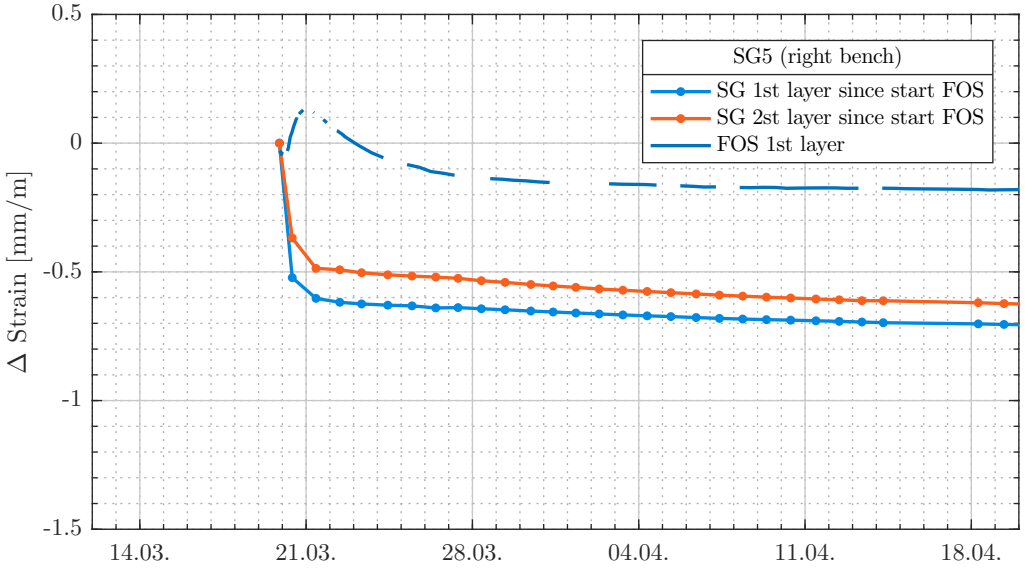

Figure 7.13: Comparison of the evolution of change in strain of the fibre-optic sensing cables in circumferential direction with the strain gages at SG5 (here called right bench).

For the invert point (Figure 7.14) the course of the changes in strain at the first layer show a fairly good agreement both in shape and magnitude. The slight divergence (about 0.2 mm/m) may again be caused by the different locations of the sensors inside the lining as explained before.

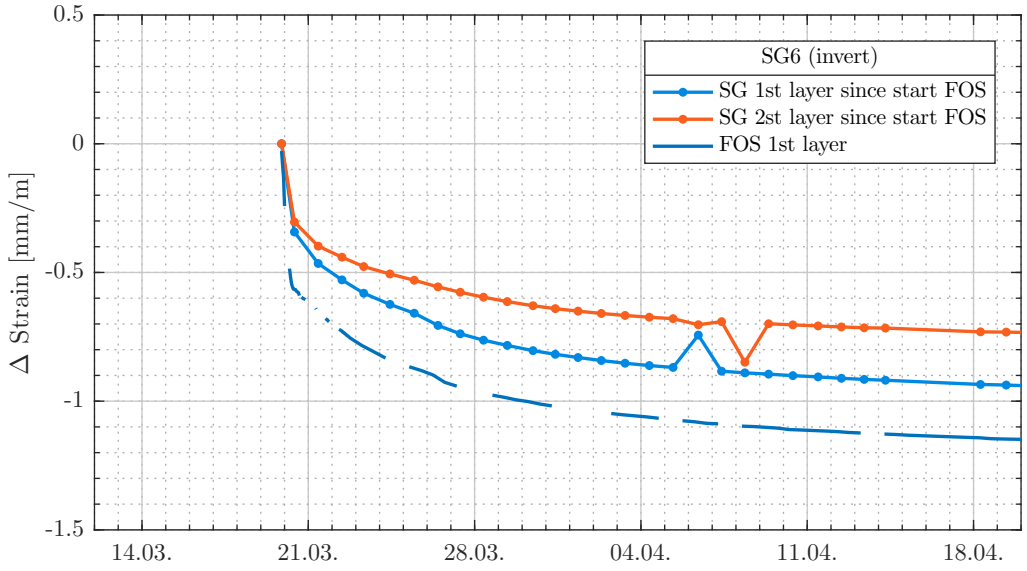

Figure 7.14: Comparison of the evolution of change in strain of the fibre-optic sensing cables in circumferential direction with the strain gages at SG6 (bottom of the invert).

7.4 Comparison FOS with Calculations of TUNNEL:SUITE

This section shows a comparison of the changes in strain recorded by the fibre-optic measurement system and strain calculated by the software TUNNEL:SUITE.

The software solution TUNNEL:SUITE can be utilised to present and analyse geotechnical measurement data and is used for the entire SBT project. State diagrams (influence curves), distance-time diagrams, displacement paths, calculated strains within the lining as well as a full 3D visualisation of the degree of utilisation of the lining can be displayed with this software (TUNNEL:MONITOR, 2004).

Due to the intern mechanism of TUNNEL:SUITE computing the strains utilising geometrical changes of the monitoring targets (vertical and horizontal displacements), the position of the targets are considered as points of discontinuities (mathematical issue) along the circumference of the tunnel. Therefore, interpolated points in between the monitoring points, here called evaluation points (EPs), are used for the comparison as they provide a better representation of the intended outcome.

Note that for the calculation of the strains TUNNEL:SUITE uses the chord length between the monitoring points since the movement of interpolated points is not known. Further calculations are applied to transfer the strain to the tunnel lining. Figure 7.15 shows the location of these evaluation points in reference to the monitoring points.

The following graphs display the changes in strain recorded by the fibre-optic measurement system for the first and second layer of fibre-optic sensing cables in circumferential direction at the top-heading and the strains calculated by TUNNEL:SUITE respectively at the four described evaluation points.

The data of the first layer of the fibre-optic sensing cables as well as the data from TUNNEL:SUITE are plotted relative to the moment of the first reading of the second layer of the fibre-optic sensing cable to get comparable graphs. The way of presenting the fibre-optic results is the same as described in section 6.1, meaning the strains are averaged over 30 cm of cable length (see Figure 6.1).

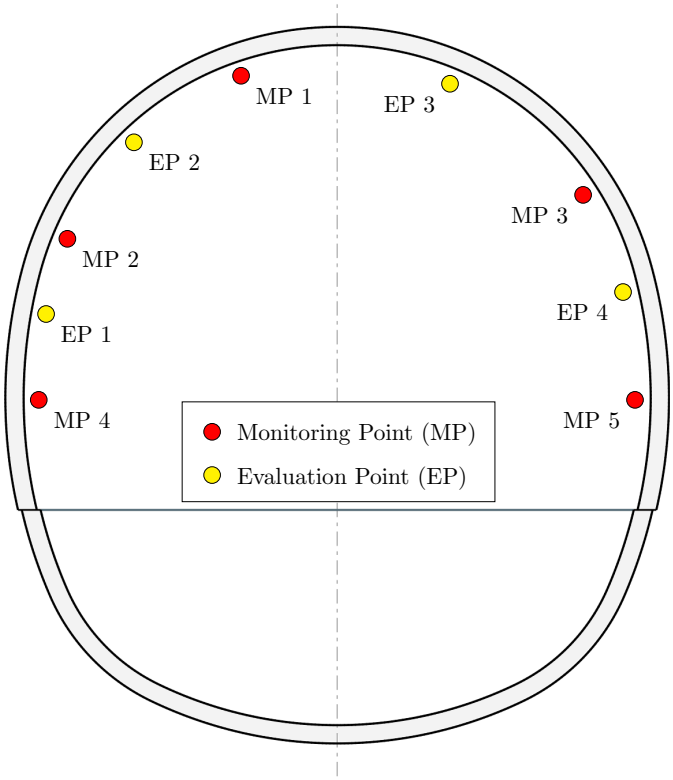

Figure 7.15: Positions of the points used for evaluation (EPs) with respect to the position of the monitoring points (MPs) for the comparison of the measured changes in strain and the calculated strain by the software Tunnel:Suite.

After a certain time (about two weeks) the changes in strain calculated by Tunnel:Suite show a non-smooth behaviour. This circumstance can be attributed to the measurement noise arising from the displacement recordings of the geodetic targets.

Therefore the following graphs also show the standard deviation (1σ) (plotted as yellow dashed line) computed via the length variations of the cord lengths between the monitoring targets as they displace over time. The average measurement precision of the 3D geodetic targets is assumed with 1 mm.

This calculation does not attribute all possible deviations since the exact computation algorithm used by Tunnel:Suite is not known and therefore only represents an approximation. It is, however, a consistent approach to observe the influence of the measurement precision of the monitoring targets on the calculated results.

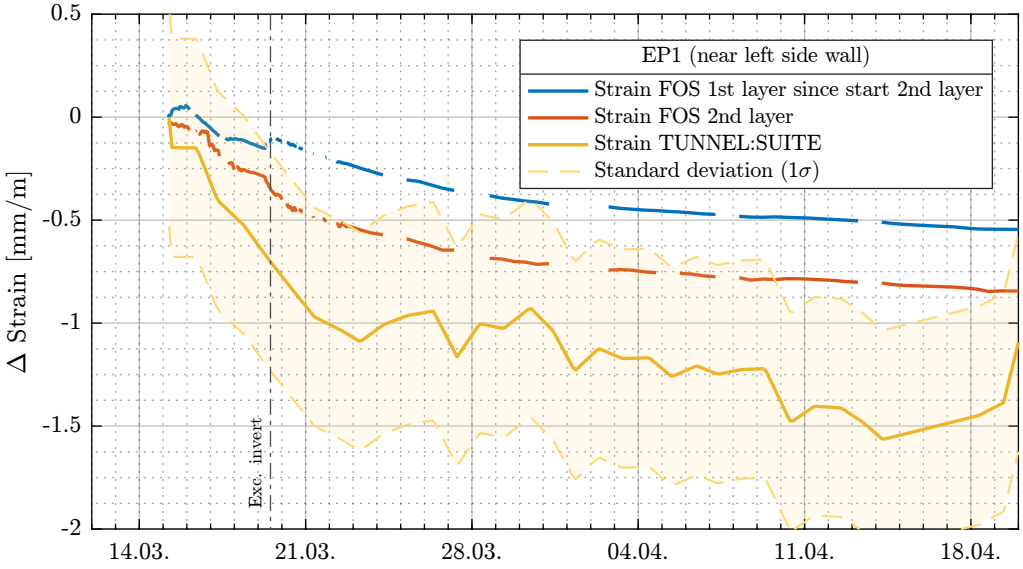

Figure 7.16: Comparison of the evolution of change in strain of the fibre-optic measurement in circumferential direction at the top-heading and the strain calculated by TUNNEL:SUITE at EP1 (near left side wall).

Figure 7.16 displays the evolution of the measured changes in strain and the strain calculated by TUNNEL:SUITE at EP1 (near left side wall). It can be seen that the recorded data shows overall a lower level of magnitude of change in strain compared the calculated strain.

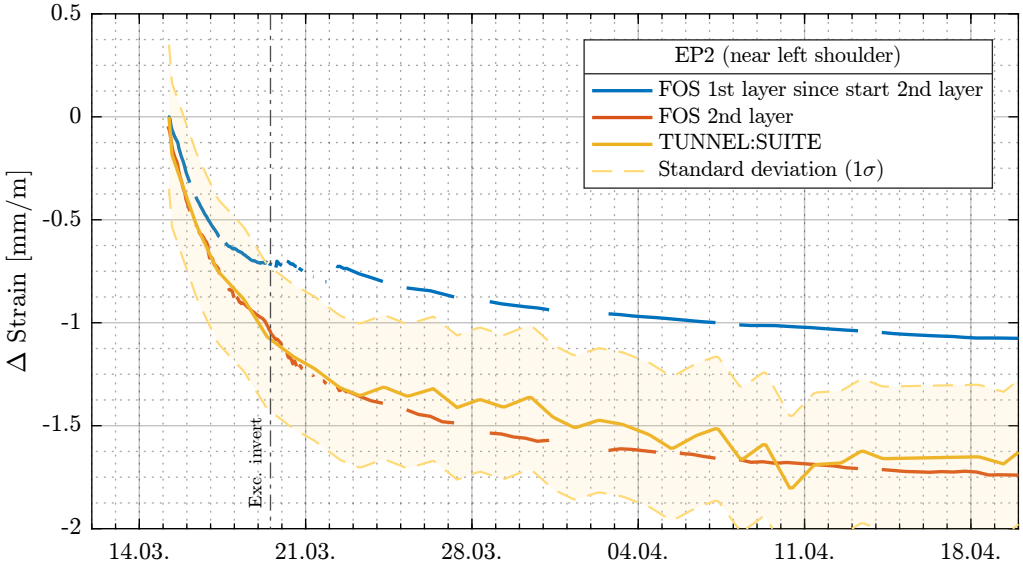

Figure 7.17: Comparison of the evolution of change in strain of the fibre-optic measurements in circumferential direction at the top-heading and the strain calculated by TUNNEL:SUITE at EP2 (near left shoulder).

Figure 7.17 shows the evolution of the measured changes in strain and the strain calculated by TUNNEL:SUITE at EP2 (near left shoulder). It can be seen that the recorded data of the second layer of the fibre-optic sensing cable shows a very good agreement with the calculated strain. The first layer of the fibre-optic sensing cable shows overall a lower level of magnitude than the calculated one.

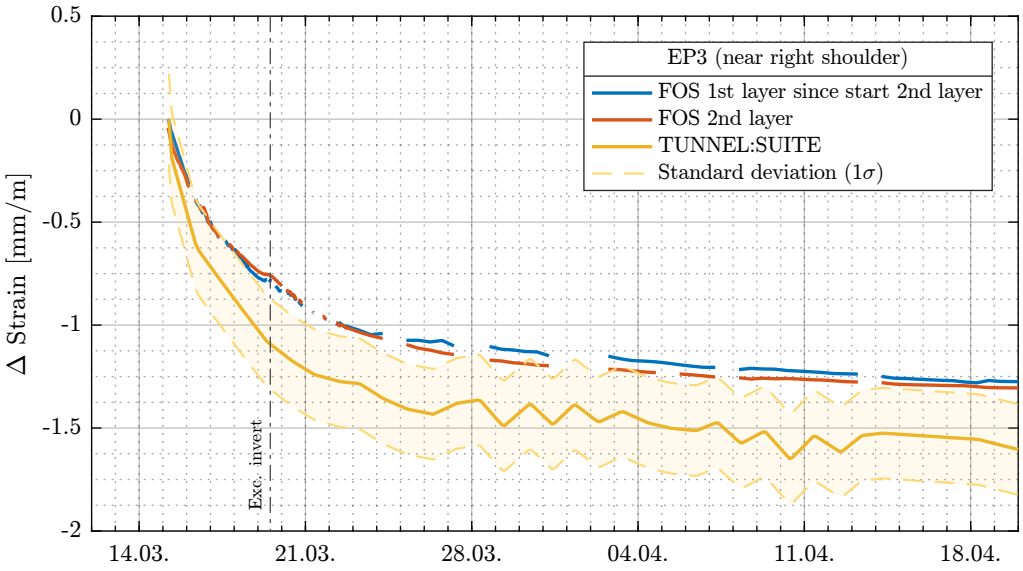

Figure 7.18: Comparison of the evolution of change in strain of the fibre-optic measurement in circumferential direction at the top-heading and the strain calculated by TUNNEL:SUITE at EP3 (near right shoulder).

In Figure 7.18 the evolution of the measured changes in strain and the strain calculated by TUNNEL:SUITE at EP3 (near right side wall) are displayed. It can be seen that the recorded data show a lower level of magnitude then the calculated one, the course, however, is very similar.

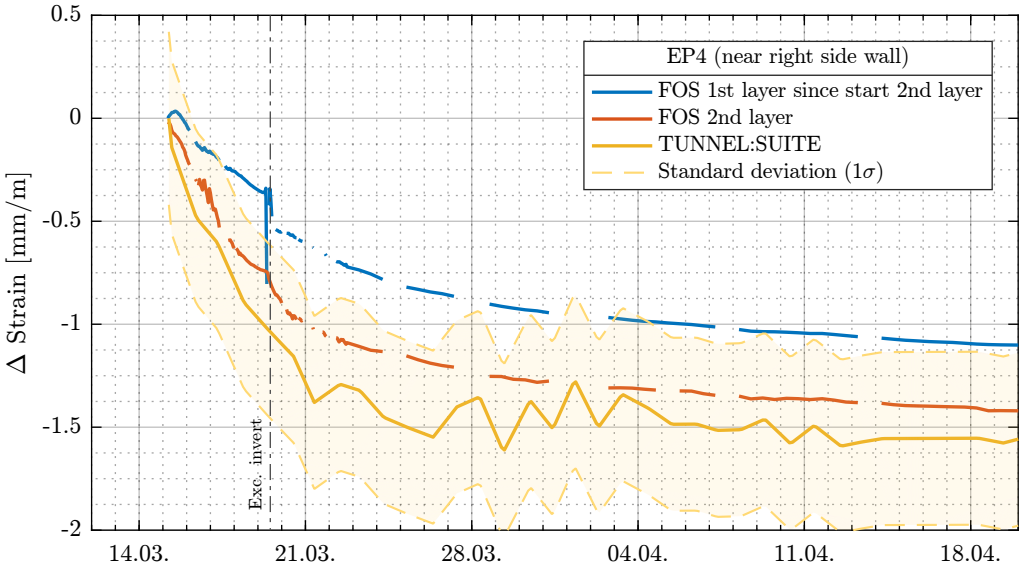

Figure 7.19: Comparison of the evolution of change in strain of the fibre-optic measurement in circumferential direction at the top-heading and the strain calculated by TUNNEL:SUITE at EP4 (near right side wall).

Figure 7.19 depicts the evolution of the measured changes in strain and the strain calculated by TUNNEL:SUITE at EP4 (near right shoulder). It can be seen that the recorded data show a lower level of magnitude then the calculated one, the course however is very similar.

To visualise the differences between the measured changes in strain and the calculated ones, Figure 7.20 shows the absolute distribution of changes in strain along the circumference of the tunnel at the given cross-section for an exemplary moment in time. Both layers of fibre-optic sensing cables are graphed in this plot (only compression present) as well as the strain computed by TUNNEL:SUITE.

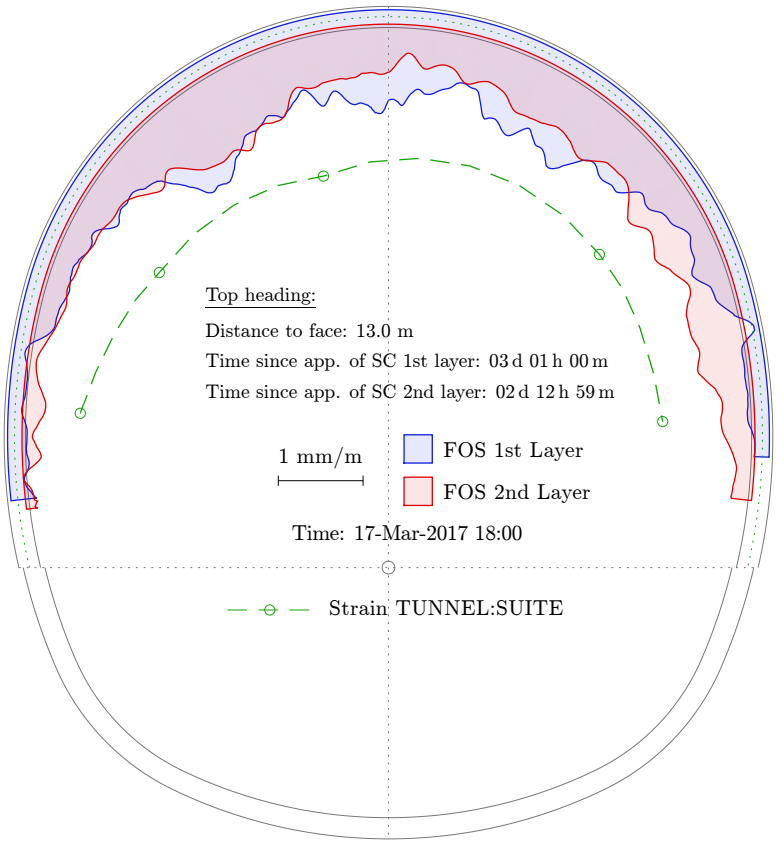

Figure 7.20: Comparison of the distribution of change in strain of the fibre-optic measurement in circumferential direction and the strain calculated by TUNNEL:SUITE (circles showing the monitoring points) for an exemplary moment in time.

The results are plotted orthogonal to the tunnel perimeter (analogous to the results presented in section 6.2). Note that the calculated strains of TUNNEL:SUITE are graphed beginning in the middle of the lining (dotted line), whereas the zero level of the measured strains is the respective cable line at its actual position within the lining.

Looking at the shown results, the fact that the calculated strains are larger in magnitude than the measured ones can be observed. Nevertheless, the overall back calculated strains show a fairly good agreement concerning the development over time. The differences in magnitude of the compared strains lie within a decent range considering the precision at which the displacements of the monitoring targets can be measured on site, which are then used by TUNNEL:SUITE to calculate the strains.

The fact that the calculated strains are larger than the measured strains can be seen as a conservative basis for further calculations done by TUNNEL:SUITE, e.g. the degree of utilisation of the lining, and for geotechnical judgement (e.g. evaluation of current excavation method and support measures).

8 Conclusion

8.1 Summary

In this thesis the planning, the installation and the evaluation of the recorded data of fibre-optic sensing cables within the shotcrete lining of a conventional tunnel drive are shown.

In a prior conducted pre-test important boundary conditions like cable type, cable layout or fixation method are evaluated in order to plan and conduct the main test in an optimal way. The main test itself comprises multiple lines of fibre-optic sensing cables installed in two different directions as well as at two different layers within the lining of the top-heading and of the invert to directly measure and record changes in strain. The installation process takes place during regular ongoing tunnelling and can be realised in about one and a half hours for both directions per layer for the installation at the top-heading and around two hours for each layer (both directions) at the invert.

In addition to the fibre-optic measurements, strain gages and pressure cells are installed in the cross-section under investigation to validate the data of the fibre-optic sensors.

The results of the conducted fibre-optic measurements are presented in different graphs, which show the development of the changes in strain over time, as well as with plots that show the distribution of the changes in strain around the circumference of the tunnel at a specific moment in time.

The fibre-optic results are compared to the results of the additional installed strain gages, showing a good overall conformity in both magnitude and shape for multiple investigated points along the tunnel perimeter. Furthermore, the fibre-optic results are compared to computed strains of the software Tunnel:Suite to investigate the integrity of the calculation approach used by this software.

8.2 Discussion

This thesis shows that the implementation of fibre-optic sensing cables in a tunnel lining has great potential due to some advantages in comparison to the conventional measuring techniques for recording strains within the lining (strain gages) in tunnelling. Also informations gained by 3D displacement monitoring targets can be supplemented with the data of the fibre-optic measurement system.

First of all it has to be mentioned that on the one hand, strains calculated with displacement recordings of monitoring targets are after all 'just' calculated values that can only be as coherent as the theoretical model on which the calculation is based on. On the other hand, devices like strain gages, which (directly) measure the changes in strain within the lining, are typically installed only at certain points along the tunnel circumference and can therefore only provide local information at these specific positions.

With the implementation of the fibre-optic sensing cables, recordings of the changes in strain within the lining are possible along the entire cable length, meaning also in between the positions of the monitoring targets or potential strain gages, as the whole fibre is a sensor.

The time consumption for the whole implementation process lies within a reasonable range considering the additional data gain and that the installation of the strain gages and pressure cells took more than twice as long as the installation of the fibre-optic instrumentation for this specific application.

On the downside the data processing and an appropriate presentation of the results is much more complex and therefore – at the moment – slower compared to the conventional displacement data presentation. However, as the data processing and the system as a whole are still under development, this circumstance can be resolved for future installations by improving the routines for processing and presentation.

Furthermore, it takes more time to install the fibre-optic sensing cables than to mount five geodetic monitoring targets, a circumstance which is, however, justifiable due to the additional gained information concerning the strain situation as described above. Nevertheless, no indication of any occurring displacements nor their specific direction can be made with the fibre-optic system which makes the use of monitoring targets essential.

Yet the biggest drawback for such a distributed fibre-optic system are its present costs, which are currently way higher than the mentioned conventional monitoring devices. Especially the measuring unit (OBR) is a major cost factor for such a project.

The used cable type *BRUsens strain V3* has shown that it can withstand the harsh environmental conditions inside a tunnel during its installation process and the given stress situation within the lining at the chainage under investigation due to its special steel armouring. The structured surface assures optimal bonding with the shotcrete. No indication of slippage could be observed. The provided accuracy of up to 1 µm/m and the achieved resolution of 2 cm are considered sufficient enough for the comparison with other monitoring data or to perform further research.

The fixation method of the fibre-optic sensing cables with cable ties offers a quick and adequate possibility to mount the individual cable lines. This can be done by the workers on site which confirms the general applicability of this system under the rather rough conditions of a tunnelling construction site. Simultaneously, the fixation is robust enough to sustain the application of shotcrete under full spraying performance. The used protective tube containing the cable for temperature compensation has shown a good performance as the smooth surface inside provides minor frictional resistance.

8.3 Outlook

As shown in this thesis, the implementation of fibre-optic sensing cables to directly record the changes in strain within the shotcrete lining of a tunnel is possible, but certain limitations at the given installation are present, which, however, could be improved for future applications.

For instance, the round length at the chainage of the main test with only 1 m is relatively short for the installation of cables in longitudinal direction. Respecting the minimal bending radius of the cables, the actual length in longitudinal direction is rather short. For possible installations and recordings in this direction a chainage with a larger round length is recommended.

Because of the unexpected and unrealistic behaviour of the linear standard coefficient of the used cable *BRUsens strain V3* to determine temperature values, it would be recommended to insert an additional, 'special temperature' cable into the protective tube, which houses the cable for temperature compensation of the measured changes in strain in order to directly measure the temperature development within the lining.

With the results of the fibre-optic strain measurement, a possible statement on the overall, real-time loading situation of the tunnel lining can be made in correlation with the geological situation documented at the respective chainage. Pressure cells provide – like the previously mentioned strain gages – only local information.

Furthermore, the stress distribution of the lining could be back calculated from the measured strains using different approaches like the improved Rate of Flow Method proposed by Aldrian (1991) (original Rate of Flow Method proposed by Schubert (1988)) or the much more recent adoption by Entfellner (2017), who made some modifications regarding the time dependent behaviour of the Young's modulus and compressive strength of modern shotcrete. Even more sophisticated models like the newly developed shotcrete model presented by Paternesi et al. (2016) or the thermochemomechanical material model proposed by Hellmich (1999) could be used. The latter is the basis of the software Tunnel:Suite for computing stresses from calculated strains.

For future applications it would be conceivable to measure more than one cross-section at once by simply connecting them via supply cables. With certain preparations a follow-up measurement of the installed fibre-optic sensing cables even after the construction of the inner lining would be possible, for instance, to investigate the long term structural integrity of the outer lining.

Bibliography

[Aldrian 1991] Aldrian, W. 1991. *Beitrag zum Materialverhalten von früh belastetem Spritzbeton.* PhD thesis, Montanuniversität Leoben, Austria.

[de Battista et al. 2015] Battista, N. de, Elshafie, M., Soga, K., Williamson, M., Hazelden, G. & Hsu, Y. S.: Strain monitoring using embedded distributed fibre optic sensors in a sprayed concrete tunnel lining during the excavation of cross-passages. In: *Proceedings of the 7th International Conference on Structural Health Monitoring of Intelligent Infrastructure* (2015), July. – Torino, Italy.

[Brugg Kabel 2012a] Brugg Kabel, AG: *Datasheet: BRUsens strain V3.* Version: 2012/09/12 Rev. 02 TH. Brugg, Switzerland, 2012.

[Brugg Kabel 2012b] Brugg Kabel, AG: *Datasheet: BRUsens strain V9.* Version: 2012/01/31 Rev. 01 TH. Brugg, Switzerland, 2012.

[Brugg Kabel 2013] Brugg Kabel, AG: *Datasheet: BRUsens temperature 85°C.* Version: 2013/02/22 Rev. 04 TH. Brugg, Switzerland, 2013.

[Davila Mendez 2016] Davila Mendez, J. M. 2016. *Displacements Analysis in Layered Rock Masses.* PhD thesis, Institute of Rock Mechanics and Tunnelling, Graz University of Technology, Austria.

[Entfellner 2017] Entfellner, M. 2017. *Prediction of Displacements and Shotcrete Lining Utilization – Decision strategy for a timely application of ductile support systems in conventional tunnelling.* Master's thesis, Institute of Rock Mechanics and Tunnelling, Graz University of Technology, Austria.

[Gehwolf et al. 2016] Gehwolf, P., Monsberger, C., Barwart, S., Wenighofer, R., Galler, R., Lienhart, W., Haberler-Weber, M., Moritz, B., Barwart, C. & Lange, A.: Deformation measurements of tunnel segments at a newly developed test rig. In: *Geomechanics and Tunnelling* 9 (2016), June, No. 3, pp. 180 – 187.

[Geokon 2016] Geokon, Incorporated: *Datasheet: 4200 Series: Concrete Embedment Strain Gages.* Version: Doc. Rev. H.1, 10/16. New Hampshire, USA, 2016.

[Geokon 2017] Geokon, Incorporated: *Datasheet: Model 4850: NATM Style Shotcrete Stress Cell.* Version: Doc. Rev. K.1, 01/17. New Hampshire, USA, 2017.

[Hellmich 1999] Hellmich, C. 1999. *Shotcrete as Part of the New Austrian Tunneling Method: From Thermochemomechanical Material Modeling to Structural Analysis and Safety Assessment of Tunnels.* PhD thesis, Institute for Strength of Materials, Vienna University of Technology, Austria.

[Lienhart 2015] Lienhart, W.: *Geotechnical Monitoring, lecture notes.* Lecture 8: Fiber Optic Sensors: An Overview, Part II, slide 9. 2015. – Institute of Engineering Geodesy and Measurement Systems, Graz University of Technology, Austria.

[Lin & Thaduri 2006] Lin, M. W. & Thaduri, J.: Structural Damage Detection Using an Embedded ETDR Distributed Strain Sensor. In: *Journal Of Intelligent Material Systems and Structures* 17 (2006), May, pp. 423 – 430.

[Lin et al. 2005] Lin, M. W., Thaduri, J. & Abatan, A. O.: Development of an electrical time domain reflectometry (ETDR) distributed strain sensor. In: *Measurement Science and Technology* 16 (2005), June, pp. 1495 – 1505.

[Luna Innovations 2014] Luna Innovations, Incorporated: *Datasheet: Optical Backscatter Reflectometer (Model OBR 4600).* LTOBR4600 REV.004 02/13/2014. Roanoke, USA, 2014.

[Monsberger et al. 2016] Monsberger, C., Woschitz, H. & Hayden, M.: Deformation Measurement of a Driven Pile Using Distributed Fiber-Optic Sensing. In: *Journal of applied geodesy* 10 (2016), March, No. 1, pp. 61 – 69.

[Monsberger et al. 2017] Monsberger, C., Woschitz, H., Lienhart, W. & Racansky, V.: Performance assessment of geotechnical structural elements using distributed fiber optic sensing. In: *Proc. SPIE 10168, Sensors and Smart Structures Technologies for Civil, Mechanical, and Aerospace Systems* (2017), April. – Portland, USA.

[Moser et al. 2016] Moser, F., Lienhart, W., Woschitz, H. & Schuller, H.: Long-term monitoring of reinforced earth structures using distributed fiber optic sensing. In: *Journal of Civil Structural Health Monitoring* 6 (2016), July, No. 3, pp. 321 – 327.

[ÖBB-Infrastruktur 2014] ÖBB-Infrastruktur, Aktiengesellschaft: *Geotechnische Prognose Untertage.* Semmering Basistunnel – Baulos SBT 1.1, Tunnel Gloggnitz. 2014.

[ÖBB-Infrastruktur 2015] ÖBB-Infrastruktur, Aktiengesellschaft: *ÖBB Corporate Blog: Die Bauabschnitte des Semmering Basistunnels.* `https://blog.oebb.at/die-bauabschnitte-des-semmering-basistunnels/`. Version: 15. August 2015. – (Cited 12. July 2017)

[ÖBB-Infrastruktur 2016] ÖBB-Infrastruktur, Aktiengesellschaft: *Semmering-Basistunnel – Die neue Dimension des Reisens (Infofolder).* 2016.

[ÖBB-Infrastruktur 2017a] ÖBB-Infrastruktur, Aktiengesellschaft: *Baugeologische Kurzzeitprognose VGLO-1 & 2: Subhorizontalschnitt.* Semmering Basistunnel – Baulos SBT 1.1, Tunnel Gloggnitz. 2017.

[ÖBB-Infrastruktur 2017b] ÖBB-Infrastruktur, Aktiengesellschaft: *Protokoll Baugeologische Vortriebsdokumentation.* Semmering Basistunnel – Baulos SBT 1.1, Tunnel Gloggnitz. 2017. – Tunnelmeter 1423.2, 1439.2 und 1441.2.

[Paternesi et al. 2016] Paternesi, A., Schweiger, H. F. & Schubert, P.: Verification of a rheological constitutive model for shotcrete through back-analysis. In: *Geomechanics and Tunnelling* 9 (2016), August, No. 4, pp. 356 – 360.

[Schubert 1988] Schubert, P.: Beitrag zum rheologischen Verhalten von Spritzbeton. In: *Felsbau* 6 (1988), No. 3, pp. 150 – 153.

[Schuller et al. 2014] Schuller, H., Riepler, F. & Schachinger, T.: Preliminary works for the new Semmering Base Tunnel – geotechnical monitoring of slope stabilization measures and earth retaining structures. In: *Geomechanics and Tunnelling* 7 (2014), August, No. 4, pp. 339 – 352.

[Singer et al. 2009] Singer, J., Grafinger, H. & Thuro, K.: Überwachung der Deformation einer temporären Kalottensohle mit Time Domain Reflectometry. In: *Geomechanics and Tunnelling* 2 (2009), June, No. 3, pp. 238 – 249.

[Singer et al. 2011] Singer, J., Thuro, K., Sambeth, U. & Stump, R.: Deformationsmessungen mit Time Domain Reflectometry (TDR) zur Hangbewegungs- und Bauwerksüberwachung – Möglichkeiten und Grenzen. In: *Tagungsbeiträge: 8. Österreichische Geotechniktagung, Wien* (2011), February, pp. 377 – 386.

[Tunnel:Monitor 2004] Tunnel:Monitor: *Gruppe* Tunnel:Monitor. iC consulenten Ziviltechniker GesmbH, IGT Geotechnik und Tunnelbau Ziviltechniker G.m.b.H., 3G Gruppe Geotechnik Graz ZT GmbH. 2004.

[Woschitz et al. 2015] Woschitz, H., Klug, F. & Lienhart, W.: Design and calibration of a fiber optic monitoring system for the determination of segment joint movements inside a hydro power dam. In: *Journal of Light Wave Technology* 33 (2015), June, No. 12, pp. 2652 – 2657.